


Classification of electronic nematicity in three-dimensional crystals and quasicrystalsMatthias Hecker ¹, Anant Rastogi,¹ Daniel F. Agterberg,² and Rafael M. Fernandes¹¹*School of Physics and Astronomy, University of Minnesota, Minneapolis 55455, Minnesota, USA*²*Department of Physics, University of Wisconsin-Milwaukee, Milwaukee 53201, Wisconsin, USA*

(Received 4 March 2024; revised 6 June 2024; accepted 10 June 2024; published 25 June 2024)

Electronic nematic order has been reported in a rich landscape of materials, encompassing not only a range of intertwined correlated and topological phenomena but also different underlying lattice symmetries. Motivated by these findings, we investigate the behavior of electronic nematicity as the spherical symmetry of three-dimensional (3D) space is systematically lowered by the lattice environment. We consider all 32 crystallographic point groups as well as four major classes of quasicrystalline point groups, given the recent observations of electronic phases of interest in quasicrystalline materials and artificial twisted quasicrystals. Valuable insights are gained by establishing a mapping between the five-component charge-quadrupolar nematic order parameter of the electronic fluid and the 3D tensorial order parameter of nematic liquid crystals. We find that a uniaxial nematic state is only generically realized in polyhedral point groups (icosahedral and cubic), with the nematic director pointing along different sets of rotational symmetry axes. Interestingly, icosahedral point groups are the only ones in which the five nematic order parameter components transform as the same irreducible representation, making them the closest analog of 3D isotropic nematics. In axial point groups, one of the nematic components is always condensed, whereas the other four components decompose into an in-plane and an out-of-plane nematic doublet, resulting in biaxial nematic ground states. Because these two nematic doublets behave as Z_q clock order parameters, this allows us to identify the types of crystals and quasicrystals that can host interesting electronic nematic phenomena enabled by the critical properties of the $q \geq 4$ clock model, such as emergent continuous nematic fluctuations in 3D, critical phases with quasi-long-range nematic order in two dimensions (2D), and Ashkin-Teller nematicity in 2D.

DOI: [10.1103/PhysRevB.109.235148](https://doi.org/10.1103/PhysRevB.109.235148)**I. INTRODUCTION**

Fingerprints typical of electronic nematic behavior have been experimentally seen in a wide range of settings, such as unconventional cuprates [1–5] and iron-based superconductors [6–11], quantum Hall systems [12,13], correlated oxides [14], doped topological insulators [15,16], twisted moiré systems [17–20], f -electron materials [21–24], kagome metals [25], colossal magnetoresistance compounds [26], triangular antiferromagnets [27–31], topological semimetals [32], and optical lattices [33]. As its name suggests, this state of matter is the quantum analog of classical nematic liquid crystals [34,35] because it causes the spontaneous breaking of a discrete rotational symmetry of the system while preserving its properties under translations [36]. At first, the term electronic nematicity was coined to describe the ordered state that emerges upon the partial melting of an underlying charge or spin stripe state that restores the translational symmetry of a correlated metal or insulator, in close analogy to the smectic-to-nematic transition of liquid crystals [36–40]. More recently, this concept of a so-called vestigial nematic phase was extended to the case of multicomponent superconductors, which were shown in certain circumstances to support a partially melted state that restores the U(1) gauge symmetry but keeps the rotational symmetry of the pairing state broken [41,42]. Since the seminal work of Ref. [36], the term electronic nematicity has been broadly employed to refer to any spontaneous rotational-symmetry-breaking

phase that is driven by electronic interactions (as opposed to elastic interactions) and that does not break additional symmetries—for recent reviews, see Refs. [43–46]. This includes the case of weakly interacting Fermi liquids that undergo a charge $l = 2$ Pomeranchuk instability via a Stoner-like mechanism [47–51], which is particularly favored when the electronic band structure is close to a van Hove singularity and thus has an enhanced density of states [52,53]. Another example of electronic nematicity under this definition are insulating and metallic multi-orbital systems that display ferroquadrupolar order [54]. Extensions of this concept to states that break rotational and time-reversal or inversion symmetries have also been studied [55–60].

The main difference between electronic nematic materials and nematic liquid crystals is that, in the former, rotational symmetry is already explicitly broken by the underlying lattice, whereas the latter has full rotational symmetry. As a result, the electronic nematic order parameter always breaks a discrete symmetry that lowers the point group of the crystal, and all nematic collective modes in the ordered state are gapped. Historically, much of the theoretical investigations on electronic nematicity have focused on strongly anisotropic layered systems and “planar” nematic order parameters [37,48–51,61–63]. Perhaps the most well recognized example is the electronically driven breaking of C_{4z} symmetry (i.e., fourfold rotations about the z axis), in which case the electronic nematic order parameter

is Ising-like [39,64–73]. We emphasize that although such a nematic transition is, on symmetry grounds, equivalent to a tetragonal-to-orthorhombic structural transition, the microscopic mechanisms responsible for the spontaneously broken symmetry are completely different [9]. The fact that electronic nematic phenomena have been heavily studied in tetragonal lattices is not surprising, since the initial experimental observations were on tetragonal (or nearly tetragonal) compounds such as bilayer ruthenates [14], cuprates [1], and iron pnictides [6,7]. More recently, experimental reports of the spontaneous breaking of C_{3z} symmetry (i.e., threefold rotations about the z axis) by electronic degrees of freedom in hexagonal and trigonal systems such as doped Bi_2Se_3 [15,16], twisted multilayer graphene [17–20], and triangular antiferromagnets [27–31] have motivated a deeper theoretical investigation of three-state Potts electronic nematic order parameters [41,57,74–81].

The diversity of systems in which electronic nematicity has been observed indicates that a broader description and systematic classification of this phenomenon is timely. Indeed, there is a rich landscape of crystalline symmetries whose effects on electronic nematic order remain to be explored in depth. This includes cubic systems such as EuB_6 [26] and CaSn_3 [32], which have been reported to display anisotropic properties consistent with nematicity. Besides crystals, quasicrystals [82,83] have been recently found to display electronically ordered states of interest such as superconductivity [84,85], magnetism [86], and quantum criticality [87], raising interesting questions about how electronic nematicity would be manifested in systems that lack periodicity but possess orientational order. This includes not only quasicrystal materials with icosahedral, dodecagonal, decagonal, and octagonal symmetries [88–91] but also artificial quasicrystals that can be assembled in the laboratory by twisting two periodic crystals by specific angles [85,92–96]. Moreover, besides the planar nematic order parameters studied in layered systems, there are additional nematic channels available. Indeed, in terms of the usual electronic operators $\hat{\psi}_{k\sigma}$, the nematic order parameters can be expressed as the expectation values of the quadrupolar charge operator [48], $d_i \equiv \sum_{k,\sigma} \langle f_i(\hat{\mathbf{k}}) \hat{\psi}_{k\sigma}^\dagger \hat{\psi}_{k\sigma} \rangle$. Since there are five d -wave form factors $f_i(\hat{\mathbf{k}})$, one must consider, in the most general case, a nematic order parameter \mathbf{d} with five components:

$$\mathbf{d} = \begin{pmatrix} d_{\frac{1}{\sqrt{3}}(2z^2-x^2-y^2)} \\ d_{x^2-y^2} \\ d_{2yz} \\ d_{2xz} \\ d_{2xy} \end{pmatrix}, \quad (1)$$

where the subscript denotes the corresponding d -wave form factor in Cartesian coordinates. This opens the possibility of realizing “out-of-plane” nematic order in materials that are not strongly anisotropic, such as d_{2xz} and d_{2yz} , beyond the widely investigated “in-plane” nematic states corresponding to $d_{x^2-y^2}$ and d_{2xy} .

In this paper, we perform a systematic and thorough classification of electronic nematic order in all crystalline and quasicrystalline point groups. Specifically, we derive the

Landau expansions and determine the universal properties of the nematic transitions associated with the different allowed types of in-plane and out-of-plane nematic order parameters d_i for a given point group. To gain further insight into how the reduced rotational symmetry of the underlying crystalline or quasicrystalline environment constrains nematicity, we establish a direct relationship between the five-component charge-quadrupolar nematic order parameter \mathbf{d} in Eq. (1), which describes the electronic fluid, and the full rank-2 traceless symmetric tensor $Q_{\mu\mu'}$ that describes nematic liquid crystals in general [34,35]. We find it illuminating to write the latter in the eigenstate basis:

$$Q_{\mu\mu'} = q_1(n_\mu n_{\mu'} - \frac{1}{3}\delta_{\mu\mu'}) - q_2(m_\mu m_{\mu'} - l_\mu l_{\mu'}), \quad (2)$$

where q_1 and q_2 are scalars and $\mathbf{n}, \mathbf{m}, \mathbf{l}$ form a complete set of orthonormal vectors in three-dimensional space. When $q_2 = 0$ or $q_2 = q_1$, $Q_{\mu\mu'}$ describes a uniaxial nematic state with a uniquely defined nematic director \mathbf{n} or \mathbf{m} , respectively; in all other cases, $Q_{\mu\mu'}$ describes a biaxial nematic state [97]. While in liquid crystals these axes determine the orientation of the constituent molecules, in metallic systems they are manifested in the Fermi surface of the nematic state. Thus, by establishing the relationship between the five free parameters encompassed by $q_1, q_2, \mathbf{n}, \mathbf{m}, \mathbf{l}$ in Eq. (2) and the five charge-quadrupolar order parameters encoded in \mathbf{d} in Eq. (1), we determine the characteristic Fermi surface distortion patterns in the nematic states of every point group studied.

To perform the analysis in a transparent and insightful way, we start from the isotropic three-dimensional system, described by the orthogonal group $O(3) = \text{SO}(3) \times \{E, I\}$, from which all crystallographic and noncrystallographic point groups can be obtained by systematically reducing the symmetry according to group theory. Here, $\text{SO}(3)$ contains arbitrary rotations about any three-dimensional axis, I denotes inversion, and E denotes the identity operation. Figure 1 illustrates the well-known path by which the $O(3)$ symmetry is systematically lowered to yield all point groups. First, one needs to distinguish between two types of point groups: the polyhedral groups and the axial groups. There are only seven polyhedral groups: three tetrahedral and two octahedral groups, which form the cubic crystal system, and two icosahedral groups, which describe a large number of quasicrystals.

In contrast, there is an infinite number of axial groups, all of which are subgroups of $D_{\infty h} = \text{SO}(2) \times \{E, I\} \times \{E, C_{2x}\}$, which describes a two-dimensional isotropic system and contains arbitrary rotations about the z axis, twofold rotations about any in-plane axis, inversion, and reflection with respect to the plane. The axial groups are further subdivided into the seven different groups outlined in Fig. 1: $D_{nh}, D_{nd}, C_{nh}, D_n, S_{2n}, C_{nv}$, and C_n , which contain discrete n -fold rotations around the axis perpendicular to the plane and, in some cases, twofold rotations about an axis parallel to the plane. Enforcing the crystallographic restriction theorem leads to 27 crystallographic axial point groups, which are then divided into six crystal systems: hexagonal (seven groups), trigonal (five groups), tetragonal (seven groups), orthorhombic (three groups), monoclinic (three groups), and triclinic (two groups). Together with the five polyhedral cubic groups, they constitute the 32 crystallographic point groups and seven crystal

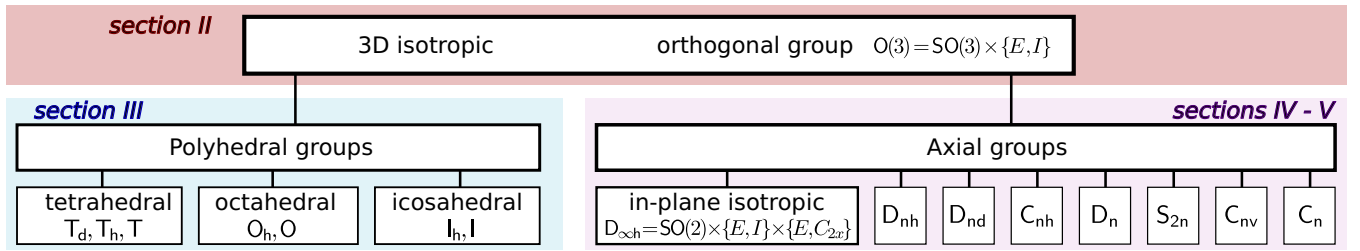


FIG. 1. Schematics of the systematic classification performed in this paper of electronic nematicity in crystalline and quasicrystalline systems. The analysis starts from the ideal isotropic three-dimensional system, described by the orthogonal group $O(3)$ (Sec. II). The spherical symmetry is systematically lowered, leading to two different sets of groups: the seven polyhedral groups (Sec. III) and the seven classes of axial groups. The latter are subgroups of D_{oh} , which describes a two-dimensional isotropic system. Axial groups include 27 crystallographic point groups (Sec. IV) as well as the noncrystallographic dodecagonal, decagonal, and octagonal point groups that describe quasicrystals (Sec. V).

systems. Importantly, the noncrystallographic point groups can still describe materials that are nonperiodic and that can host nontrivial electronic states [88,89]. Thus, in this paper, we also focus on the noncrystallographic point groups that describe quasicrystals, namely, the polyhedral icosahedral groups as well as the axial dodecagonal, decagonal, and octagonal point groups.

Of course, several of our results for the character of the nematic transition in certain point groups recover well-established results obtained in previous symmetry analyses of two-dimensional nematics [43,44,46], structural and ferroelastic transitions [98–100], multipolar order [56,101], and intertwined orders [102]. We emphasize that our main goal here is to provide a complete, self-contained classification of electronic nematicity in crystals and quasicrystals by systematically determining how the removal of symmetries impacts the general structure of the tensorial nematic order parameter (2) via its relationship with the five-component charge-quadrupolar order parameter (1). Our results are summarized in Tables I and II in Sec. VI, and their derivations are shown in Secs. II–V and Appendixes D–G. For the convenience of the reader not interested in the technical details of our analysis, we outline here the main results.

(1) The icosahedral quasicrystalline point groups are the only ones for which the five components of the nematic order parameter (1) transform together as a single five-dimensional irreducible representation. The nematic transition is first order within mean field due to a cubic invariant in the Landau expansion. Depending on the signs of the Landau coefficients, the nematic director that characterizes the uniaxial nematic ground state aligns itself with either the ten axes of threefold rotational symmetry or the six axes of fivefold rotational symmetry of the quasicrystal. In the former case, the residual point group is crystalline (trigonal) whereas in the latter, it is quasicrystalline (decagonal).

(2) The components of the nematic order parameter \mathbf{d} in the cubic crystal groups split into separate triplet and doublet order parameters. The triplet behaves as a Z_4 Potts order parameter, giving rise to a uniaxial nematic state in which the director is parallel to one of four axes of threefold rotational symmetry of the crystal (i.e., the space diagonals). The doublet behaves as a Z_3 Potts (which is equivalent to the Z_3 clock) order parameter, and the three nematic axes point along the coordinate axes. In the cubic groups for which the coordinate

axes are also axes of fourfold rotational symmetry, the nematic ground state is uniaxial, otherwise, it is biaxial. The nematic transitions are, again, first order within mean field.

(3) In any axial group, the nematic component $d_{\frac{1}{\sqrt{3}}(2z^2 - x^2 - y^2)}$ is necessarily nonzero, which changes the shape of the Fermi surface in the symmetry-unbroken phase from spherical to cylindrical. The other four components are decomposed into at least two independent nematic doublets, the in-plane $\mathbf{d}^{\text{ip}} = (d_{x^2 - y^2}, d_{2xy})^T$ and the out-of-plane $\mathbf{d}^{\text{op}} = (d_{2yz}, d_{2xz})^T$. The nematic ground state is always biaxial for the axial groups, unless the Landau parameters are fine tuned. In most cases, at least one of the nematic axes aligns with a high-symmetry in-plane direction.

(4) Each nematic doublet in the axial groups behaves as a Z_q clock order parameter. If the group has $(2n)$ -fold rotational symmetry, $q = n$ for \mathbf{d}^{ip} and $q = 2n$ for \mathbf{d}^{op} . If the group has $(2n + 1)$ -fold rotational symmetry, $q = 2n + 1$ for both \mathbf{d}^{ip} and \mathbf{d}^{op} . In three dimensions, the q -state clock model is known to undergo an XY transition for $q \geq 4$, similarly to the isotropic two-dimensional (2D) nematic case. In two dimensions, the Z_q clock model displays an intermediate critical phase with quasi-long-range order for $q \geq 5$ and an Ashkin-Teller phase transition with nonuniversal critical exponents for $q = 4$. A first-order transition occurs for $q = 3$ and above the upper critical dimension $d_u \gtrsim 2$. If the axial group lacks in-plane rotational symmetry axes, or if \mathbf{d}^{ip} and \mathbf{d}^{op} have the same transformation properties, the clock term in the Landau expansion acquires a nonuniversal offset, which we denote as the Z_q^* clock model.

(5) The main difference between hexagonal and trigonal crystals is that, in the latter, \mathbf{d}^{ip} and \mathbf{d}^{op} are not independent, which has a significant impact on the character of the nematic transition. In tetragonal crystals, \mathbf{d}^{ip} is further decomposed into two one-component Ising-like order parameters. Orthorhombic, monoclinic, and triclinic crystals are described by Abelian point groups, which only admit one-dimensional irreducible representations. As a result, any nematic transition must be Ising-like.

(6) In dodecagonal, decagonal, and octagonal quasicrystals, both nematic doublets behave as Z_q clock order parameters with $q \geq 4$. This makes axial quasicrystals interesting platforms to realize exotic nematicity enabled by the critical properties of the $q \geq 4$ clock model, such as emergent

XY nematic fluctuations and critical nematic phases displaying quasi-long-range order.

The organization of the paper, schematically shown in Fig. 1, is as follows: Section II introduces the formalism and presents the results for nematicity in the three-dimensional isotropic system. The case of polyhedral groups, i.e., cubic crystal system and icosahedral quasicrystals, is discussed in Sec. III. Section IV presents the properties of electronic nematic order in the isotropic two-dimensional system and in the axial crystallographic groups (hexagonal, trigonal, tetragonal, orthorhombic, monoclinic, and triclinic crystal systems). The cases of dodecagonal, decagonal, and octagonal quasicrystalline axial groups are presented in Sec. V. Section VI contains our concluding remarks as well as a summary of our results for the crystalline point groups in Table I and for the quasicrystalline point groups in Table II. Appendix A contains additional details about isotropic nematicity. Appendix B explains the concept of symmetrized decomposition of products of irreducible representations, whereas Appendix C shows details of the minimization of the nematic Landau expansion in icosahedral systems. Appendix D presents details of electronic nematic order in cubic crystals without fourfold rotational symmetry axes. Appendixes E, F, and G derive the properties of electronic nematicity, respectively, in hexagonal, trigonal, and tetragonal point groups that lack in-plane rotational symmetry axes.

II. ELECTRONIC NEMATICITY IN A THREE-DIMENSIONAL ISOTROPIC SYSTEM

A. Representations of the nematic order parameter

To set the stage for the remainder of the paper, we first review the properties of electronic nematicity in three-dimensional (3D) isotropic systems, i.e. systems that are fully rotational invariant. In classical nematics, the order parameter is a “headless vector” associated with the orientation of the elongated molecules that form the liquid crystal. It is conveniently expressed in terms of the symmetric traceless tensor $Q_{\mu\mu'} = \langle a_\mu a_{\mu'} - \frac{1}{3} \delta_{\mu\mu'} a^2 \rangle$, with $\mu, \mu' = 1, 2, 3$ and the director $\mathbf{a} = (a_1, a_2, a_3)$ [34,35]. The generalization to the quantum (i.e. electronic) case has been widely discussed in the literature [48,97]. In terms of the electronic annihilation (creation) operators $\hat{\psi}_\mathbf{k}$ ($\hat{\psi}_\mathbf{k}^\dagger$), the tensorial order parameter is given by

$$Q_{\mu\mu'} = \frac{1}{k_F^2} \sum_{\mathbf{k}, \sigma} \langle \mathcal{F}_{\mu\mu'}(\mathbf{k}) \hat{\psi}_{\mathbf{k}\sigma}^\dagger \hat{\psi}_{\mathbf{k}\sigma} \rangle, \quad (3)$$

with momentum \mathbf{k} , Fermi momentum k_F , spin $\sigma = \uparrow, \downarrow$, and the d -wave form factor $\mathcal{F}_{\mu\mu'}(\mathbf{k}) = 2(k_\mu k_{\mu'} - \frac{1}{3} \delta_{\mu\mu'} k^2)$. Generalizations to multi-orbital systems are straightforward, but will not be covered here [71,101]. Thus, the components of the electronic nematic order parameter correspond to quadrupolar

charge order which, in the theory of interacting Fermi liquids, corresponds to an angular momentum $l = 2$ Pomeranchuk instability of the Fermi liquid in the singlet channel [47]. The condensation of the tensor order parameter Q leads to a distortion of the otherwise spherically symmetric Fermi surface, thus breaking the rotational invariance of the isotropic system:

$$\epsilon_{\mathbf{k}} = \frac{k^2}{2m} - \mu_0 + \frac{1}{2} \text{tr}[Q\mathcal{F}(\mathbf{k})]. \quad (4)$$

Here, m is the effective electron mass and μ_0 , the chemical potential. For concreteness, and to better visualize the fingerprints of nematicity on the electronic degrees of freedom, our analysis will focus on metals. Of course, the symmetry properties of the nematic state would be the same in insulators.

Being a traceless symmetric tensor, Q has five independent components. Thus, it is also convenient to express nematic phenomena in terms of a five-component “vector” $\mathbf{d} = (d_1, d_2, d_3, d_4, d_5)$. To derive the symmetry properties of this vector, we note that a 3D isotropic system is described by the continuous (orthogonal) group $O(3) = SO(3) \times \{E, I\}$, which combines the full rotation group $SO(3)$ with the inversion operation I (here, E denotes the identity operation). Thus, in group-theory notation, the five-component nematic vector \mathbf{d} transforms according to the five-dimensional irreducible representation (IR) $\Gamma_{j=2}^+$ of the orthogonal group $O(3)$. Note that the superscript $+$ ($-$) indicates an inversion-even (inversion-odd) IR.

Such a five-component order parameter can be obtained in a straightforward way as a bilinear \mathbf{M} constructed from the coordinate vector $\mathbf{r} = (x, y, z)$, which in turn transforms according to the three-dimensional vector IR $\Gamma_{j=1}^-$. That such a bilinear \mathbf{M} in the $\Gamma_{j=2}^+$ channel exists follows from the product decomposition $\Gamma_{j=1}^- \otimes \Gamma_{j=1}^- = \Gamma_{j=0}^+ \oplus \Gamma_{j=2}^+ \oplus \Gamma_{j=1}^+$. Writing the bilinear components as $M_i = r_\mu \lambda_{\mu\mu'}^{j=2,i} r_{\mu'}$ with $i \in \{1, \dots, 5\}$ and $\mu \in \{1, 2, 3\}$, we obtain the five matrices $\lambda^{j=2}$ from the transformation condition

$$\mathcal{R}_{-,j=1}^T(g) \lambda^{j=2,i} \mathcal{R}_{-,j=1}(g) = \mathcal{R}_{+,j=2}(g)_{ii'} \lambda^{j=2,i'}, \quad (5)$$

where $\mathcal{R}_{\pm,j}(g)$ denotes the 5×5 transformation matrix of a symmetry element g associated with the IR Γ_j^\pm . The symmetry elements $g = (\vartheta, \hat{\ell}, \mathcal{I})$ are parametrized in terms of the rotation angle ϑ around the unit rotation axis $\hat{\ell}$ and the index $\mathcal{I} = \pm 1$ for inversion being applied ($\mathcal{I} = -1$) or not ($\mathcal{I} = +1$). Therefore, the transformation matrices are given by $\mathcal{R}_{+,j}(g) = \mathcal{R}_j(\vartheta, \hat{\ell})$ and $\mathcal{R}_{-,j}(g) = \mathcal{I} \mathcal{R}_j(\vartheta, \hat{\ell})$ where $\mathcal{R}_j(\vartheta, \hat{\ell}) = \exp(-i\vartheta \mathbf{J}^{(j)} \cdot \hat{\ell})$ are the well-known $(2j+1) \times (2j+1)$ -dimensional rotation matrices. Using the $\mathbf{J}^{(j)}$ matrices outlined in Appendix A, one finds the five matrices $\lambda^{j=2}$ in (5) to be identical to the five symmetric Gell-Mann matrices,

$$\lambda^{j=2} = \left\{ \frac{1}{\sqrt{3}} \begin{pmatrix} -1 & 0 & 0 \\ 0 & -1 & 0 \\ 0 & 0 & 2 \end{pmatrix}, \begin{pmatrix} 1 & 0 & 0 \\ 0 & -1 & 0 \\ 0 & 0 & 0 \end{pmatrix}, \begin{pmatrix} 0 & 0 & 0 \\ 0 & 0 & 1 \\ 0 & 1 & 0 \end{pmatrix}, \begin{pmatrix} 0 & 0 & 1 \\ 0 & 0 & 0 \\ 1 & 0 & 0 \end{pmatrix}, \begin{pmatrix} 0 & 1 & 0 \\ 1 & 0 & 0 \\ 0 & 0 & 0 \end{pmatrix} \right\}. \quad (6)$$

We can now label the five nematic components of \mathbf{d} as polynomials of the coordinate vector $\mathbf{r} = (x, y, z)$, according to their symmetry properties encoded in the bilinear \mathbf{M} :

$$\mathbf{d} = \begin{pmatrix} d_1 \\ d_2 \\ d_3 \\ d_4 \\ d_5 \end{pmatrix} = \begin{pmatrix} d_{\frac{1}{\sqrt{3}}(2z^2-x^2-y^2)} \\ d_{x^2-y^2} \\ d_{2yz} \\ d_{2xz} \\ d_{2xy} \end{pmatrix}. \quad (7)$$

Unsurprisingly, the five components of \mathbf{d} correspond to the five d -wave form factors written as tesseral harmonics. The symmetric Gell-Mann matrices (6) also conveniently establish the relationship between the tensor notation Q and the vector notation \mathbf{d} :

$$Q = \mathbf{d} \cdot \boldsymbol{\lambda}^{j=2}, \quad \mathbf{d} = \text{tr}[Q\boldsymbol{\lambda}^{j=2}]/2, \quad (8)$$

which, in explicit form, gives

$$Q = \begin{pmatrix} d_2 - \frac{1}{\sqrt{3}}d_1 & d_5 & d_4 \\ d_5 & -d_2 - \frac{1}{\sqrt{3}}d_1 & d_3 \\ d_4 & d_3 & \frac{2}{\sqrt{3}}d_1 \end{pmatrix}. \quad (9)$$

In this work, we interchangeably use the tensor notation Q (9) and the five-component vector notation \mathbf{d} (7). Moreover, throughout this work, we use the following transformation relation for the nematic order parameter:

$$\mathbf{d} \xrightarrow{g} \mathcal{R}_{+,j=2}(g)\mathbf{d}, \quad (10)$$

such that the transformation matrices are fixed by the set of given symmetry elements g . This is particularly useful as it uniquely defines the multicomponent nematic channels within reduced symmetry systems where $\mathcal{R}_{+,j=2}(g)$ is block diagonal, such as crystal lattices.

A convenient representation of the nematic tensor Q (9) is in terms of its eigenbasis. In this representation, which we denote the (\mathbf{nml}) representation, the nematic tensor becomes

$$Q_{\mu\mu'} = \sqrt{3}|\mathbf{d}| \cos \alpha (n_\mu n_{\mu'} - \frac{1}{3}\delta_{\mu\mu'}) - |\mathbf{d}| \sin \alpha (m_\mu m_{\mu'} - l_\mu l_{\mu'}), \quad (11)$$

where the angle α determines the eigenvalues while the unit vectors $\mathbf{n}, \mathbf{m}, \mathbf{l}$ span the eigenspace of the matrix (9). As a set of orthonormal eigenvectors, $\mathbf{n}, \mathbf{m}, \mathbf{l}$ obey the orthogonality relations $\mathbf{n} \cdot \mathbf{m} = \mathbf{n} \cdot \mathbf{l} = \mathbf{m} \cdot \mathbf{l} = 0$, as well as the completeness relation

$$n_\mu n_{\mu'} + m_\mu m_{\mu'} + l_\mu l_{\mu'} = \delta_{\mu\mu'}, \quad (12)$$

valid for any μ, μ' . One reason why the (\mathbf{nml}) representation is particularly useful is because the tensor (11) is readily diagonalized using the orthogonal matrix $U = (\mathbf{n}, \mathbf{m}, \mathbf{l})$,

$$Q^d = U^T Q U = \frac{2|\mathbf{d}|}{\sqrt{3}} \begin{pmatrix} \cos(\alpha) & 0 & 0 \\ 0 & \cos(\alpha + \frac{2\pi}{3}) & 0 \\ 0 & 0 & \cos(\alpha + \frac{4\pi}{3}) \end{pmatrix}. \quad (13)$$

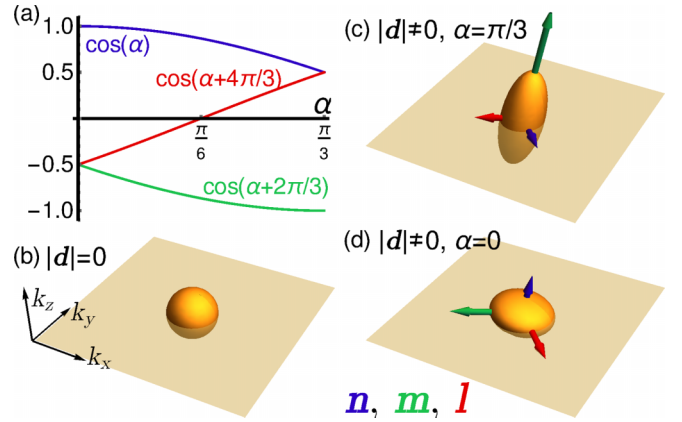


FIG. 2. (a) Eigenvalues of the tensorial nematic order parameter Q (13), in units of $2|\mathbf{d}|/\sqrt{3}$, as a function of the parameter α . The eigenvalues are colored according to their corresponding eigenvector \mathbf{n} (blue), \mathbf{m} (green), and \mathbf{l} (red), see Eq. (14). Note that for $\alpha = 0, \pi/3$, two eigenvalues are degenerate and the corresponding nematic state is uniaxial. (b)–(d) Fermi surfaces (32) of the 3D isotropic system in the absence [panel (b)] or presence of nematic order in the ground state $\alpha = \pi/3$ [panel (c), corresponding to a tensile nematic distortion] and $\alpha = 0$ [panel (d), corresponding to a compressive nematic distortion]. The nematic axes $\mathbf{n}, \mathbf{m}, \mathbf{l}$ are also shown; for visual purposes, they are rescaled by the corresponding value of the Fermi momentum along that direction, $2.25 k_F$ ($\{\mathbf{n}, \mathbf{m}, \mathbf{l}\}$).

Moreover, in this representation, we can use Eq. (8) to write the five-component vector \mathbf{d} (7) as

$$\mathbf{d} = \frac{|\mathbf{d}|}{\sqrt{3}} \left\{ \cos(\alpha) (n_\mu \lambda_{\mu\mu'}^{j=2} n_{\mu'}) + \cos\left(\alpha + \frac{2\pi}{3}\right) (m_\mu \lambda_{\mu\mu'}^{j=2} m_{\mu'}) + \cos\left(\alpha + \frac{4\pi}{3}\right) (l_\mu \lambda_{\mu\mu'}^{j=2} l_{\mu'}) \right\}, \quad (14)$$

where summation over μ, μ' is implied. The parametrization of the orthonormal eigenvectors $\mathbf{n}, \mathbf{m}, \mathbf{l}$ involves three angles and it is not unique, see Appendix A for details. Importantly, to ensure a one-to-one mapping between Eqs. (9) and (11), the eigenvalue-angle α must be restricted to the range $[0, \pi/3]$. Plotting the three eigenvalues as a function of α in Fig. 2(a) makes it clear that the smallest eigenvalue is always related to \mathbf{m} whereas the largest one is associated with \mathbf{n} , see also Eq. (14). Moreover, the figure also reveals two special points, $\alpha = 0, \pi/3$, for which two eigenvalues are degenerate—either the smallest eigenvalue (for $\alpha = 0$) or the largest eigenvalue (for $\alpha = \pi/3$), corresponding to a uniaxial nematic state. For later convenience, we note that in the (\mathbf{nml}) representation of Eq. (14), a sign change in \mathbf{d} corresponds to changing $\alpha \rightarrow \frac{\pi}{3} - \alpha$ and swapping $\mathbf{n} \leftrightarrow \mathbf{m}$:

$$-d[|\mathbf{d}|, \alpha, \mathbf{n}, \mathbf{m}, \mathbf{l}] = d\left[|\mathbf{d}|, \frac{\pi}{3} - \alpha, \mathbf{m}, \mathbf{n}, \mathbf{l}\right]. \quad (15)$$

Here, $|\mathbf{d}| \geq 0$ should be understood as the radial variable of the coordinates $(|\mathbf{d}|, \alpha, \mathbf{n}, \mathbf{m}, \mathbf{l})$.

B. Minimization of the nematic free energy

The value of the angle α that determines the eigenvalues of the nematic order parameter Q or \mathbf{d} , see Eqs. (13) and (14),

can be obtained by minimizing the corresponding Landau expansion. The symmetry-allowed terms in the Landau expansion can be obtained by decomposing the products of the nontrivial IR that defines the order parameter and then picking the terms in the decomposition that transform trivially under the group operations. One way to unambiguously determine these terms, which will be very useful once we consider point groups, is through the so-called decomposition of the symmetrized product, see Appendix B for details. This special decomposition removes any redundancy related to the anti-symmetric channels and avoids the double-counting that one would encounter by considering the nonsymmetrized product. With the order parameter \mathbf{d} transforming according to the IR $\Gamma_{j=2}^+$, the decomposition of the symmetrized products for each Landau expansion order becomes

$$[\otimes_{l=1}^2 \Gamma_2^+]_s = \Gamma_0^+ \oplus \Gamma_2^+ \oplus \Gamma_4^+, \quad (16)$$

$$[\otimes_{l=1}^3 \Gamma_2^+]_s = \Gamma_0^+ \oplus \Gamma_2^+ \oplus \Gamma_3^+ \oplus \Gamma_4^+ \oplus \Gamma_6^+, \quad (17)$$

$$[\otimes_{l=1}^4 \Gamma_2^+]_s = \Gamma_0^+ \oplus 2\Gamma_2^+ \oplus 2\Gamma_4^+ \oplus \Gamma_5^+ \oplus \Gamma_6^+ \oplus \Gamma_8^+. \quad (18)$$

Here, we use the abbreviated tensor product notation, e.g., $\otimes_{l=1}^3 \Gamma_2^+ = \Gamma_2^+ \otimes \Gamma_2^+ \otimes \Gamma_2^+$, and the subscript s to indicate that only the symmetrized product is considered. The symmetrized decompositions (16)–(18) imply the existence of one Landau invariant per expansion order, since there is exactly one trivial channel (Γ_0^+) per expansion order. To systematically identify these invariants, it is useful to first determine the bilinears associated with each IR in Eq. (16), which we denote by $D^{j=0} = |\mathbf{d}|^2$ (Γ_0^+), $D^{j=2}$ (Γ_2^+) and $D^{j=4}$ (Γ_4^+). Solving the respective transformation conditions, similar to Eq. (5), leads to the five-component vector

$$\mathbf{D}^{j=2} = \begin{pmatrix} d_1^2 - d_2^2 + \frac{1}{2}(d_3^2 + d_4^2 - 2d_5^2) \\ -2d_1d_2 - \frac{\sqrt{3}}{2}(d_3^2 - d_4^2) \\ (d_1 - \sqrt{3}d_2)d_3 + \sqrt{3}d_4d_5 \\ (d_1 + \sqrt{3}d_2)d_4 + \sqrt{3}d_3d_5 \\ -2d_1d_5 + \sqrt{3}d_3d_4 \end{pmatrix}, \quad (19)$$

and the nine-component vector $\mathbf{D}^{j=4}$ given in Eq. (A10) in Appendix A. Since $\mathbf{D}^{j=2}$ is quadratic in d_i , it is straightforward to construct the cubic invariant that appears in the symmetrized decomposition in Eq. (17). Specifically, since \mathbf{d} and $\mathbf{D}^{j=2}$ transform as the same IR $\Gamma_{j=2}^+$, their scalar product must transform trivially and thus appear in the free-energy expansion:

$$\mathbf{d} \cdot \mathbf{D}^{j=2} = \frac{\sqrt{3}}{2} \text{tr}[Q^3] = |\mathbf{d}|^3 \cos(3\alpha). \quad (20)$$

In the last step, we employed the (nml) representation (11)–(14) to further simplify the expression. As for the quartic decomposition in Eq. (18), since there is only one term in the symmetrized product that transforms trivially, we can readily identify it as $D^{j=0}D^{j=0} = |\mathbf{d}|^4$. Therefore, the resulting nematic Landau expansion is given by the action

$$S[|\mathbf{d}|, \alpha] = \int_{\mathbf{x}} \{r_0 |\mathbf{d}|^2 + g |\mathbf{d}|^3 \cos(3\alpha) + u |\mathbf{d}|^4\}, \quad (21)$$

where $\mathbf{x} = (\mathbf{r}, \tau)$ comprises position and imaginary time, $\int_{\mathbf{x}} \equiv \int d^3r \int_0^{1/T} d\tau$, r_0 is the control parameter that tunes the system across a nematic transition, and g, u are cubic and quartic Landau parameters, respectively. We opted to represent the Landau expansion in terms of an action rather than a free energy in order to explicitly account for the temporal dependence of the nematic order parameter, which is necessary in the case of a quantum phase transition. For a thermal transition, we can write $r_0 = a_0(T - T_0)$ with $a_0 > 0$ and T_0 a reference temperature, such that the free energy is given by $F = ST_0$.

We note that the action (21) does not depend on the orientation of the nematic axes \mathbf{n}, \mathbf{m} , and \mathbf{l} , which is a manifestation of the full rotational invariance of the 3D isotropic system. Although the expansion (21) resembles that of a three-state Potts or clock model (Z_3 model), it is important to emphasize that $\alpha \in [0, \frac{\pi}{3}]$ and that \mathbf{d} is a five-component vector. Minimization with respect to α gives the mean-field ground-state angle:

$$\alpha_0 = \frac{\pi}{3} \left(\frac{1 + \text{sign}(g)}{2} \right), \quad (22)$$

i.e., the angle is either $\alpha_0 = 0$ (for $g < 0$) or $\alpha_0 = \pi/3$ (for $g > 0$). In either case, the effective action in terms of $|\mathbf{d}|$ alone assumes the form

$$\mathcal{S}_{\text{eff}}[|\mathbf{d}|] = \int_{\mathbf{x}} \{r_0 |\mathbf{d}|^2 - |g| |\mathbf{d}|^3 + u |\mathbf{d}|^4\}. \quad (23)$$

The existence of a negative cubic term implies that, within a mean-field solution, the isotropic nematic transition is first order. Another important property of the $\alpha_0 = 0, \pi/3$ solutions is that they correspond to uniaxial nematic states, i.e., states that only depend on one eigenvector and for which two eigenvalues are degenerate [97]. This can be seen directly from Eq. (11): when $\alpha = 0$, the second term vanishes and we obtain

$$\mathcal{Q}_{\mu\mu'}[\alpha = 0] = \sqrt{3} |\mathbf{d}| (n_\mu n_{\mu'} - \frac{1}{3} \delta_{\mu\mu'}), \quad (24)$$

which corresponds to a nematic director along \mathbf{n} . Correspondingly, for $\alpha = \pi/3$, we have $\sqrt{3} \cos \alpha = \sin \alpha = \sqrt{3}/2$; using the completeness relation (12) we find

$$\mathcal{Q}_{\mu\mu'}[\alpha = \pi/3] = -\sqrt{3} |\mathbf{d}| (m_\mu m_{\mu'} - \frac{1}{3} \delta_{\mu\mu'}), \quad (25)$$

corresponding to a nematic director along \mathbf{m} . Similarly, inserting the two α_0 values into the nematic order parameter (14) gives

$$\mathbf{d}[\alpha = 0] = (\sqrt{3}/2) |\mathbf{d}| n_\mu \lambda_{\mu\mu'}^{j=2} n_{\mu'}, \quad (26)$$

$$\mathbf{d}[\alpha = \pi/3] = -(\sqrt{3}/2) |\mathbf{d}| m_\mu \lambda_{\mu\mu'}^{j=2} m_{\mu'}, \quad (27)$$

where we used, once again, the completeness relation (12) as well as the fact that $\text{tr}(\lambda^{j=2,i}) = 0$. Note that (27) is just the negative of (26), in accordance with (15). Clearly, the continuous rotational symmetry of the isotropic system is spontaneously broken in the nematic ground state, as the nematic director \mathbf{n} (or \mathbf{m}) can point in any direction.

In the case of a metallic system, these distortion patterns are manifested in the Fermi surface of the nematic state, and the nematic instability is nothing but an $l = 2$ Pomeranchuk instability in the charge channel. The corresponding electronic

dispersion (4) can be conveniently rewritten in the (nml) representation. Using Eq. (13), we find

$$\epsilon_k = \frac{k^2}{2m} - \mu_0 + \frac{1}{2} \text{tr}[Q_d U^T \mathcal{F}(\mathbf{k}) U]. \quad (28)$$

The transformed matrix $U^T \mathcal{F}(\mathbf{k}) U$ is given by

$$\begin{aligned} U^T \mathcal{F}(\mathbf{k}) U &= \begin{pmatrix} \mathbf{n}^T \\ \mathbf{m}^T \\ \mathbf{l}^T \end{pmatrix} \mathcal{F}(\mathbf{k})(\mathbf{n}, \mathbf{m}, \mathbf{l}) \\ &= \begin{pmatrix} \mathbf{n}^T \mathcal{F}(\mathbf{k}) \mathbf{n} & \mathbf{n}^T \mathcal{F}(\mathbf{k}) \mathbf{m} & \mathbf{n}^T \mathcal{F}(\mathbf{k}) \mathbf{l} \\ \mathbf{m}^T \mathcal{F}(\mathbf{k}) \mathbf{n} & \mathbf{m}^T \mathcal{F}(\mathbf{k}) \mathbf{m} & \mathbf{m}^T \mathcal{F}(\mathbf{k}) \mathbf{l} \\ \mathbf{l}^T \mathcal{F}(\mathbf{k}) \mathbf{n} & \mathbf{l}^T \mathcal{F}(\mathbf{k}) \mathbf{m} & \mathbf{l}^T \mathcal{F}(\mathbf{k}) \mathbf{l} \end{pmatrix}. \end{aligned} \quad (29)$$

Using the fact that

$$\mathbf{v}^T \mathcal{F}(\mathbf{k}) \mathbf{w} = 2(\mathbf{k} \cdot \mathbf{v})(\mathbf{k} \cdot \mathbf{w}) - \frac{2}{3} k^2 (\mathbf{v} \cdot \mathbf{w}), \quad (30)$$

and performing the matrix product, we find

$$\begin{aligned} \epsilon_k &= \frac{k^2}{2m} - \mu_0 + \frac{2|\mathbf{d}|k^2}{\sqrt{3}} \left[(\hat{\mathbf{k}} \cdot \mathbf{n})^2 \cos(\alpha) \right. \\ &\quad \left. + (\hat{\mathbf{k}} \cdot \mathbf{m})^2 \cos\left(\alpha + \frac{2\pi}{3}\right) + (\hat{\mathbf{k}} \cdot \mathbf{l})^2 \cos\left(\alpha + \frac{4\pi}{3}\right) \right], \end{aligned} \quad (31)$$

with $\hat{\mathbf{k}} = \mathbf{k}/|\mathbf{k}|$. Here, we used $\sum_{\nu=0}^2 \cos(\alpha + \nu \frac{2\pi}{3}) = 0$.

The Fermi wave vector of the dispersion (31) can be readily obtained as a function of $\hat{\mathbf{k}}$:

$$\begin{aligned} k_F(\hat{\mathbf{k}}) &= k_{F,0} \left\{ 1 + \frac{4m|\mathbf{d}|}{\sqrt{3}} \left[(\hat{\mathbf{k}} \cdot \mathbf{m})^2 \cos\left(\alpha + \frac{2\pi}{3}\right) \right. \right. \\ &\quad \left. \left. + (\hat{\mathbf{k}} \cdot \mathbf{l})^2 \cos\left(\alpha + \frac{4\pi}{3}\right) + (\hat{\mathbf{k}} \cdot \mathbf{n})^2 \cos(\alpha) \right] \right\}^{-\frac{1}{2}}, \end{aligned} \quad (32)$$

where we defined the isotropic Fermi momentum $k_{F,0} = \sqrt{2m\mu_0}$. Using the results of Fig. 2(a), we conclude that the Fermi wave vector is longest along the \mathbf{m} axis, $k_{F,\max} = k_F(\hat{\mathbf{k}} = \pm \mathbf{m})$, and shortest along the \mathbf{n} directions, $k_{F,\min} = k_F(\hat{\mathbf{k}} = \pm \mathbf{n})$. Therefore, we identify \mathbf{m} and \mathbf{n} as the long and short nematic axes of the distorted Fermi surface, respectively. Moreover, when $\alpha = 0$ ($g < 0$), the Fermi momentum along the \mathbf{l} direction is as large as the Fermi momentum along \mathbf{m} , resulting in a Fermi surface with the shape of an oblate spheroid; we dub this a ‘‘compressive’’ nematic deformation, and associate the nematic director to \mathbf{n} . In contrast, when $\alpha = \pi/3$ ($g > 0$), the Fermi momenta along \mathbf{l} and along the short axes \mathbf{n} are equivalent, resulting in a Fermi surface with the shape of a prolate spheroid, which we associate with a ‘‘tensile’’ nematic deformation. The nematic director in this case is parallel to \mathbf{m} .

We plot the Fermi surface (32) associated with the two mean-field nematic ground states $\alpha = \pi/3, 0$ in Figs. 2(c) and 2(d) with nematic magnitude $|\mathbf{d}| = 1/(3m)$, together with the undistorted Fermi surface in Fig. 2(b). The same nematic magnitude is employed in all figures in this work. Additionally, we also plot the corresponding eigenvectors $\mathbf{n}, \mathbf{m}, \mathbf{l}$

rescaled by $2.25 k_F(\mathbf{n})$, $2.25 k_F(\mathbf{m})$, $2.25 k_F(\mathbf{l})$, respectively, to better visualize the long and short axes in each case. Regardless of the value of g , the resulting Fermi surface is always a uniaxial ellipsoid, which has the shape of either an oblate spheroid [$\alpha = 0, g < 0$, resulting in the compressive distortion of Fig. 2(d)] or a prolate spheroid [$\alpha = \pi/3, g > 0$, resulting in the tensile distortion of Fig. 2(c)]. Importantly, the uniaxial vector \mathbf{n} or \mathbf{m} can point in any direction, reflecting the spontaneous breaking of the continuous rotational symmetry below the nematic transition.

III. ELECTRONIC NEMATICITY IN POLYHEDRAL POINT GROUPS

Once full rotational symmetry is explicitly broken, the system is described in terms of point groups, which, in contrast with the continuous orthogonal group $O(3)$, are finite groups. When investigating electronically ordered states, it is customary to focus on the 32 crystallographic point groups, which have at most twofold, threefold, fourfold, or sixfold rotation symmetry. However, quasicrystals [82,83] have been recently shown to realize various electronically driven phenomena observed in periodic crystals [90,91], such as superconductivity [84,85], magnetism [86], and quantum criticality [87]. While nematicity has not yet been observed in quasicrystalline environments, it is interesting to analyze this possibility not only to establish valuable predictions for future experiments, but also to gain deep insights about the structure of electronic nematicity as the symmetries of the nonisotropic system are systematically reduced. Therefore, in this paper, we will not restrict our analysis to crystallographic point groups only, but will also consider electronic nematicity in point groups that describe icosahedral, dodecahedral, decagonal, and octagonal quasicrystals, as well as twisted quasicrystals [85,92–96].

There are two different classes of point groups, namely, polyhedral groups (which do not have axial symmetry) and axial groups (which, as the name implies, have cylindrical symmetry). As we show below, in what concerns nematicity, the polyhedral groups are special, since none of the five elements of the vector \mathbf{d} transform as a trivial IR. In fact, they always transform as multidimensional IRs, which can be either two dimensional, three dimensional, or five dimensional. This makes a description of electronic nematicity in the (nml) representation particularly insightful and convenient. In contrast, in the axial groups, at least one of the elements of \mathbf{d} transforms trivially, and the other components transform either as two-dimensional IRs or as one-dimensional IRs. As we see, this does not preclude a description in terms of the (nml) representation.

The seven existing polyhedral groups, which are the focus of this section, are depicted in Fig. 1 and include two octahedral, three tetrahedral, and two icosahedral point groups. The octahedral and tetrahedral groups define the cubic crystal system, whereas the icosahedral groups describe a large class of quasicrystals [89].

The two icosahedral groups I and $I_h = I \times \{E, I\}$ have a total of 60 and 120 symmetry elements. Those are constructed from twofold (15 axes), threefold (10 axes), and fivefold (6 axes) rotations. For later convenience, we explicitly list the

sets of six fivefold and the ten threefold rotation axes:

$$\mathcal{V}_5^{\text{ico}} = \left\{ \begin{pmatrix} \pm\alpha_+^{(5)} \\ \alpha_-^{(5)} \\ 0 \end{pmatrix}, \begin{pmatrix} 0 \\ \pm\alpha_+^{(5)} \\ \alpha_-^{(5)} \end{pmatrix}, \begin{pmatrix} \alpha_-^{(5)} \\ 0 \\ \pm\alpha_+^{(5)} \end{pmatrix} \right\}, \quad (33)$$

$$\mathcal{V}_3^{\text{ico}} = \left\{ \begin{pmatrix} \pm\alpha_+^{(3)} \\ \alpha_+^{(3)} \\ 0 \end{pmatrix}, \begin{pmatrix} 0 \\ \pm\alpha_-^{(3)} \\ \alpha_+^{(3)} \end{pmatrix}, \begin{pmatrix} \alpha_+^{(3)} \\ 0 \\ \pm\alpha_-^{(3)} \end{pmatrix}, \mathcal{V}_{111} \right\}. \quad (34)$$

Here, we defined $\alpha_{\pm}^{(3)} = \frac{1}{\sqrt{6}}\sqrt{3 \pm \sqrt{5}}$, $\alpha_{\pm}^{(5)} = \frac{1}{\sqrt{10}}\sqrt{5 \pm \sqrt{5}}$, as well as the set

$$\mathcal{V}_{111} = \frac{1}{\sqrt{3}} \left\{ \begin{pmatrix} 1 \\ 1 \\ 1 \end{pmatrix}, \begin{pmatrix} -1 \\ -1 \\ 1 \end{pmatrix}, \begin{pmatrix} 1 \\ -1 \\ -1 \end{pmatrix}, \begin{pmatrix} -1 \\ 1 \\ -1 \end{pmatrix} \right\}, \quad (35)$$

containing the four corners of a tetrahedron. The five octahedral and tetrahedral point groups, which form the cubic crystal system, have much fewer elements, and can be conveniently expressed as

$$\text{T} = \{E, C_{3\alpha}^{\pm 1}\} \times \{E, C_{2z}\} \times \{E, C_{2x}\}, \quad (36)$$

$$\text{T}_h = \text{T} \times \{E, I\}, \quad (37)$$

$$\text{T}_d = \text{T} \times \{E, IC_{4z}\}, \quad (38)$$

$$\text{O} = \text{T} \times \{E, C_{4z}\}, \quad (39)$$

$$\text{O}_h = \text{T} \times \{E, C_{4z}\} \times \{E, I\}. \quad (40)$$

Within the cubic crystal system (36)–(39), O_h is the supergroup, since all the other ones are subgroups to O_h . The characteristic elements of the T group comprise four threefold rotation axes $\hat{\ell} \in \mathcal{V}^{111}$, see Eq. (35), as well as three twofold rotation axes $\hat{\ell} \in \mathcal{V}^{100}$, where

$$\mathcal{V}^{100} = \{\hat{e}_x, \hat{e}_y, \hat{e}_z\}. \quad (41)$$

For instance, the element $C_{3\alpha}^{\pm 1}$ denotes a rotation by an angle $\vartheta = \pm 2\pi/3$ about the axis $\hat{\ell} = (1, 1, 1)/\sqrt{3}$. Similarly, C_{2z} corresponds to a $\vartheta = 2\pi/2$ rotation about $\hat{\ell} = \hat{e}_z$.

A. Icosahedral quasicrystals

Within the polyhedral point groups, the icosahedral class contains the largest number of symmetry elements. In fact, the large number of symmetry elements forces the five-component order parameter \mathbf{d} to still transform as a five-dimensional IR. In other words, in an icosahedral environment the nematic order parameter is not symmetry-decomposed but remains the five-dimensional expression (7), i.e.,

$$\mathbf{d} \xrightarrow{\text{icosahedral}} \mathbf{d}. \quad (42)$$

This property is unique to icosahedral quasicrystals as no other crystallographic or noncrystallographic point group allows for a five-component IR. For concreteness, in this section we focus on the larger group I_h , but our results also apply to the group I. Within I_h , the order parameter transforms according to the five-dimensional IR H_g . While both the isotropic $\text{O}(3)$ and the icosahedral I_h environments host five-component nematic order parameters, the preferred directions of the nematic director in the latter should be severely restricted due to the finite number of symmetry axes. Therefore,

because the system lacks a continuous rotational symmetry, the nematic ground state of an icosahedral quasicrystal should be qualitatively different from the isotropic case. Mathematically, this difference should be reflected in the corresponding nematic Landau expansion, which we now derive.

Here, and in all subsequent sections of this paper, we follow the same strategy to derive the Landau expansion. First, we compute the decomposition, for each expansion order, of the symmetrized products of the IR according to which the nematic order parameter transforms (see Appendix B). We find

$$[\otimes_{j=1}^2 H_g]_s = A_g \oplus G_g \oplus 2H_g, \quad (43)$$

$$[\otimes_{j=1}^3 H_g]_s = 2A_g \oplus T_{1g} \oplus T_{2g} \oplus 3G_g \oplus 3H_g, \quad (44)$$

$$[\otimes_{j=1}^4 H_g]_s = 2A_g \oplus 2T_{1g} \oplus 2T_{2g} \oplus 4G_g \oplus 8H_g. \quad (45)$$

Therefore, the Landau expansion up to fourth order contains a total of five invariants (i.e., five terms that transform as the trivial IR A_g), in contrast with the three invariants of the isotropic case, see Eqs. (16)–(18). To construct these five invariants it is convenient to determine the bilinear combinations associated with Eq. (43), which we denote by $D^{A_g} = |\mathbf{d}|^2$, D^{G_g} , $D^{H_g,1}$, and $D^{H_g,2}$. Note that the two H_g bilinears are degenerate. As explained in Appendix C, we choose a representation where $D^{H_g,1} = D^{j=2}$, as defined in Eq. (19), and

$$D^{H_g,2} = \mathcal{R}_5(-\phi_0) \begin{pmatrix} \tilde{d}_1^2 - \tilde{d}_2^2 + \frac{1}{2}(\tilde{d}_3^2 + \tilde{d}_4^2 - 2\tilde{d}_5^2) \\ -2\tilde{d}_1\tilde{d}_2 - \frac{\sqrt{3}}{2}(\tilde{d}_3^2 - \tilde{d}_4^2) \\ (\tilde{d}_1 - \sqrt{3}\tilde{d}_2)\tilde{d}_3 + \sqrt{3}\tilde{d}_4\tilde{d}_5 \\ (\tilde{d}_1 + \sqrt{3}\tilde{d}_2)\tilde{d}_4 + \sqrt{3}\tilde{d}_3\tilde{d}_5 \\ -2\tilde{d}_1\tilde{d}_5 + \sqrt{3}\tilde{d}_3\tilde{d}_4 \end{pmatrix}. \quad (46)$$

Here, we introduced $\tilde{\mathbf{d}} = \mathcal{R}_5(\phi_0)\mathbf{d}$ with angle $\phi_0 = \arccos(-1/4)$ and the particular rotation matrix

$$\mathcal{R}_5(\phi) = \begin{pmatrix} \cos \phi & \sin \phi & 0 & 0 & 0 \\ -\sin \phi & \cos \phi & 0 & 0 & 0 \\ 0 & 0 & 1 & 0 & 0 \\ 0 & 0 & 0 & 1 & 0 \\ 0 & 0 & 0 & 0 & 1 \end{pmatrix}. \quad (47)$$

Correspondingly, the two H_g bilinears are related through the equation $D^{H_g,2} = \mathcal{R}_5(-\phi_0)D^{H_g,1}|_{\mathbf{d} \rightarrow \tilde{\mathbf{d}}}$, and thus have the same magnitude $|D^{H_g,1}| = |D^{H_g,2}| = |\mathbf{d}|^2$. For our purposes, we do not need D^{G_g} , although it can be derived in a straightforward way. With the aid of the two H_g bilinears, the five A_g invariants in Eqs. (43)–(45) can be constructed as $|\mathbf{d}|^2$, $|\mathbf{d}|^4$, $\mathbf{d} \cdot D^{H_g,1}$, $\mathbf{d} \cdot D^{H_g,2}$, and $D^{H_g,1} \cdot D^{H_g,2}$. The resulting nematic Landau action becomes

$$\mathcal{S} = \int_{\mathbf{x}} \{r_0 |\mathbf{d}|^2 + |\mathbf{d}|^3 (g_1 \hat{\mathbf{d}} \cdot \hat{D}^{H_g,1} + g_2 \hat{\mathbf{d}} \cdot \hat{D}^{H_g,2}) + |\mathbf{d}|^4 (u_1 + u_2 \hat{D}^{H_g,1} \cdot \hat{D}^{H_g,2})\}, \quad (48)$$

with the unit vectors $\hat{\mathbf{d}} = \mathbf{d}/|\mathbf{d}|$ and $\hat{D}^{H_g,1/2} = D^{H_g,1/2}/|\mathbf{d}|^2$, the cubic coefficients g_1 and g_2 , and the quartic coefficients u_1 and u_2 , which are restricted to $0 \leq |u_2| < u_1$ in order for the action to be bounded. Since the action (48) has not

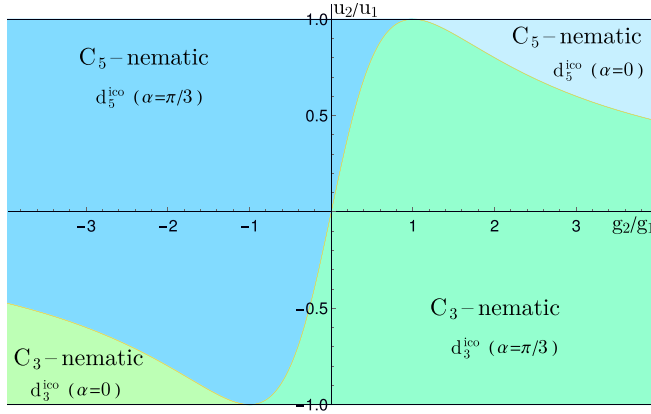


FIG. 3. Nematic mean-field phase diagram of an icosahedral quasicrystal obtained by a mean-field minimization of the action (48). The parameters u_1 , u_2 and g_1 , g_2 are the quartic and cubic Landau coefficients, respectively. Each state is characterized by the angle α denoting either a tensile nematic state ($\alpha = \pi/3$) or a compressive nematic state ($\alpha = 0$), see Eq. (14). In this figure, we set $g_1 > 0$. The case $g_1 < 0$ is recovered by switching ($\alpha = 0$) \leftrightarrow ($\alpha = \pi/3$).

been explored in the literature, we first establish the corresponding mean-field ground-state phase diagram. The details of the derivation are given in Appendix C; here, we focus on the numerically obtained phase diagram shown in Fig. 3 in the $(g_2/g_1, u_2/u_1)$ parameter space. Clearly, the Landau expansion (48) has two distinct ground-state phases, which we dub C_3 nematic and C_5 nematic, based on the residual rotational symmetry of each state. Note that in this projected phase diagram, we implicitly assume that the value of the quadratic coefficient r_0 is small enough such that the system is in the nematic phase. In other words, this phase diagram does not determine when the nematic transition takes place. Instead, it expresses which nematic state is selected below the nematic transition temperature for a given set of higher-order Landau coefficients.

We first discuss the C_3 nematic phase, by focusing on the parameter regime $\text{sign } g_1 = \text{sign } g_2$ and $u_2 < 0$ (bottom-right quadrant in Fig. 3). In this region, the condition $\hat{D}^{H_g,1} = \hat{D}^{H_g,2} = -\text{sign } g_1 \hat{d}$ minimizes not only the two cubic terms of Eq. (48), but also the anisotropic quartic term, i.e., all three direction-dependent terms are simultaneously minimized. This condition is satisfied for 10 directions of the nematic order parameter \hat{d} , which are associated with the ten threefold symmetry axes $\mathcal{V}_3^{\text{ico}}$ in Eq. (34). Indeed, in the (nml) representation (14), the C_3 nematic ground state is given by

$$g_1 > 0: \quad \mathbf{d}_{3,i}^{\text{ico}} = \mathbf{d}[|\mathbf{d}|, \alpha = \pi/3, \mathbf{n}_i, \mathbf{m}_i = \mathcal{V}_{3,i}^{\text{ico}}, \mathbf{l}_i], \quad (49)$$

$$g_1 < 0: \quad \mathbf{d}_{3,i}^{\text{ico}} = \mathbf{d}[|\mathbf{d}|, \alpha = 0, \mathbf{n}_i = \mathcal{V}_{3,i}^{\text{ico}}, \mathbf{m}_i, \mathbf{l}_i], \quad (50)$$

with $i = 1, \dots, 10$. Since $\alpha = \pi/3$ or $\alpha = 0$, both ground states are uniaxial, see Eqs. (26) and (27), with the state described by Eq. (49) being a tensile nematic state ($\alpha = \pi/3$) and the state described by Eq. (50) being a compressive nematic state ($\alpha = 0$). In Fig. 4(a), we plot the Fermi-surface distortion associated with the tensile C_3 nematic ground state (49) using Eq. (31). Note that, while strictly speaking,

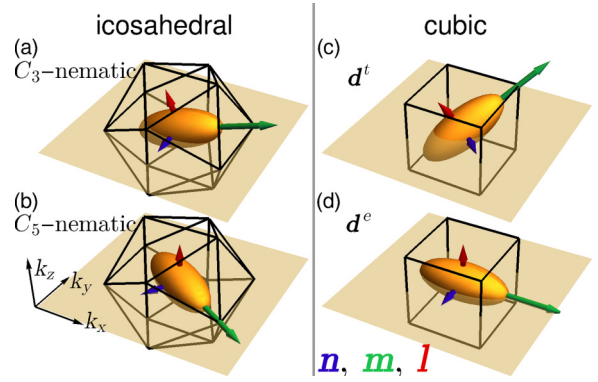


FIG. 4. Distorted Fermi surface in the nematic phase, as given by Eq. (32), plotted together with the nematic axes \mathbf{n} , \mathbf{m} , \mathbf{l} . (a) Icosahedral C_3 nematic state (49); (b) icosahedral C_5 nematic state (51); (c) cubic triplet (T_{2g}) state (62); (d) cubic doublet (E_g) state (70). In all cases, the $\alpha = \pi/3$ (tensile) state is plotted, and the nematic director is parallel to \mathbf{m} . The unit vectors $\{\mathbf{n}, \mathbf{m}, \mathbf{l}\}$ are rescaled by $2.2 k_F$ ($\{\mathbf{n}, \mathbf{m}, \mathbf{l}\}$), respectively.

the crystal momentum is not a good quantum number for a quasicrystal, plotting Eq. (32) is useful to visualize, even if perturbatively only, the effect of the broken rotational symmetry on the otherwise spherically symmetric electronic charge distribution. To visualize the allowed directions of the nematic director \mathbf{m} , we draw in the same figure an icosahedron concentric to the Fermi surface, which consists of 20 identical equilateral triangles. Clearly, the long axis \mathbf{m} points towards the center of one these equilateral triangles. Since there are 20 such triangles, and because $\pm \mathbf{m}$ are identical nematic states, there are indeed ten degenerate states. Because \mathbf{n}_i or \mathbf{m}_i can only point along ten symmetry-related directions, the broken symmetry is discrete. Note that the resulting point group in this case is D_{3d} . While it belongs to the crystallographic trigonal system, this does not imply that the quasicrystal will become a crystal rather than an incommensurate crystal. Nevertheless, it is interesting that a nematic transition changes the point group from noncrystallographic to crystallographic.

To discuss the C_5 nematic phase, we consider the parameter range $\text{sign } g_1 = -\text{sign } g_2$ and $u_2 > 0$, corresponding to the top-left quadrant in the phase diagram of Fig. 3. In this case, the simultaneous minimization of the three anisotropic terms of the action (48) is achieved by the condition $\hat{D}^{H_g,1} = -\hat{D}^{H_g,2} = -\text{sign } g_1 \hat{d}$. This condition, in turn, is satisfied for six directions of \hat{d} that are associated with the six fivefold symmetry axes $\mathcal{V}_5^{\text{ico}}$ in Eq. (33). In analogy to the C_3 nematic phase, the C_5 nematic ground state is uniaxial and parametrized as

$$g_1 > 0: \quad \mathbf{d}_{5,i}^{\text{ico}} = \mathbf{d}[|\mathbf{d}|, \alpha = \pi/3, \mathbf{n}_i, \mathbf{m}_i = \mathcal{V}_{5,i}^{\text{ico}}, \mathbf{l}_i], \quad (51)$$

$$g_1 < 0: \quad \mathbf{d}_{5,i}^{\text{ico}} = \mathbf{d}[|\mathbf{d}|, \alpha = 0, \mathbf{n}_i = \mathcal{V}_{5,i}^{\text{ico}}, \mathbf{m}_i, \mathbf{l}_i], \quad (52)$$

where $i = 1, \dots, 6$. We visualize the tensile Fermi-surface distortion associated with the tensile state (51) in Fig. 4(b). In the C_5 nematic phase, the nematic director \mathbf{m} aligns with the corners of the icosahedron. Since there are twelve such corners, we find indeed six degenerate C_5 nematic states. The residual symmetries inside the nematic phase result in the

point group D_{5d} , which is also a noncrystallographic point group.

The nematic phase diagram in Fig. 3 shows that the C_3 nematic state (49) and the C_5 nematic state (51) actually occupy the entire phase space, including regions where not all three anisotropic terms in (48) can be satisfied simultaneously. As shown in the top-right and bottom-left corner, a tensile ground state can become a compressive one upon traversing the phase diagram.

B. Cubic crystals

Candidate nematic materials with cubic symmetry include the colossal magnetoresistance compound EuB_6 [26] and the topological semimetal CaSn_3 [32]. The cubic crystal system consists of two octahedral point groups (O_h , O) and three tetrahedral point groups (T_h , T_d , T). In all five cases, the reduced symmetry with respect to the icosahedral point group leads to a symmetry decomposition of the five-component nematic order parameter \mathbf{d} (7) according to

$$\mathbf{d} \xrightarrow{\text{cubic}} (\mathbf{d}^e, \mathbf{d}^t)^T, \quad (53)$$

where the doublet \mathbf{d}^e and the triplet \mathbf{d}^t nematic vectors are given by

$$\mathbf{d}^e = \begin{pmatrix} d_1 \\ d_2 \end{pmatrix} = \begin{pmatrix} d \frac{1}{\sqrt{3}} (2z^2 - x^2 - y^2) \\ d_{x^2 - y^2} \end{pmatrix} = |\mathbf{d}^e| \begin{pmatrix} \cos \gamma_e \\ \sin \gamma_e \end{pmatrix}, \quad (54)$$

$$\mathbf{d}^t = (d_3, d_4, d_5)^T = (d_{2yz}, d_{2xz}, d_{2xy})^T. \quad (55)$$

In terms of the IRs of the five groups (O_h , O , T_h , T_d , T), \mathbf{d}^t always transforms as a three-dimensional IR (T_{2g} , T_2 , T_g , T_2 , and T , respectively) whereas \mathbf{d}^e transforms as a two-dimensional IR (E_g , E , $E_g \oplus \bar{E}_g$, E , and $E \oplus \bar{E}$, respectively). Our goal is to derive the Landau expansions for both types of nematics and then determine the mean-field ground states in the (nml) representation (14). For concreteness, we focus on the most symmetric cubic point group O_h and comment on the extension to the other four cubic point groups in the end of this section.

We begin with the nematic triplet order parameter \mathbf{d}^t (55), which transforms as the T_{2g} IR of O_h . The decomposition of the symmetrized product for each expansion order gives

$$[\otimes_{j=1}^2 T_{2g}]_s = A_{1g} \oplus E_g \oplus T_{2g}, \quad (56)$$

$$[\otimes_{j=1}^3 T_{2g}]_s = A_{1g} \oplus T_{1g} \oplus 2T_{2g}, \quad (57)$$

$$[\otimes_{j=1}^4 T_{2g}]_s = 2A_{1g} \oplus 2E_g \oplus T_{1g} \oplus 2T_{2g}, \quad (58)$$

which implies the existence of four invariants in the Landau expansion up to fourth order. To systematically construct them, it is convenient to exploit the bilinears associated with the quadratic decomposition, Eq. (56). We find that $D^{A_{1g}} = |\mathbf{d}^t|^2$ and

$$\mathbf{D}^{E_g} = \begin{pmatrix} \frac{1}{\sqrt{3}}(2d_5^2 - d_3^2 - d_4^2) \\ (d_3^2 - d_4^2) \end{pmatrix}, \quad \mathbf{D}^{T_{2g}} = \begin{pmatrix} 2d_4d_5 \\ 2d_3d_5 \\ 2d_3d_4 \end{pmatrix}. \quad (59)$$

In terms of these bilinears, the four invariants become $|\mathbf{d}^t|^2$ to quadratic order, $\mathbf{d}^t \cdot \mathbf{D}^{T_{2g}}$ to cubic order, and $|\mathbf{d}^t|^4$ and $\mathbf{D}^{T_{2g}}$

$\mathbf{D}^{T_{2g}}$ to quartic order. Note that the quartic term could equally be written in terms of $\mathbf{D}^{E_g} \cdot \mathbf{D}^{E_g}$ by using the Fierz identity $\mathbf{D}^{E_g} \cdot \mathbf{D}^{E_g} = \frac{4}{3} |\mathbf{d}^t|^4 - \mathbf{D}^{T_{2g}} \cdot \mathbf{D}^{T_{2g}}$. Therefore, the resulting Landau expansion is

$$\mathcal{S} = \int_{\mathbf{x}} \{ r_0 |\mathbf{d}^t|^2 + g d_3 d_4 d_5 + u_1 |\mathbf{d}^t|^4 + u_2 (d_3^2 d_4^2 + d_3^2 d_5^2 + d_4^2 d_5^2) \}, \quad (60)$$

with the cubic and quartic Landau coefficients g , u_1 , u_2 . The Landau expansion (60) is the same as that of the four-state Potts model (Z_4 Potts) [103]. It is well established that the upper critical dimension of this model is below three, $d_u < 3$ [104]. Consequently, a mean-field solution of Eq. (60) is appropriate, resulting in a first-order transition and in a fourfold degenerate ground-state manifold given by $\mathbf{d}_{0,i}^t = \text{sign}(-g) |\mathcal{V}_i^{Z_4}|$ with $i = 1, \dots, 4$ and

$$\mathcal{V}^{Z_4} = \frac{1}{\sqrt{3}} \left\{ \begin{pmatrix} 1 \\ 1 \\ 1 \end{pmatrix}, \begin{pmatrix} -1 \\ -1 \\ 1 \end{pmatrix}, \begin{pmatrix} 1 \\ -1 \\ -1 \end{pmatrix}, \begin{pmatrix} -1 \\ 1 \\ -1 \end{pmatrix} \right\}. \quad (61)$$

This fourfold degeneracy is associated with the four threefold symmetry axes \mathcal{V}^{111} defined in Eq. (35). Indeed, in the (nml) representation of Eq. (14), these four states are given by

$$g > 0: \quad \mathbf{d}_{0,i}^t = \mathbf{d}[|\mathbf{d}^t|, \alpha = \pi/3, \mathbf{n}_i, \mathbf{m}_i = \mathcal{V}_i^{111}, \mathbf{l}_i], \quad (62)$$

$$g < 0: \quad \mathbf{d}_{0,i}^t = \mathbf{d}[|\mathbf{d}^t|, \alpha = 0, \mathbf{n}_i = \mathcal{V}_i^{111}, \mathbf{m}_i, \mathbf{l}_i]. \quad (63)$$

Since $\alpha = \pi/3$ or $\alpha = 0$, the nematic states (62) and (63) are uniaxial [recall Eqs. (26) and (27)], and the nematic director is determined by either \mathbf{m} or \mathbf{n} , respectively. In Fig. 4(c), we show the distorted Fermi surface associated with the tensile (i.e., $\alpha = \pi/3$) nematic state, Eq. (62). Note that the nematic director \mathbf{m} points towards the corners of the cube that is concentric to the Fermi surface. Since there are eight such corners, the number of degenerate states is four, since $\pm \mathbf{m}$ correspond to the same state.

Next, we consider the nematic doublet order parameter \mathbf{d}^e (54), which transforms as the E_g IR of O_h . Following the same procedure as above, we first perform the decomposition of the symmetrized product for each Landau-expansion order:

$$[\otimes_{j=1}^2 E_g]_s = A_{1g} \oplus E_g, \quad (64)$$

$$[\otimes_{j=1}^3 E_g]_s = A_{1g} \oplus A_{2g} \oplus E_g, \quad (65)$$

$$[\otimes_{j=1}^4 E_g]_s = A_{1g} \oplus 2E_g, \quad (66)$$

which reveals the existence of one A_{1g} invariant per expansion order. The bilinear combinations in Eq. (64) can be readily obtained:

$$D^{A_{1g}} = |\mathbf{d}^e|^2, \quad \mathbf{D}^{E_g} = |\mathbf{d}^e|^2 \begin{pmatrix} \cos 2\gamma_e \\ -\sin 2\gamma_e \end{pmatrix}. \quad (67)$$

Using these bilinears, we can express the three invariants as $|\mathbf{d}^e|^2$, $|\mathbf{d}^e|^4$, and $\mathbf{d}^e \cdot \mathbf{D}^{E_g}$, such that the nematic Landau expansion becomes:

$$\mathcal{S} = \int_{\mathbf{x}} \{ r_0 |\mathbf{d}^e|^2 + g |\mathbf{d}^e|^3 \cos(3\gamma_e) + u |\mathbf{d}^e|^4 \}. \quad (68)$$

The nematic action (68) has the same Landau expansion as the three-state Potts model (Z_3 Potts) [104]. We note that the three-state Potts model is in the same universality class as the three-state clock model (Z_3 clock), so we use these terms interchangeably in the remainder of the paper. We discuss further the differences between Z_q Potts and Z_q clock models in Sec. IV. The key point is that the upper critical dimension of the Z_3 Potts (which is equivalent to the Z_3 clock) model is $d_u < 3$. Therefore, as in the case of the triplet nematic, a mean-field solution of Eq. (68) is appropriate. We find a threefold degenerate ground-state manifold given by $\mathbf{d}_{0,i}^e = \text{sign}(-g)|\mathbf{d}^e|V_i^{Z_3}$ with $i = 1, 2, 3$ and

$$V^{Z_3} = \left\{ \begin{pmatrix} 1 \\ 0 \end{pmatrix}, \frac{1}{2} \begin{pmatrix} -1 \\ \sqrt{3} \end{pmatrix}, \frac{1}{2} \begin{pmatrix} -1 \\ -\sqrt{3} \end{pmatrix} \right\}. \quad (69)$$

This threefold degeneracy is related to the three fourfold rotation axes V^{100} in Eq. (41), which are parallel to the three coordinate axes. This can be directly seen upon writing the nematic ground state in the (nml) representation (14):

$$g > 0: \quad \mathbf{d}_{0,i}^e = \mathbf{d}[|\mathbf{d}^e|, \alpha = \pi/3, \mathbf{n}_i, \mathbf{m}_i = V_i^{100}, I_i], \quad (70)$$

$$g < 0: \quad \mathbf{d}_{0,i}^e = \mathbf{d}[|\mathbf{d}^e|, \alpha = 0, \mathbf{n}_i = V_i^{100}, \mathbf{m}_i, I_i]. \quad (71)$$

As in the case of the T_{2g} (triplet) nematic, the E_g (doublet) nematic state is uniaxial with the nematic director \mathbf{m} or \mathbf{n} pointing along one of the three coordinate axes. This is illustrated in Fig. 4(d), where we plot the Fermi-surface distortion associated with the tensile (i.e. $\alpha = \pi/3$) state given by Eq. (70).

While the analysis performed above focused on the O_h group, the same general results hold for the doublet and triplet nematics of the other four cubic point groups, as shown in Table I. It is important to note, however, that the case of the nematic doublet order parameter \mathbf{d}^e in the tetrahedral point groups T_h and T needs to be treated slightly differently, because \mathbf{d}^e transforms according to a *complex* IR, which allows for additional invariants in the Landau expansion, which in turn make the nematic state biaxial rather than uniaxial. A detailed derivation of this case is presented in Appendix D.

IV. ELECTRONIC NEMATICITY IN CRYSTALLOGRAPHIC AXIAL POINT GROUPS

In contrast with the family of polyhedral point groups, which encompasses the seven point groups discussed in Sec. III, there is an infinite number of axial groups. Their defining property, as the name indicates, is their underlying cylindrical symmetry, which implies that the system is invariant under some n -fold proper or improper rotation with respect to the z axis. This symmetry can be accompanied by additional symmetries related to inversion or twofold rotations with respect to in-plane axes, resulting in a total of seven series of axial groups, as shown in Fig. 1. They can be constructed from two axial group series corresponding to the cyclic group C_n and the group S_{2n} :

$$C_n = \{E, C_{nz}, C_{nz}^2, \dots, C_{nz}^{n-1}\}, \quad n \in [2, 3, \dots, \infty], \quad (72)$$

$$S_{2n} = \{E, S_{2nz}, S_{2nz}^2, \dots, S_{2nz}^{2n-1}\}, \quad n \in [2, 3, \dots, \infty]. \quad (73)$$

Here, E is the identity operation, C_{nz} corresponds to an n -fold rotation with respect to the z axis, and the improper rotation (or rotoinversion) operation S_{nz} is defined as a proper rotation C_{nz} followed by a reflection with respect to the horizontal mirror, $S_{nz} = IC_{2z}C_{nz}$. Note that we can also extend these definitions to include the groups $C_1 = \{E\}$ and $S_2 = C_i = \{E, I\}$. The remaining five infinite series of axial groups are obtained from C_n or S_{2n} in the following way:

$$D_n = C_n \times \{E, C_{2x}\}, \quad (74)$$

$$C_{nv} = C_n \times \{E, IC_{2x}\}, \quad (75)$$

$$C_{nh} = C_n \times \{E, IC_{2z}\}, \quad (76)$$

$$D_{nd} = S_{2n} \times \{E, C_{2x}\}, \quad (77)$$

$$D_{nh} = C_n \times \{E, IC_{2z}\} \times \{E, C_{2x}\}, \quad (78)$$

where I denotes inversion and C_{2x} , twofold rotation with respect to the in-plane x axis. Note that the compositions IC_{2z} and IC_{2x} correspond to reflections with respect to the horizontal and vertical mirrors (denoted σ_h and σ_v), whereas $IC_{2y}C_{4z} = S_{4z}C_{2x}$ corresponds to a reflection with respect to the diagonal mirror (denoted σ_d).

Upon imposing the crystallographic restriction theorem, one finds 27 crystallographic axial point groups corresponding to the following six crystal systems: hexagonal, trigonal, tetragonal, orthorhombic, monoclinic, and triclinic. Together with the five crystallographic polyhedral point groups discussed in Sec. III that form the cubic crystal system, one finds 32 crystallographic point groups. While this section focuses on the 27 crystallographic axial groups, we discuss noncrystallographic axial point groups that are relevant to quasicrystalline materials [86,88,89,91,105] (octagonal, decagonal, and dodecagonal) and to twisted quasicrystals [93–95,106] in Sec. V.

A. Two-dimensional isotropic systems

To set the stage for the analysis of electronic nematicity in axial groups, it is instructive to analyze the case in which the system has full in-plane rotational symmetry. To describe such a system, one possibility would be to consider the continuous $SO(2)$ group, which describes 2D rotations and is equivalent to C_∞ defined in Eq. (72). However, for our purposes, it is more convenient to consider the continuous dihedral group $D_{\infty h}$, since all other axial groups are subgroups of $D_{\infty h}$. Formally, the elements of this group include continuous proper and improper 2D rotations as well as a horizontal mirror, i.e., $D_{\infty h} = SO(2) \times \{E, I\} \times \{E, C_{2x}\}$. Hereafter, we simply refer to such a system as a 2D isotropic system.

In the 2D isotropic case, the five-dimensional nematic order parameter \mathbf{d} (7) decomposes into three separate channels,

$$\mathbf{d} \xrightarrow{\text{in-plane isotropic}} (\underline{d}_1, \mathbf{d}^{\text{ip}}, \mathbf{d}^{\text{op}})^T. \quad (79)$$

The first component $d_1 = d \frac{1}{\sqrt{3}}(2z^2 - x^2 - y^2)$ transforms as the trivial IR A_{1g} of $D_{\infty h}$, which we indicate by the underline in the expression above. The other components \mathbf{d}^{ip} and \mathbf{d}^{op} are two-component ‘‘vectors’’ (i.e., doublets) that transform as different two-dimensional IRs of $D_{\infty h}$, E_{2g} , and E_{1g} , respectively.

They are given by

$$\mathbf{d}^{\text{ip}} = \begin{pmatrix} d_2 \\ d_5 \end{pmatrix} = \begin{pmatrix} d_{x^2-y^2} \\ d_{2xy} \end{pmatrix} = |\mathbf{d}^{\text{ip}}| \begin{pmatrix} \cos \gamma_{\text{ip}} \\ \sin \gamma_{\text{ip}} \end{pmatrix}, \quad (80)$$

$$\mathbf{d}^{\text{op}} = \begin{pmatrix} d_3 \\ d_4 \end{pmatrix} = \begin{pmatrix} d_{2yz} \\ d_{2xz} \end{pmatrix} = |\mathbf{d}^{\text{op}}| \begin{pmatrix} \cos \gamma_{\text{op}} \\ \sin \gamma_{\text{op}} \end{pmatrix}, \quad (81)$$

where we introduced a polar parametrization in terms of the angles γ_{ip} and γ_{op} . The superscripts ip and op are used to indicate that the condensation of the order parameter promotes an in-plane or out-of-plane distortion of the Fermi surface, respectively. Importantly, as explained in Sec. II, we are using the transformation rule in Eq. (10) to define the nematic order parameter for all point groups, which results in the definitions (80), (81). In the literature, one often uses a point-group-specific basis to define the nematic order parameter, resulting in definitions such as $\tilde{\mathbf{d}}^{\text{ip}} = (d_{x^2-y^2}, -d_{2xy})^T$ and $\tilde{\mathbf{d}}^{\text{op}} = (d_{2yz}, -d_{2xz})^T$ [107]. Further implications arising from different definitions are discussed in Sec. VI. Of course, the final results do not depend on the basis used to express the nematic order parameter.

We emphasize that, because the nematic component d_1 transforms trivially in $D_{\infty h}$, it will do so for all axial groups. Therefore, $d_{\frac{1}{\sqrt{3}}(2z^2-x^2-y^2)}$ should not be interpreted as a nematic order parameter, since it is generically nonzero for any temperature or tuning parameter. Physically, from Eq. (32), $d_1 \neq 0$ corresponds to a distortion of the isotropic Fermi surface along the k_z axis, lowering its symmetry from spherical to cylindrical—as expected for an axial group. As we argue below, while d_1 does not impact the critical properties of the nematic instability, it needs to be included if one chooses to express the nematic order parameter \mathbf{d} in the (nml) representation of Eq. (14).

We now proceed to derive the Landau expansions for \mathbf{d}^{ip} and \mathbf{d}^{op} . Since they transform according to the IRs E_{2g} and E_{1g} of the infinite dihedral group $D_{\infty h}$, respectively, the number of invariants for each expansion order can be read off from the symmetrized-product decomposition:

$$[\otimes_{j=1}^{2N} E_{2g}]_s = A_{1g} \oplus_{n=1}^N E_{(4n)g}, \quad (82)$$

$$[\otimes_{j=1}^{2N-1} E_{2g}]_s = \oplus_{n=1}^N E_{(4n-2)g}, \quad (83)$$

$$[\otimes_{j=1}^{2N} E_{1g}]_s = A_{1g} \oplus_{n=1}^N E_{(2n)g}, \quad (84)$$

$$[\otimes_{j=1}^{2N-1} E_{1g}]_s = \oplus_{n=1}^N E_{(2n-1)g}, \quad (85)$$

with $N = 1, 2, 3$ and where we used a tensor summation notation, e.g., $\oplus_{n=1}^2 E_{(4n)g} = E_{4g} \oplus E_{8g}$. The decompositions (82)–(85) are carried out up to sixth order in order to emphasize that no A_{1g} invariants occur other than $|\mathbf{d}^{\text{ip}}|^{2N}$ and $|\mathbf{d}^{\text{op}}|^{2N}$, i.e., the invariants only occur at even order. Consequently, the Landau expansions for the in-plane and out-of-plane nematic order parameters become

$$\begin{aligned} \mathcal{S}_{\text{ip}} &= \int_{\mathbf{x}} \{r_0 |\mathbf{d}^{\text{ip}}|^2 + u |\mathbf{d}^{\text{ip}}|^4\}, \\ \mathcal{S}_{\text{op}} &= \int_{\mathbf{x}} \{\tilde{r}_0 |\mathbf{d}^{\text{op}}|^2 + \tilde{u} |\mathbf{d}^{\text{op}}|^4\}. \end{aligned} \quad (86)$$

Therefore, since \mathbf{d}^{ip} and \mathbf{d}^{op} are two-component order parameters, their actions have the same Landau expansion as the well-known XY model. Their condensation leads to a continuous symmetry breaking, since the nematic angles $\gamma_{\text{ip}}, \gamma_{\text{op}} \in [0, 2\pi]$ are not constrained by symmetry and can point in any direction.

It is illustrative to rewrite the fully isotropic nematic order parameters (80) and (81) in the (nml) representation of Eq. (14). For the description of the in-plane nematic order parameter \mathbf{d}^{ip} , it is convenient to introduce the three orthonormal vectors in cylindrical coordinates

$$\mathbf{e}_{\parallel}^A = \begin{pmatrix} \cos(\gamma_{\text{ip}}/2) \\ \sin(\gamma_{\text{ip}}/2) \\ 0 \end{pmatrix}, \quad \mathbf{e}_{\parallel}^B = \begin{pmatrix} -\sin(\gamma_{\text{ip}}/2) \\ \cos(\gamma_{\text{ip}}/2) \\ 0 \end{pmatrix}, \quad \mathbf{e}_z = \begin{pmatrix} 0 \\ 0 \\ 1 \end{pmatrix}. \quad (87)$$

The magnitude of the nematic order parameter is given by $|\mathbf{d}| = [|\mathbf{d}^{\text{ip}}|^2 + (d_1)^2]^{1/2}$, where d_1 , as explained above, is always nonzero, and can thus be considered as an intrinsic parameter characterizing the 2D isotropic system even in the absence of symmetry-breaking nematic order. Depending on the value of the ratio $-1 < d_1/|\mathbf{d}| < 1$, we find three different regimes of parameters that characterize \mathbf{d} in the (nml) representation:

$$\begin{aligned} \frac{|d_1|}{|\mathbf{d}|} \leq \frac{1}{2}: \quad & \alpha = \frac{\pi}{6} + \arcsin\left(\frac{d_1}{|\mathbf{d}|}\right), \\ & \mathbf{n} = \mathbf{e}_{\parallel}^A, \quad \mathbf{m} = \mathbf{e}_{\parallel}^B, \quad \mathbf{l} = \mathbf{e}_z, \\ \frac{|d_1|}{|\mathbf{d}|} < \frac{-1}{2}: \quad & \alpha = \arcsin\left(\frac{|d_1|}{|\mathbf{d}|}\right) - \frac{\pi}{6}, \\ & \mathbf{n} = \mathbf{e}_{\parallel}^A, \quad \mathbf{m} = \mathbf{e}_z, \quad \mathbf{l} = \mathbf{e}_{\parallel}^B, \\ \frac{|d_1|}{|\mathbf{d}|} > \frac{1}{2}: \quad & \alpha = \frac{\pi}{2} - \arcsin\left(\frac{|d_1|}{|\mathbf{d}|}\right), \\ & \mathbf{n} = \mathbf{e}_z, \quad \mathbf{m} = \mathbf{e}_{\parallel}^B, \quad \mathbf{l} = \mathbf{e}_{\parallel}^A. \end{aligned} \quad (88)$$

As for the out-of-plane nematic order parameter, we have $|\mathbf{d}| = [|\mathbf{d}^{\text{op}}|^2 + (d_1)^2]^{1/2}$ and

$$\begin{aligned} \alpha &= \frac{\pi}{6} - \arcsin[d_1/(2|\mathbf{d}|)], \\ \mathbf{n} &= \begin{pmatrix} \sin \gamma_{\text{op}} \cos \eta_{\text{op}} \\ \cos \gamma_{\text{op}} \cos \eta_{\text{op}} \\ \sin \eta_{\text{op}} \end{pmatrix}, \quad \mathbf{m} = \begin{pmatrix} \sin \gamma_{\text{op}} \sin \eta_{\text{op}} \\ \cos \gamma_{\text{op}} \sin \eta_{\text{op}} \\ -\cos \eta_{\text{op}} \end{pmatrix}, \\ \mathbf{l} &= \begin{pmatrix} \cos \gamma_{\text{op}} \\ -\sin \gamma_{\text{op}} \\ 0 \end{pmatrix}, \end{aligned} \quad (89)$$

where we defined the polar angle:

$$\begin{aligned} \eta_{\text{op}} &= -\frac{1}{2} \text{sign}(d_1) \arcsin\left(|\mathbf{d}^{\text{op}}| / \sqrt{|\mathbf{d}^{\text{op}}|^2 + \frac{3}{4}(d_1)^2}\right) \\ &\quad + \frac{\pi}{2} \frac{1 + \text{sign}(d_1)}{2}. \end{aligned} \quad (90)$$

Both the in-plane (88) and the out-of-plane (89) nematic states are generically biaxial, since $\alpha \neq 0, \pi/3$. Note that, if the contribution from the trivial nematic component is negligible,

$|d_1| \ll |\mathbf{d}^{\text{ip}}|, |\mathbf{d}^{\text{op}}|$, both states are “maximally” biaxial with $\alpha = \pi/6$ [cf. Fig. 2(a)]. In this regard, a nonzero d_1 brings the states (88) and (89) closer to the uniaxial regime. Indeed, in the limit $|d_1| \gg |\mathbf{d}^{\text{ip}}|, |\mathbf{d}^{\text{op}}|$, $\alpha \rightarrow 0, \pi/3$ in both cases, with the nematic director \mathbf{n} or \mathbf{m} pointing along the k_z axis. Interestingly, the nematic in-plane order parameter (88) also establishes a uniaxial state when $|d_1| = |\mathbf{d}^{\text{ip}}|/\sqrt{3}$, corresponding to $|d_1|/|\mathbf{d}| = 1/2$. In this fine-tuned parameter regime, there is a swap between the nematic axes that point along the k_z axis, since for $|d_1| > |\mathbf{d}^{\text{ip}}|/\sqrt{3}$ either the long or the short nematic axis (\mathbf{m} or \mathbf{n}) points out of plane, while for $|d_1| < |\mathbf{d}^{\text{ip}}|/\sqrt{3}$ the long and short nematic axes both lie within the plane. Since \mathbf{d}^{ip} and \mathbf{d}^{op} also emerge in the description of hexagonal and tetragonal lattices, we defer plotting the Fermi-surface distortion patterns triggered by the condensation of these nematic order parameters to the subsequent sections.

An alternative representation of the 2D isotropic in-plane nematic order parameter \mathbf{d}^{ip} has also been widely employed in the literature [37,48–51,61–63], building on the analogy with the classical *two-dimensional* tensorial nematic order parameter $Q_{\mu\mu'} = \langle a_\mu a_{\mu'} - \frac{1}{2} \delta_{\mu\mu'} \mathbf{a}^2 \rangle$, with director $\mathbf{a} = (a_x, a_y)$. In terms of the quadrupolar order parameters, the electronic nematic order parameter is given by

$$Q = \begin{pmatrix} d_{x^2-y^2} & d_{2xy} \\ d_{2xy} & -d_{x^2-y^2} \end{pmatrix} = \mathbf{d}^{\text{ip}} \cdot \boldsymbol{\tau}^{\text{ip}}, \quad (91)$$

where $\boldsymbol{\tau}^{\text{ip}} = (\tau^3, \tau^1)$ with Pauli matrices τ^i . This form establishes a straightforward connection between the two-component “vector” $\mathbf{d}^{\text{ip}} = (d_2, d_5)^T = (d_{x^2-y^2}, d_{2xy})^T$ and Q similar to the 3D case in Eq. (8), with the symmetric Pauli matrices replacing the symmetric Gell-Mann matrices. To preserve rotational invariance, the Landau expansion can only depend on traces of powers of Q :

$$\mathcal{S}_{\text{ip}} = \int_{\mathbf{x}} \sum_n \frac{\kappa_n}{2} \text{tr}(Q^n), \quad (92)$$

where κ_n are Landau coefficients. Using the facts that $(\mathbf{d}^{\text{ip}} \cdot \boldsymbol{\tau}^{\text{ip}})^{2n} = |\mathbf{d}^{\text{ip}}|^{2n} \tau^0$, and thus $\text{tr}[(\mathbf{d}^{\text{ip}} \cdot \boldsymbol{\tau}^{\text{ip}})^{2n+1}] = |\mathbf{d}^{\text{ip}}|^{2n} \text{tr}[\mathbf{d}^{\text{ip}} \cdot \boldsymbol{\tau}^{\text{ip}}] = 0$, we find

$$\mathcal{S}_{\text{ip}} = \int_{\mathbf{x}} \sum_n \kappa_{2n} |\mathbf{d}^{\text{ip}}|^{2n} = \int_{\mathbf{x}} \{r_0 |\mathbf{d}^{\text{ip}}|^2 + u |\mathbf{d}^{\text{ip}}|^4 + \mathcal{O}(|\mathbf{d}^{\text{ip}}|^6)\}, \quad (93)$$

which is identical to Eq. (86). When comparing with the Landau expansion of the 3D isotropic case, Eq. (21), the main difference is the absence of the cubic term. Ultimately, this can be traced back to the fundamental differences in the SU(2) and SU(3) Lie algebras, reflected in the fact that different Pauli matrices necessarily anticommute whereas different Gell-Mann matrices do not necessarily anticommute.

As discussed above in the context of Eq. (86), electronic nematicity in the 2D isotropic system (either in plane or out of plane) belongs to the XY universality class, implying the existence of a Goldstone mode in the nematically ordered state. As discussed in Refs. [48,108], the coupling between this Goldstone mode and low-energy electronic degrees of freedom can promote interesting phenomena, such as non-Fermi-liquid behavior. As we see below, the main effect of the explicit breaking of the full rotational symmetry in a lattice

described by an axial point group is the emergence of an anisotropic term in the Landau expansion:

$$\mathcal{S}_{\text{axial}} = \int_{\mathbf{x}} \{r_0 |\mathbf{d}^\alpha|^2 + u |\mathbf{d}^\alpha|^4 + h_q |\mathbf{d}^\alpha|^q \cos(q\gamma_\alpha)\}, \quad (94)$$

where q is a positive integer that is the same within the same crystal system (hexagonal, trigonal, tetragonal, orthorhombic, monoclinic, and triclinic), α can refer to ip or op, and h_q is a Landau coefficient. For the (crystallographic and non-crystallographic) axial groups that we investigated here, we found the following general result: if the group has $(2n)$ -fold symmetry, then $q = n$ for $\alpha = \text{ip}$ and $q = 2n$ for $\alpha = \text{op}$. On the other hand, if the axial group has $(2n+1)$ -fold symmetry, $q = 2n+1$ for both $\alpha = \text{ip}$ and $\alpha = \text{op}$.

We note that Eq. (94) corresponds to the Landau expansion of the q state “soft” clock model (Z_q clock), whose classical critical properties are well understood [109]. In three dimensions (and nonzero temperatures), which is the case of most relevance here, the character of the transition is (of course, $q=1$ implies explicitly broken symmetry): 3D-Ising for $q=2$, first-order for $q=3$, and 3D XY for $q \geq 4$. The latter result is a consequence of the fact that h_q is a dangerously irrelevant perturbation (in the renormalization-group sense) for $q \geq 4$, i.e., it is irrelevant at the nematic critical point but relevant inside the nematically ordered state [110–112]. Thus, even though the transition is XY-like, the ordered state does not display a Goldstone mode, but a gapped pseudo-Goldstone mode.

It is important to point out that crystals described by an axial point group can be very anisotropic and display behavior intermediate between 2D and 3D. Moreover, as we discuss in Sec. VD, twisted quasicrystals are 2D systems. In this regard, it is interesting to note that the Z_q clock model has rather unique properties in 2D [109]. While the $q=2$ model undergoes a standard 2D-Ising transition, the $q=3$ model undergoes a second-order transition despite the existence of a cubic term in the Landau expansion. More surprisingly, for $q \geq 5$, the 2D Z_q clock model undergoes two Berezinskii-Kosterlitz-Thouless (BKT) transitions: a higher-temperature BKT transition towards a critical phase with quasi-long-range order, analogous to that displayed by the XY model at nonzero temperatures, and a lower-temperature BKT transition towards a state with long-range order where the discrete clock symmetry is broken. Interestingly, for $q=4$, these two BKT transitions merge into a single line. As a result, the critical behavior of the 2D Z_4 clock model, which maps onto the 2D Ashkin-Teller model, is only weakly universal [113], since while the anomalous critical exponent is fixed to $\eta = 1/4$, the other exponents depend on the value of h_4 [114]. The crossover from 2D to 3D Z_q clock behavior has been recently discussed numerically in Ref. [112] and also indirectly in the context of quantum critical points in 2D Z_q clock systems [57–59,115,116]. Finally, we emphasize that the critical properties of the Z_q clock model are generically different from those of the Z_q Potts model, except for the special case $q=3$, where they share the same universality class [104]. For this reason, as explained in the previous section, we use the terms Z_3 clock and Z_3 Potts interchangeably.

Finally, we show in Appendixes E–G that, in the cases where the nematic order parameter transforms as a complex

IR, which reflects the lack of twofold in-plane rotation axes in the crystal, the clock term in the action (94) acquires an offset angle, which can be traced back to the existence of another anisotropic term in the Landau expansion, $\tilde{h}_q |\mathbf{d}^\alpha|^q \sin(q\gamma_\alpha)$ (see also Ref. [102]):

$$\mathcal{S}_{\text{axial}} = \int_{\mathbf{x}} \{r_0 |\mathbf{d}^\alpha|^2 + u |\mathbf{d}^\alpha|^4 + h_q |\mathbf{d}^\alpha|^q \cos(q\gamma_\alpha - \delta_0)\}. \quad (95)$$

To distinguish it from Eq. (95), we denote the Landau expansion above a Z_q^* clock model. An offset angle is also found when the two nematic doublets are “degenerate,” i.e., transform as the same IR, as is the case in trigonal point groups.

B. Hexagonal crystals

Candidate nematic systems with underlying hexagonal symmetry include $\text{Fe}_{1/3}\text{NbS}_2$ [27], the kagome metal CoSn [25], twisted bilayer graphene [17,18], and hexagonal sp^2 optical lattices [33]. The hexagonal crystal system consists of seven crystallographic axial point groups: D_{6h} , D_6 , D_{3h} , C_{6v} , C_{6h} , C_{3h} , and C_6 . In all cases, the nematic order parameter \mathbf{d} in Eq. (7) decomposes into the three channels in the same way as in the 2D isotropic case,

$$\mathbf{d} \xrightarrow{\text{hexagonal}} (\underline{d}_1, \mathbf{d}^{\text{ip}}, \mathbf{d}^{\text{op}})^T. \quad (96)$$

We recall that an underline means that the corresponding nematic component transforms as the trivial IR of the point group. The most notable difference with respect to the isotropic case is, of course, the limited number of C_{nz} or IC_{nz} symmetry elements, which reduces the continuous XY degeneracy of the nematic angles γ_{ip} and γ_{op} down to either threefold or sixfold degeneracies, as we demonstrate below. Within the hexagonal crystal system, one needs to distinguish between the sets of point groups $\{D_{6h}, D_6, D_{3h}, C_{6v}\}$ and $\{C_{6h}, C_{3h}, C_6\}$, since only the former possess the characteristic six in-plane symmetry axes

$$\begin{aligned} \mathcal{V}_1^{\text{hex}} &= \left\{ \begin{pmatrix} 1 \\ 0 \\ 0 \end{pmatrix}, \begin{pmatrix} -\frac{1}{2} \\ \frac{\sqrt{3}}{2} \\ 0 \end{pmatrix}, \begin{pmatrix} -\frac{1}{2} \\ -\frac{\sqrt{3}}{2} \\ 0 \end{pmatrix} \right\}, \\ \mathcal{V}_2^{\text{hex}} &= \left\{ \begin{pmatrix} 0 \\ 1 \\ 0 \end{pmatrix}, \begin{pmatrix} -\frac{\sqrt{3}}{2} \\ -\frac{1}{2} \\ 0 \end{pmatrix}, \begin{pmatrix} \frac{\sqrt{3}}{2} \\ -\frac{1}{2} \\ 0 \end{pmatrix} \right\}, \end{aligned} \quad (97)$$

see Eqs. (72) and (76). Mathematically, the absence of in-plane symmetry axes is manifested in the nematic doublets \mathbf{d}^{ip} and \mathbf{d}^{op} transforming according to complex IRs, which causes additional Landau invariants to emerge when compared with the generic Z_q clock Landau expansion of Eq. (94). As we show in detail in Appendix E, this additional Landau invariant for the groups $\{C_{6h}, C_{3h}, C_6\}$ can be recast as an offset angle in the clock term, see Eq. (95). In this section, we focus instead on the first set of groups, $\{D_{6h}, D_6, D_{3h}, C_{6v}\}$, for which the nematic doublets \mathbf{d}^{ip} and \mathbf{d}^{op} transform as real two-dimensional IRs. For concreteness, we show the derivation for the point group D_{6h} , where \mathbf{d}^{ip} and \mathbf{d}^{op} transform according to the IRs E_{2g} and E_{1g} , respectively. The results equally apply to the other groups of the set, $\{D_6, D_{3h}, C_{6v}\}$.

Consider first the in-plane nematic order parameter $\mathbf{d}^{\text{ip}} = (d_2, d_5)^T = (d_{x^2-y^2}, d_{2xy})^T$. The symmetrized product decomposition for each expansion order is given by

$$[\otimes_{j=1}^2 E_{2g}]_s = A_{1g} \oplus E_{2g}, \quad (98)$$

$$[\otimes_{j=1}^3 E_{2g}]_s = A_{1g} \oplus A_{2g} \oplus E_{2g}, \quad (99)$$

$$[\otimes_{j=1}^4 E_{2g}]_s = A_{1g} \oplus 2E_{2g}. \quad (100)$$

To construct the three A_{1g} Landau invariants, we derive the bilinear combinations associated with Eq. (98):

$$D_{\text{ip}}^{A_{1g}} = |\mathbf{d}^{\text{ip}}|^2, \quad \mathbf{D}_{\text{ip}}^{E_{2g}} = |\mathbf{d}^{\text{ip}}|^2 (\cos(2\gamma_{\text{ip}}), -\sin(2\gamma_{\text{ip}}))^T. \quad (101)$$

Then, the three invariants become $|\mathbf{d}^{\text{ip}}|^2$, $|\mathbf{d}^{\text{ip}}|^4$, and $\mathbf{d}^{\text{ip}} \cdot \mathbf{D}_{\text{ip}}^{E_{2g}}$, since both \mathbf{d}^{ip} and $\mathbf{D}_{\text{ip}}^{E_{2g}}$ transform as E_{2g} . The corresponding Landau expansion,

$$\mathcal{S}_{\text{ip}} = \int_{\mathbf{x}} \{r_0 |\mathbf{d}^{\text{ip}}|^2 + g_{\text{ip}} |\mathbf{d}^{\text{ip}}|^3 \cos(3\gamma_{\text{ip}}) + u |\mathbf{d}^{\text{ip}}|^4\}, \quad (102)$$

has the same form as that of the Z_3 clock model, Eq. (94), as derived elsewhere [41,57,74,79]. Correspondingly, the threefold-degenerate mean-field ground state is given by

$$\gamma_{\text{ip}}^0 = \frac{\pi}{3} \left(\frac{1 + \text{sign } g_{\text{ip}}}{2} \right) + \frac{2\pi}{3} n, \quad n = \{0, 1, 2\}. \quad (103)$$

In the (nml) representation (14), this ground state is parametrized according to Eq. (88); recall that d_1 is the symmetry-conforming nematic component, which is nonzero at any temperature or tuning parameter range. We plot the corresponding Fermi-surface distortion in Fig. 5(a) by using the general expression (32). In this figure, we chose $g_{\text{ip}} < 0$ and three values of the trivial component $d_1/|\mathbf{d}| = \{0.1, 0.5, 0.9\}$. In the top panel where $|d_1| < |\mathbf{d}^{\text{ip}}|/\sqrt{3}$, the short and long nematic axes \mathbf{n} and \mathbf{m} align, respectively, with the in-plane symmetry axes $\mathcal{V}_1^{\text{hex}}$ and $\mathcal{V}_2^{\text{hex}}$ of Eq. (97), highlighted in purple and light-blue in the figure. The three degenerate states correspond to \mathbf{m} being aligned with one of the three light-blue axes, corresponding to $\mathcal{V}_2^{\text{hex}}$ in Eq. (97). For the opposite sign $g_{\text{ip}} > 0$, the long nematic axis \mathbf{m} aligns with the purple axes, which correspond to $\mathcal{V}_1^{\text{hex}}$ in Eq. (97). The biaxial nature of the nematic order parameter is clear from the shape of the distorted Fermi surface. To see this in a transparent way, we rescaled the vectors in the figure by $2.5 k_F (\|\mathbf{n}, \mathbf{m}, \mathbf{l}\|)$ such that their length reflects the extension of the Fermi surface along the respective direction. A uniaxial nematic requires two of the vectors to have the same length, which is generally not the case here. Upon increasing $|d_1|/|\mathbf{d}|$, we demonstrate in the second panel of Fig. 5(a) how the nematic state passes through a fine-tuned uniaxial point at $|d_1| = |\mathbf{d}|/2$, according to Eq. (88). In the parameter range $|d_1| > |\mathbf{d}|/2$ [third panel of Fig. 5(a)], two nematic axes are interchanged, and the nematic state becomes gradually more in-plane isotropic.

We now discuss the case of the out-of-plane nematic doublet $\mathbf{d}^{\text{op}} = (d_3, d_4)^T = (d_{2yz}, d_{2xz})^T$, which transforms as the E_{1g} IR of D_{6h} . The decomposition of the symmetrized product

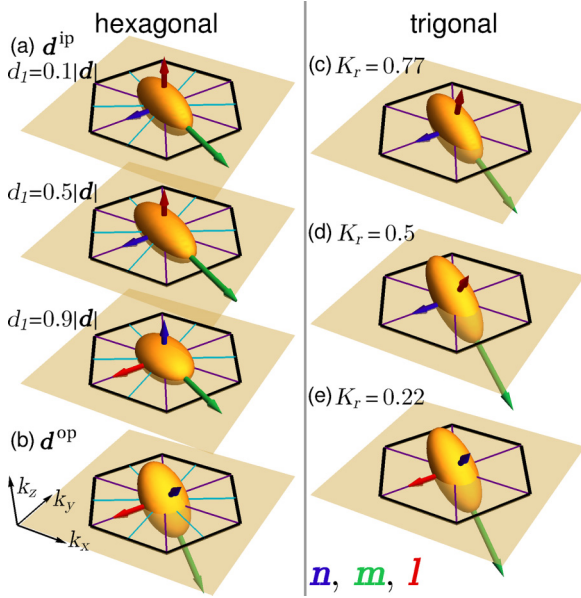


FIG. 5. Distorted Fermi surface in the nematic phase, as given by Eq. (32), plotted together with the nematic axes \mathbf{n} , \mathbf{m} , \mathbf{l} for the cases of (a) hexagonal in-plane doublet state (103) for three values of $d_1/|d|$, and (b) out-of-plane doublet state (111). (c)–(e) trigonal nematic state (139) for three values of K_r (135). The unit vectors $\{\mathbf{n}, \mathbf{m}, \mathbf{l}\}$ are rescaled by $2.5 k_F \langle \mathbf{n}, \mathbf{m}, \mathbf{l} \rangle$, respectively. Unless specified otherwise, we chose $d_1/|d| = 0.1$.

gives

$$\left[\otimes_{j=1}^2 E_{1g} \right]_s = A_{1g} \oplus E_{2g}, \quad (104)$$

$$\left[\otimes_{j=1}^3 E_{1g} \right]_s = B_{1g} \oplus B_{2g} \oplus E_{1g}, \quad (105)$$

$$\left[\otimes_{j=1}^4 E_{1g} \right]_s = A_{1g} \oplus 2E_{2g}, \quad (106)$$

$$\left[\otimes_{j=1}^5 E_{1g} \right]_s = B_{1g} \oplus B_{2g} \oplus 2E_{1g}, \quad (107)$$

$$\left[\otimes_{j=1}^6 E_{1g} \right]_s = 2A_{1g} \oplus A_{2g} \oplus 2E_{2g}. \quad (108)$$

Here, we extended the expansion to sixth-order to include the leading anisotropic invariant, i.e., the leading-order invariant that depends on the angle γ_{op} . Using the bilinears associated with Eq. (104),

$$D_{op}^{A_{1g}} = |\mathbf{d}^{op}|^2, \quad D_{op}^{E_{2g}} = |\mathbf{d}^{op}|^2 (\cos(2\gamma_{op}), -\sin(2\gamma_{op}))^T, \quad (109)$$

the four invariants can be constructed as $|\mathbf{d}^{op}|^2$, $|\mathbf{d}^{op}|^4$, $|\mathbf{d}^{op}|^6$, $(\mathbf{d}^{op} \cdot \mathbf{D}_{op}^{E_{2g}})^2$, where we used the fact that $\mathbf{d}^{op} \cdot \mathbf{D}_{op}^{E_{2g}}$ transforms as B_{1g} . The resulting nematic Landau expansion can be written as

$$\mathcal{S}_{op} = \int_{\mathbf{x}} \left\{ r_0 |\mathbf{d}^{op}|^2 + u |\mathbf{d}^{op}|^4 + u_6 |\mathbf{d}^{op}|^6 + v_6 |\mathbf{d}^{op}|^6 \cos(6\gamma_{op}) \right\} \quad (110)$$

and corresponds to the Z_6 clock model of Eq. (94). Thus, we find an important difference between the in-plane \mathbf{d}^{ip} and out-of-plane \mathbf{d}^{op} nematic order parameters in the hexagonal lattice: whereas the former undergoes a first-order transition,

the latter is expected to undergo a continuous 3D XY transition, at which the discrete nature of the nematic angle is irrelevant (in the renormalization-group sense).

The mean-field ground state of \mathbf{d}^{op} is therefore sixfold degenerate and characterized by the nematic angles

$$\gamma_{op}^0 = \frac{\pi}{6} \left(\frac{1 + \text{sign } v_6}{2} \right) + \frac{2\pi}{6} n, \quad n \in \{0, 1, \dots, 5\}. \quad (111)$$

The distorted Fermi surface associated with this ground state is shown in Fig. 5(b). In terms of the (nml) representation derived in Eq. (89), we see that, regardless of the value of the trivial nematic component d_1 , the nematic axis \mathbf{l} is always in-plane and aligned with either $\mathcal{V}_1^{\text{hex}}$ (purple) or $\mathcal{V}_2^{\text{hex}}$ (light-blue) defined in Eq. (97), depending on the sign of the Landau coefficient v_6 . The long (\mathbf{m}) and short (\mathbf{n}) nematic axes are rotated out of the plane by the tilt angle η_{op} (90), which is exactly $\pm 45^\circ$ in the limiting case $d_1 = 0$. To visualize the sixfold degeneracy of this state, it is useful to invoke the symmetry elements C_{2z} or IC_{2z} , one of which is present in every hexagonal point group. They imply the existence of a nonidentical ground-state configuration that emerges from Fig. 5(b) through a 180° rotation about the k_z axis. The key point is that, under such a rotation, $\mathbf{l} \rightarrow -\mathbf{l}$ but \mathbf{m}, \mathbf{n} are not mapped onto $-\mathbf{m}, -\mathbf{n}$. This implies that, for each of the three choices for the \mathbf{l} axis in $\mathcal{V}_1^{\text{hex}}$ or $\mathcal{V}_2^{\text{hex}}$, there are two different sets of possible \mathbf{m}, \mathbf{n} values, resulting in a sixfold degeneracy. In contrast, such a sixfold degeneracy is absent for the in-plane state \mathbf{d}^{ip} of Fig. 5(a), since \mathbf{l} remains invariant and \mathbf{m}, \mathbf{n} are mapped onto $-\mathbf{m}, -\mathbf{n}$ under a C_{2z} or IC_{2z} operation.

As we mentioned earlier, the same results derived here for D_{6h} hold for $\{D_6, D_{3h}, C_{6v}\}$ and $\{C_{6h}, C_{3h}, C_6\}$, as shown in Table I. The main difference in the latter set is that an offset angle appears in the anisotropic terms of Eqs. (102) and (110), see Appendix E, which we indicate as Z_3^* clock and Z_6^* clock models in Table I.

C. Trigonal crystals

Nematic candidate materials with an underlying trigonal structure include doped Bi_2Se_3 [15,16], van der Waals antiferromagnets FePS_3 [28,30] and NiPS_3 [29,31], as well as twisted double-bilayer graphene [19]. The axial point groups D_3, D_{3d}, C_{3v}, S_6 and C_3 form the trigonal crystal system. In what concerns nematicity, its key distinction with respect to the hexagonal crystal system, Eq. (96), is that the two nematic doublets, in-plane $\mathbf{d}^{ip} = (d_2, d_5)^T = (d_{x^2-y^2}, d_{2xy})^T$ and out of plane $\mathbf{d}^{op} = (d_3, d_4)^T = (d_{2yz}, d_{2xz})^T$, transform as the same two-dimensional IR. We thus represent the decomposition of the five-component nematic order parameter \mathbf{d} (7) as

$$\mathbf{d} \xrightarrow{\text{trigonal}} (\underline{d}_1, \{\mathbf{d}^{ip}, \mathbf{d}^{op}\})^T, \quad (112)$$

where the curly brackets are used to indicate degeneracy, i.e., nematic components that transform as the same IR. Analogously to the hexagonal case, we must also distinguish the trigonal group sets $\{D_3, D_{3d}, C_{3v}\}$ and $\{S_6, C_3\}$, as the latter lacks the in-plane symmetry directions encompassed by $\mathcal{V}_1^{\text{hex}}, \mathcal{V}_2^{\text{hex}}$ in Eq. (97). This case, for which \mathbf{d}^{ip} and \mathbf{d}^{op} transform as a complex IR, is discussed in Appendix F. Here, as a representative of the group set $\{D_3, D_{3d}, C_{3v}\}$, we focus our analysis

on the point group C_{3v} , for which \mathbf{d}^{ip} and \mathbf{d}^{op} transform as the IR E . Repeating the same steps as in the other sections, we perform the symmetrized product decomposition:

$$[\otimes_{j=1}^2 E]_s = A_1 \oplus E, \quad [\otimes_{j=1}^3 E]_s = A_1 \oplus A_2 \oplus E, \quad (113)$$

$$[\otimes_{j=1}^4 E]_s = A_1 \oplus 2E. \quad (114)$$

Clearly, this decomposition is analogous to that of the E_{2g} IR in the hexagonal case, see Eqs. (98)–(102). This suggests that, individually, each doublet \mathbf{d}^{ip} and \mathbf{d}^{op} would behave as a Z_3 clock order parameter. Here, however, we must focus on the combined four-component vector $\mathbf{d}^E = (\mathbf{d}^{\text{ip}}, \mathbf{d}^{\text{op}})$, which transforms as $(E \oplus E)$. Its symmetrized decomposition, in turn, gives 13 invariants up to fourth-order in the Landau expansion:

$$[\otimes_{j=1}^2 (E \oplus E)]_s = 3A_1 \oplus A_2 \oplus 3E, \quad (115)$$

$$[\otimes_{j=1}^3 (E \oplus E)]_s = 4A_1 \oplus 4A_2 \oplus 6E, \quad (116)$$

$$[\otimes_{j=1}^4 (E \oplus E)]_s = 6A_1 \oplus 3A_2 \oplus 13E. \quad (117)$$

To systematically construct them, we use the seven bilinears that appear in the decomposition (115). These include the four bilinears that transform as one-dimensional IRs

$$\begin{aligned} D_{\text{ip}}^{A_1} &= |\mathbf{d}^{\text{ip}}|^2, & D_{\text{io}}^{A_1} &= |\mathbf{d}^{\text{ip}}||\mathbf{d}^{\text{op}}| \cos(\gamma_{\text{ip}} - \gamma_{\text{op}}), \\ D_{\text{op}}^{A_1} &= |\mathbf{d}^{\text{op}}|^2, & D_{\text{io}}^{A_2} &= |\mathbf{d}^{\text{ip}}||\mathbf{d}^{\text{op}}| \sin(\gamma_{\text{ip}} - \gamma_{\text{op}}), \end{aligned} \quad (118)$$

and the three bilinears that transform as two-dimensional IRs

$$\begin{aligned} \mathbf{D}_{\text{ip}}^E &= |\mathbf{d}^{\text{ip}}|^2 \begin{pmatrix} \cos(2\gamma_{\text{ip}}) \\ -\sin(2\gamma_{\text{ip}}) \end{pmatrix}, \\ \mathbf{D}_{\text{io}}^E &= |\mathbf{d}^{\text{ip}}||\mathbf{d}^{\text{op}}| \begin{pmatrix} \cos(\gamma_{\text{ip}} + \gamma_{\text{op}}) \\ -\sin(\gamma_{\text{ip}} + \gamma_{\text{op}}) \end{pmatrix}, \\ \mathbf{D}_{\text{op}}^E &= |\mathbf{d}^{\text{op}}|^2 \begin{pmatrix} \cos(2\gamma_{\text{op}}) \\ -\sin(2\gamma_{\text{op}}) \end{pmatrix}. \end{aligned} \quad (119)$$

It is now straightforward to construct the 13 invariants, each associated with a Landau coefficient. The three quadratic bilinears are given by $D_{\text{ip}}^{A_1}$, $D_{\text{op}}^{A_1}$, and $D_{\text{io}}^{A_1}$, whereas the four cubic invariants are $\mathbf{d}^{\text{ip}} \cdot \mathbf{D}_{\text{ip}}^E$, $\mathbf{d}^{\text{op}} \cdot \mathbf{D}_{\text{op}}^E$, $\mathbf{d}^{\text{ip}} \cdot \mathbf{D}_{\text{io}}^E$, and $\mathbf{d}^{\text{op}} \cdot \mathbf{D}_{\text{io}}^E$. As for the quartic invariants, they are given by the squares of the quadratic invariants $(D_{\text{ip}}^{A_1})^2$ and $(D_{\text{op}}^{A_1})^2$, the cross terms $D_{\text{ip}}^{A_1} D_{\text{op}}^{A_1}$, $D_{\text{ip}}^{A_1} D_{\text{io}}^{A_1}$ and $D_{\text{op}}^{A_1} D_{\text{io}}^{A_1}$, as well as $(D_{\text{io}}^{A_1})^2 - (D_{\text{io}}^{A_2})^2$. Writing the action as $\mathcal{S} = \mathcal{S}_2 + \mathcal{S}_3 + \mathcal{S}_4$, we thus have

$$\mathcal{S}_2 = \int_{\mathbf{x}} \{r_{\text{ip}}(\mathbf{d}^{\text{ip}})^2 + r_{\text{op}}(\mathbf{d}^{\text{op}})^2 + r_{\text{io}}(\mathbf{d}^{\text{ip}} \cdot \mathbf{d}^{\text{op}})\}, \quad (120)$$

$$\begin{aligned} \mathcal{S}_3 &= \int_{\mathbf{x}} \{g_{\text{ip}}|\mathbf{d}^{\text{ip}}|^3 \mathbf{c}_{3\gamma_{\text{ip}}} + g_1|\mathbf{d}^{\text{ip}}|^2|\mathbf{d}^{\text{op}}| \mathbf{c}_{2\gamma_{\text{ip}}+\gamma_{\text{op}}} \\ &\quad + g_{\text{op}}|\mathbf{d}^{\text{op}}|^3 \mathbf{c}_{3\gamma_{\text{op}}} + g_2|\mathbf{d}^{\text{ip}}||\mathbf{d}^{\text{op}}|^2 \mathbf{c}_{\gamma_{\text{ip}}+2\gamma_{\text{op}}}\}, \end{aligned} \quad (121)$$

$$\begin{aligned} \mathcal{S}_4 &= \int_{\mathbf{x}} \{u_{\text{ip}}|\mathbf{d}^{\text{ip}}|^4 + |\mathbf{d}^{\text{ip}}||\mathbf{d}^{\text{op}}|[u_1|\mathbf{d}^{\text{ip}}|^2 + u_2|\mathbf{d}^{\text{op}}|^2] \mathbf{c}_{\gamma_{\text{ip}}-\gamma_{\text{op}}} \\ &\quad + u_{\text{op}}|\mathbf{d}^{\text{op}}|^4 + |\mathbf{d}^{\text{ip}}|^2|\mathbf{d}^{\text{op}}|^2 [u_{\text{io}}^0 + u_{\text{io}}^c \mathbf{c}_{2\gamma_{\text{ip}}-2\gamma_{\text{op}}}] \}. \end{aligned} \quad (122)$$

To avoid cumbersome notations, we define $\mathbf{c}_\gamma \equiv \cos \gamma$. As expected, the degeneracy between \mathbf{d}^{ip} and \mathbf{d}^{op} is manifested in the quadratic mixing term $\mathbf{d}^{\text{ip}} \cdot \mathbf{d}^{\text{op}}$.

To determine the mean-field ground state, we first diagonalize the quadratic part \mathcal{S}_2 (120) to determine the combination of $(\mathbf{d}^{\text{ip}}, \mathbf{d}^{\text{op}})$ that orders first. We find

$$\mathcal{S}_2 = \int_{\mathbf{x}} \{\lambda_+ |\mathbf{d}^+|^2 + \lambda_- |\mathbf{d}^-|^2\}, \quad (123)$$

with the eigenvalues

$$\lambda_{\pm} = \frac{1}{2} (r_{\text{ip}} + r_{\text{op}} \pm \sqrt{(r_{\text{ip}} - r_{\text{op}})^2 + r_{\text{io}}^2}), \quad (124)$$

and the eigenvectors

$$\begin{pmatrix} \mathbf{d}^+ \\ \mathbf{d}^- \end{pmatrix} = U^T \begin{pmatrix} \mathbf{d}^{\text{ip}} \\ \mathbf{d}^{\text{op}} \end{pmatrix} = \begin{pmatrix} \text{sign}(r_{\text{io}})\beta_+ \mathbf{d}^{\text{ip}} + \beta_- \mathbf{d}^{\text{op}} \\ -\text{sign}(r_{\text{io}})\beta_- \mathbf{d}^{\text{ip}} + \beta_+ \mathbf{d}^{\text{op}} \end{pmatrix}. \quad (125)$$

In these expressions, we defined

$$\beta_{\pm} = \frac{1}{\sqrt{2}} \sqrt{1 \pm \frac{r_{\text{ip}} - r_{\text{op}}}{\sqrt{(r_{\text{ip}} - r_{\text{op}})^2 + r_{\text{io}}^2}}}, \quad (126)$$

and the unitary matrix

$$U = \begin{pmatrix} \beta_+ \text{sign} r_{\text{io}} & 0 & -\beta_- \text{sign} r_{\text{io}} & 0 \\ 0 & \beta_+ \text{sign} r_{\text{io}} & 0 & -\beta_- \text{sign} r_{\text{io}} \\ \beta_- & 0 & \beta_+ & 0 \\ 0 & \beta_- & 0 & \beta_+ \end{pmatrix}. \quad (127)$$

By construction, $\lambda_- < \lambda_+$, which implies that the order parameter combination \mathbf{d}^- is the one that condenses. The order parameter combination \mathbf{d}^+ , on the other hand, is a fluctuating field that primarily renormalizes the action for \mathbf{d}^- . Therefore, to proceed, we consider only terms that are quadratic or linear in \mathbf{d}^+ (Gaussian approximation). Introducing the parametrization $\mathbf{d}^{\pm} = |\mathbf{d}^{\pm}|(\cos \gamma_{\pm}, \sin \gamma_{\pm})$, we can rewrite the action as $\mathcal{S} = \mathcal{S}_- + \mathcal{S}_{+-}$ with

$$\mathcal{S}_- = \int_{\mathbf{x}} \{\lambda_- |\mathbf{d}^-|^2 + g_- |\mathbf{d}^-|^3 \cos(3\gamma_-) + u_- |\mathbf{d}^-|^4\}, \quad (128)$$

$$\mathcal{S}_{+-} = \int_{\mathbf{x}} \{\lambda_+ |\mathbf{d}^+|^2 + \tilde{g}_2 |\mathbf{d}^+||\mathbf{d}^-|^2 \cos(\gamma_+ + 2\gamma_-)\}. \quad (129)$$

Here, the Landau coefficients g_- , \tilde{g}_2 , and u_- can in principle be expressed in terms of the original Landau coefficients of Eqs. (120)–(122) by applying the unitary transformation U of Eq. (127). Since the \mathbf{d}^+ action is Gaussian, the minimization of \mathcal{S}_+ is straightforward and gives \mathbf{d}^+ in terms of \mathbf{d}^- :

$$|\mathbf{d}^+| = \frac{|\tilde{g}_2|}{2\lambda_+} |\mathbf{d}^-|^2, \quad \gamma_+ = -2\gamma_- + \left(\frac{1 + \text{sign} \tilde{g}_2}{2} \right) \pi. \quad (130)$$

Substituting it back in \mathcal{S} , we find the Landau expansion in terms of the ordering field \mathbf{d}^- alone:

$$\mathcal{S} = \int_{\mathbf{x}} \{\lambda_- |\mathbf{d}^-|^2 + g_- |\mathbf{d}^-|^3 \cos(3\gamma_-) + \tilde{u}_- |\mathbf{d}^-|^4\}, \quad (131)$$

with the reduced quartic coefficient $\tilde{u}_- = u_- - \tilde{g}_2^2/4\lambda_+$.

The central result is that the nematic action (131) has the same form as the Landau expansion of the Z_3 clock model,

see Eq. (94) and Ref. [107]. Therefore, in all trigonal crystals, the nematic transition belongs to the 3D Z_3 Potts/clock “universality class”, which actually corresponds to a mean-field first-order transition. Indeed, minimization of Eq. (131) reveals three degenerate ground states:

$$\gamma_-^0 = \frac{\pi}{3} \left(\frac{1 + \text{sign } g_-}{2} \right) + \frac{2\pi}{3} n, \quad n \in \{0, 1, 2\}. \quad (132)$$

Substitution in Eq. (130) shows that, in the ground state, \mathbf{d}^+ and \mathbf{d}^- are collinear:

$$\begin{pmatrix} \cos \gamma_+^0 \\ \sin \gamma_+^0 \end{pmatrix} = \text{sign}(g_- \tilde{g}_2) \begin{pmatrix} \cos \gamma_-^0 \\ \sin \gamma_-^0 \end{pmatrix}. \quad (133)$$

Therefore, using Eq. (125), we find that the nematic in-plane and out-of-plane doublets are also collinear, and thus can be parametrized as

$$\mathbf{d}^{\text{ip}} = |\mathbf{d}^E| \cos \delta_E \begin{pmatrix} \cos \gamma_-^0 \\ \sin \gamma_-^0 \end{pmatrix}, \quad \mathbf{d}^{\text{op}} = |\mathbf{d}^E| \sin \delta_E \begin{pmatrix} \cos \gamma_-^0 \\ \sin \gamma_-^0 \end{pmatrix}, \quad (134)$$

where $\delta_E \in [0, \pi]$ and $|\mathbf{d}^E| = (|\mathbf{d}^{\text{ip}}|^2 + |\mathbf{d}^{\text{op}}|^2)^{1/2}$ are determined by the Landau coefficients.

To express the trigonal nematic ground state (134) in the (\mathbf{nml}) representation (14), it is convenient to define two new quantities (recall the d_1 is the nonzero symmetry-preserving nematic component)

$$K_r = -\frac{\sqrt{3} \text{sign}(g_-)}{2} \cos(\delta_E) \frac{|\mathbf{d}^E|}{|\mathbf{d}|} - \frac{d_1}{2|\mathbf{d}|} \in [-1, 1], \quad (135)$$

$$K'_r = -\frac{\text{sign}(g_-)}{2} \cos(\delta_E) \frac{|\mathbf{d}^E|}{|\mathbf{d}|} + \frac{\sqrt{3} d_1}{2|\mathbf{d}|} \in [-1, 1], \quad (136)$$

as well as the tilt angle $\eta_0 \in [0, \frac{\pi}{2}]$

$$\eta_0 = \frac{\pi}{2} \frac{1 + \text{sign} K'_r}{2} - \frac{\text{sign} K'_r}{2} \arccos \left(\frac{|K'_r|}{\sqrt{1 - |K_r|^2}} \right), \quad (137)$$

and the three orthonormal vectors

$$\begin{aligned} \mathbf{e}_{\parallel} &= \begin{pmatrix} \cos \gamma_-^0 \\ -\sin \gamma_-^0 \\ 0 \end{pmatrix}, \quad \mathbf{e}_{\perp}^A = \begin{pmatrix} \sin \gamma_-^0 \cos \eta_0 \\ \cos \gamma_-^0 \cos \eta_0 \\ \sin \eta_0 \end{pmatrix}, \\ \mathbf{e}_{\perp}^B &= \begin{pmatrix} \sin \gamma_-^0 \sin \eta_0 \\ \cos \gamma_-^0 \sin \eta_0 \\ -\cos \eta_0 \end{pmatrix}. \end{aligned} \quad (138)$$

Note that \mathbf{e}_{\parallel} points along one of the six high-symmetry directions of the hexagonal point groups, given by $\mathcal{V}_1^{\text{hex}}$ and $\mathcal{V}_2^{\text{hex}}$ in Eq. (97). Indeed, the trigonal nematic angle γ_-^0 in Eq. (132) assumes the same values as the in-plane hexagonal nematic angles γ_{ip}^0 in Eq. (103).

In terms of these quantities, the trigonal nematic state (134) can be conveniently expressed in the (\mathbf{nml}) notation via

$$\begin{aligned} |K_r| \leq \frac{1}{2}: \quad \alpha &= \frac{\pi}{6} + \arcsin(K_r), \\ \mathbf{n} &= \mathbf{e}_{\perp}^A, \quad \mathbf{m} = \mathbf{e}_{\perp}^B, \quad \mathbf{l} = \mathbf{e}_{\parallel}, \end{aligned}$$

$$\begin{aligned} K_r < \frac{-1}{2}: \quad \alpha &= \arcsin(|K_r|) - \frac{\pi}{6}, \\ \mathbf{n} &= \mathbf{e}_{\perp}^A, \quad \mathbf{m} = \mathbf{e}_{\parallel}, \quad \mathbf{l} = \mathbf{e}_{\perp}^B, \\ K_r > \frac{1}{2}: \quad \alpha &= \frac{\pi}{2} - \arcsin(|K_r|), \\ \mathbf{n} &= \mathbf{e}_{\parallel}, \quad \mathbf{m} = \mathbf{e}_{\perp}^B, \quad \mathbf{l} = \mathbf{e}_{\perp}^A. \end{aligned} \quad (139)$$

The similarity to the in-plane nematic state of the 2D isotropic system, Eq. (88), is apparent—indeed, one can verify that upon setting $\delta_E = 0$ (pure in-plane nematicity) one recovers the exact same equations. Conversely, upon setting $\delta_E = \pi/2$ (pure out-of-plane nematicity), the out-of-plane isotropic nematic solution (89) is recovered. Therefore, the trigonal nematic state is generally biaxial with $\alpha \neq 0, \pi/3$, except for the special point $|K_r| = 1/2$, where it becomes uniaxial. In Figs. 5(c)–5(e), we plot the Fermi surface distortion in the trigonal nematic state (139) for three representative values of K_r , encompassing each of the three regimes above. For $|K_r| < \frac{1}{2}$, shown in Fig. 5(e), the nematic distortion is qualitatively similar to that caused by an out-of-plane hexagonal order parameter \mathbf{d}^{op} [Fig. 5(b)], since the nematic axis $\mathbf{l} = \mathbf{e}_{\parallel}$ aligns with one of the three in-plane symmetry axes, represented by the purple lines in the figure [corresponding to $\mathcal{V}_1^{\text{hex}}$ in Eq. (97)]. The key difference is that the trigonal groups do not possess the symmetry elements C_{2z} or IC_{2z} , such that a 180° degree rotation about the k_z axis does not lead to a degenerate state. As a result, what used to be a Z_6 degenerate state in the hexagonal case [Fig. 5(b)] splits into two sets of Z_3 degenerate states in the trigonal case, one for each sign of g_- [Eq. (132)]. In the regime $|K_r| > 1/2$, plotted in Fig. 5(c), the trigonal nematic state has either the long (\mathbf{m}) or the short (\mathbf{n}) nematic axis aligned with an in-plane symmetry axis \mathbf{e}_{\parallel} , which for $g_- < 0$ corresponds to $\mathcal{V}_1^{\text{hex}}$. This state resembles the in-plane nematic state of the hexagonal lattice depicted in Fig. 5(a), albeit slightly rotated out of plane. Exactly at $|K_r| = 1/2$, $\alpha = 0, \pi/3$ and the nematic state is uniaxial, as shown in Fig. 5(d). The properties of the nematic state of all trigonal groups are summarized in Table I.

D. Tetragonal crystals

Most nematic materials studied in the literature have tetragonal symmetry, namely: the iron pnictides [6–11,65,66,68,72,73], the cuprates [1–5,39,64,70], the correlated oxide $\text{Sr}_3\text{Ru}_2\text{O}_7$ [14,67], as well as the f -electron materials YbRu_2Ge_2 [22], CeRhIn_5 [21], TmVO_4 [24], and CeAuSb_2 [23]. In any of the seven tetragonal point groups, the five-component nematic order parameter \mathbf{d} (7) is decomposed as

$$\mathbf{d} \xrightarrow{\text{tetragonal}} (d_{\perp}, d_2, d_5, \mathbf{d}^{\text{op}})^T. \quad (140)$$

Hence, in contrast to the 2D isotropic system (79), as well as to the hexagonal and trigonal lattices, in tetragonal crystals the nematic in-plane doublet $\mathbf{d}^{\text{ip}} = (d_2, d_5)^T$ is further decomposed into the two channels $d_2 = d_{x^2-y^2}$ and $d_5 = d_{2xy}$, which transform as nontrivial one-dimensional IRs. Thus, the tetragonal crystal system is the highest-symmetry crystal for which a nontrivial nematic component exists that does not transform as a multidimensional IR.

There are seven different axial point groups in the tetragonal crystal system: $\{D_{4h}, D_4, C_{4v}, D_{2d}\}$, which possess in-plane twofold rotational symmetry axes, and $\{C_{4h}, C_4, S_4\}$, which do not possess such axes. As in the previous subsections, the two sets need to be treated slightly differently, since in the latter the out-of-plane nematic order parameter \mathbf{d}^{op} transforms as a complex IR and $\{d_2, d_5\}$ transform as the same one-dimensional IR. In this section we will focus on the first set, illustrating the results for the point group D_{4h} , while leaving the discussion of the second set of point groups to Appendix G.

In D_{4h} , the single-component order parameters $d_2 = d_{x^2-y^2}$ and $d_5 = d_{2xy}$ transform according to the IRs B_{1g} and B_{2g} , respectively, while the out-of-plane doublet $\mathbf{d}^{\text{op}} = (d_3, d_4)^T = (d_{2yz}, d_{2xz})^T$ transforms as the IR E_g . As single-component real-valued order parameters, both d_2 and d_5 are Ising variables that undergo a Z_2 Ising transition described by the action

$$\mathcal{S}_v = \int_x \{r_v |d_v|^2 + u_v |d_v|^4\}, \quad (141)$$

with $v = \{2, 5\}$. We note that this Landau expansion could also be recast in terms of the in-plane nematic doublet $\mathbf{d}^{\text{ip}} = (d_2, d_5)^T = (d_{x^2-y^2}, d_{2xy})^T$ as an effective Z_2 clock model, see Eq. (94):

$$\mathcal{S}_{\text{ip}} = \int_x \{r_0 |\mathbf{d}^{\text{ip}}|^2 + h_2 |\mathbf{d}^{\text{ip}}|^2 \cos(2\gamma_{\text{ip}}) + O(|\mathbf{d}^{\text{ip}}|^4)\}. \quad (142)$$

The second term is nothing but $h_2(d_2^2 - d_5^2)$, which implies that the transitions toward d_2 and d_5 electronic nematic order take place at different values of the control parameter, $r_0 = -h_2$ for d_2 and $r_0 = h_2$ for d_5 . The symmetry here also allows for an additional biquadratic term $d_2^2 d_5^2$. One could in principle integrate out the fluctuations of the subleading channel, whose effect on the leading channel will only be important if h_2 is small. Thus, the Landau coefficients r_v and u_v in Eq. (141) should be understood as renormalized Landau coefficients of the ‘‘original’’ in-plane nematic action.

The $d_2 = d_{x^2-y^2}$ and $d_5 = d_{2xy}$ Ising-nematic order parameters are the types of nematic order most widely studied in the literature [39,64–73]. Whereas one often describes them in terms of an effective 2D nematic order parameter, see Eq. (91), it is straightforward to describe them in the (\mathbf{nml}) representation by employing Eq. (88) with the additional constraint of $\gamma_{\text{ip}} = \{0, \pi\}$ for d_2 [corresponding to $h_2 < 0$ in Eq. (142)] and $\gamma_{\text{ip}} = \{\pi/2, 3\pi/2\}$ for d_5 [corresponding to $h_2 > 0$ in Eq. (142)]. The corresponding Fermi surface distortions are shown in Figs. 6(a) and 6(b). For the $d_2 = d_{x^2-y^2}$ state, the in-plane nematic axes align with the in-plane principal axes $\mathcal{V}_1^{\text{tet}}$ (light-blue) while for $d_5 = d_{2xy}$ they align with the in-plane diagonal axes $\mathcal{V}_2^{\text{tet}}$ (purple), with

$$\mathcal{V}_1^{\text{tet}} = \left\{ \begin{pmatrix} 1 \\ 0 \\ 0 \end{pmatrix}, \begin{pmatrix} 0 \\ 1 \\ 0 \end{pmatrix} \right\}, \quad \mathcal{V}_2^{\text{tet}} = \left\{ \frac{1}{\sqrt{2}} \begin{pmatrix} 1 \\ 1 \\ 0 \end{pmatrix}, \frac{1}{\sqrt{2}} \begin{pmatrix} 1 \\ -1 \\ 0 \end{pmatrix} \right\}. \quad (143)$$

Therefore, the Z_2 character of the Ising-nematic order parameter is associated with the C_{4z} operation (90° rotation about the k_z axis). Recall that the alignment of the $\mathbf{n}, \mathbf{m}, \mathbf{l}$ axes in Eq. (88), which determines which nematic axes are in-plane, depends on the ratio $d_1/|\mathbf{d}|$ between the trivial (i.e.

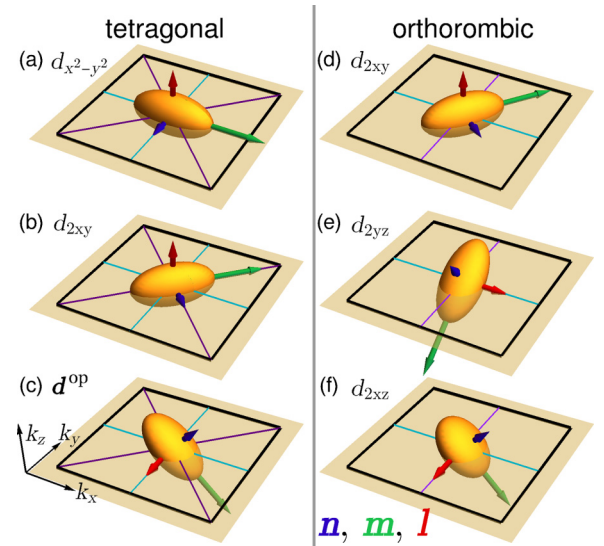


FIG. 6. Distorted Fermi surface in the nematic phase, as given by Eq. (32), plotted together with the nematic axes $\mathbf{n}, \mathbf{m}, \mathbf{l}$ for the cases of (a), (b) tetragonal in-plane $d_2 = d_{x^2-y^2}$ and $d_5 = d_{2xy}$ states (141), (c) tetragonal out-of-plane doublet state \mathbf{d}^{op} (149), (d)–(f) orthorhombic nematic states $d_5 = d_{2xy}$, $d_3 = d_{2yz}$ and $d_4 = d_{2xz}$. The unit vectors $\{\mathbf{n}, \mathbf{m}, \mathbf{l}\}$ are rescaled by $2.25 k_F \{(\mathbf{n}, \mathbf{m}, \mathbf{l})\}$, respectively. For the tetragonal and orthorhombic cases we chose the trivial components as $d_1/|\mathbf{d}| = 0.1$ and $(|\mathbf{d}^e|/|\mathbf{d}|, \gamma_e) = (0.3, 1.1)$, respectively.

symmetry-preserving) nematic component $d_1 = d_{\frac{1}{\sqrt{3}}(2z^2 - x^2 - y^2)}$ and $|\mathbf{d}| = (d_v^2 + d_1^2)^{1/2}$, with $v = \{2, 5\}$.

To derive the Landau invariants for the out-of-plane nematic order parameter \mathbf{d}^{op} we compute, once again, the decomposition of the symmetrized product for each expansion order,

$$[\otimes_{j=1}^2 E_g]_s = A_{1g} \oplus B_{1g} \oplus B_{2g}, \quad (144)$$

$$[\otimes_{j=1}^3 E_g]_s = 2E_g, \quad (145)$$

$$[\otimes_{j=1}^4 E_g]_s = 2A_{1g} \oplus A_{2g} \oplus B_{1g} \oplus B_{2g}. \quad (146)$$

From the bilinears associated with Eq. (144), $D_{\text{op}}^{A_{1g}} = |\mathbf{d}^{\text{op}}|^2$, and

$$D_{\text{op}}^{B_{1g}} = |\mathbf{d}^{\text{op}}|^2 \cos(2\gamma_{\text{op}}), \quad D_{\text{op}}^{B_{2g}} = |\mathbf{d}^{\text{op}}|^2 \sin(2\gamma_{\text{op}}), \quad (147)$$

we can readily identify the three Landau invariants as $|\mathbf{d}^{\text{op}}|^2$, $|\mathbf{d}^{\text{op}}|^4$, and $(D_{\text{op}}^{B_{1g}})^2 - (D_{\text{op}}^{B_{2g}})^2$. We then obtain the Landau expansion

$$\mathcal{S}_{\text{op}} = \int_x \{r_0 |\mathbf{d}^{\text{op}}|^2 + u |\mathbf{d}^{\text{op}}|^4 + v_4 |\mathbf{d}^{\text{op}}|^4 \cos(4\gamma_{\text{op}})\}, \quad (148)$$

which corresponds to the Z_4 clock model of Eq. (94). The fourfold degenerate ground-state is parametrized by

$$\gamma_{\text{op}}^0 = \frac{\pi}{4} \left(\frac{1 + \text{sign} v_4}{2} \right) + \frac{2\pi}{4} n, \quad n \in \{0, 1, 2, 3\}. \quad (149)$$

Therefore, the out-of-plane nematic transition in a tetragonal crystal belongs to the 3D XY universality class; we emphasize that such a critical behavior may only emerge very close to the

transition, depending on the degree of out-of-plane anisotropy of the system.

The corresponding representation of Eq. (149) in the (nml) formalism can be directly read off from Eq. (89). Figure 6(c) shows the corresponding Fermi surface distortion, with the nematic axis l aligned with the in-plane high-symmetry axes of either $\mathcal{V}_1^{\text{tet}}$ (light-blue) or $\mathcal{V}_2^{\text{tet}}$ (purple) [see Eq. (143)], depending on the sign of v_4 . The fourfold degeneracy of the ground state arises from the two axes in either $\mathcal{V}_1^{\text{tet}}$ or $\mathcal{V}_2^{\text{tet}}$ with each l can align, combined with the two sets of directions of n, m that are related by a C_{2z} symmetry operation (which is present in all tetragonal groups). A summary of the results for all tetragonal crystal groups is presented in Table I, combining the analysis of this section with that of Appendix G.

E. Orthorhombic, monoclinic, and triclinic crystals

In the remaining three crystal systems—orthorhombic, monoclinic, and triclinic—all the point groups are Abelian, and as such do not admit multidimensional IRs (real or complex). As a result, all nematic components transform as one-dimensional IRs, implying that the nontrivial nematic components behave as Z_2 Ising order parameters. Another key difference between these axial groups and the other ones previously analyzed in this section is that at least one of the components of $\mathbf{d}^{\text{ip}} = (d_2, d_5)^T = (d_{x^2-y^2}, d_{2xy})^T$ and $\mathbf{d}^{\text{op}} = (d_3, d_4)^T = (d_{2yz}, d_{2xz})^T$ transform as the trivial IR, like $d_1 = d_{\frac{1}{\sqrt{3}}(2z^2-x^2-y^2)}$.

We start with the orthorhombic crystal system, described by the three point groups $\{D_{2h}, D_2, C_{2v}\}$. In terms of the IR of these groups, the five nematic components \mathbf{d} (7) are decomposed according to

$$\mathbf{d} \xrightarrow{\text{orthorhombic}} (\underline{d_1}, \underline{d_2}, d_3, d_4, d_5)^T. \quad (150)$$

The first two components $\{d_1, d_2\}$, highlighted by the underline, transform trivially under the groups symmetry operations and thus are generically nonzero. The remaining three components $d_3 = d_{2yz}, d_4 = d_{2xz}$, and $d_5 = d_{2xy}$ correspond to shear distortions of the Fermi surface, and transform according to three different one-dimensional IRs, as shown explicitly in Table I. As such, they all undergo a Z_2 Ising transition described by an action analogous to Eq. (141).

These three Ising-nematic states can be expressed in the (nml) representation provided that one also includes the nonzero trivial components $\mathbf{d}^e = (d_1, d_2) = |\mathbf{d}^e|(\cos \gamma_e, \sin \gamma_e)$. In the case of the nematic order parameter $d_5 = d_{2xy}$, one can directly apply the in-plane isotropic parametrization of Eq. (88) with $|\mathbf{d}| = (d_5^2 + |\mathbf{d}^e|^2)^{1/2}$ and $\tan \gamma_{\text{ip}} = d_5/d_2$. The resulting Fermi surface distortion, calculated via Eq. (32), is shown in Fig. 6(d). Since d_2 is always nonzero, the in-plane nematic axes \mathbf{e}_\parallel^A and \mathbf{e}_\parallel^B defined in Eq. (87) are never aligned with $\mathcal{V}_2^{\text{tet}}$ in Eq. (143), which is consistent with the fact that $\mathcal{V}_2^{\text{tet}}$ are not high-symmetry directions in orthorhombic crystals. Note that one of the nematic axes is aligned with the k_z axis. The Z_2 degeneracy is associated with the C_{2x} (C_{2y}) or IC_{2x} (IC_{2y}) symmetry operations, corresponding to in-plane twofold rotations or vertical mirror reflections of the nematic axes in Fig. 6(d).

As for the nematic order parameters d_3 and d_4 , one cannot just apply the out-of-plane parametrization of Eq. (89), since d_2 , which is a component of \mathbf{d}^{ip} , is always nonzero. To express d_3 and d_4 in the (nml) representation, it is convenient to define the auxiliary variables

$$c_k^e = \frac{|\mathbf{d}^e|}{|\mathbf{d}|} \cos\left(\gamma_e - \frac{k\pi}{3}\right), \quad s_k^e = \frac{|\mathbf{d}^e|}{|\mathbf{d}|} \sin\left(\gamma_e - \frac{k\pi}{3}\right), \quad (151)$$

with $k = \{2, 4\}$ and $|\mathbf{d}| = [|\mathbf{d}^e|^2 + (d_3)^2 + (d_4)^2]^{1/2}$. We then define the angles

$$\eta_3^\pm = \frac{1}{2} \frac{d_3}{|d_3|} \arccos\left(\frac{|s_2^e|}{\sqrt{1 - (c_2^e)^2}}\right) \pm \frac{1 + \text{sign}(s_2^e)}{2} \frac{\pi}{2}, \quad (152)$$

$$\eta_4^\pm = \frac{1}{2} \frac{d_4}{|d_4|} \arccos\left(\frac{|s_4^e|}{\sqrt{1 - (c_4^e)^2}}\right) \pm \frac{1 + \text{sign}(s_4^e)}{2} \frac{\pi}{2}, \quad (153)$$

and, from them, the four unit vectors

$$\begin{aligned} \mathbf{e}_A^{yz} &= (0, \sin \eta_3^+, \cos \eta_3^-)^T, & \mathbf{e}_B^{yz} &= (0, \cos \eta_3^-, -\sin \eta_3^+)^T, \\ \mathbf{e}_A^{zx} &= (\cos \eta_4^-, 0, \sin \eta_4^+)^T, & \mathbf{e}_B^{zx} &= (-\sin \eta_4^+, 0, \cos \eta_4^-)^T. \end{aligned} \quad (154)$$

Now, the nematic order parameter $d_3 = d_{2yz}$ can be conveniently expressed in the (nml) representation via

$$\begin{aligned} |c_2^e| \leq \frac{1}{2}: & \quad \alpha = \frac{\pi}{6} + \arcsin(c_2^e), \\ & \quad \mathbf{n} = \mathbf{e}_A^{yz}, \quad \mathbf{m} = \mathbf{e}_B^{yz}, \quad \mathbf{l} = \mathbf{e}_x, \\ c_2^e < -\frac{1}{2}: & \quad \alpha = \arcsin(|c_2^e|) - \frac{\pi}{6}, \\ & \quad \mathbf{n} = \mathbf{e}_A^{yz}, \quad \mathbf{m} = \mathbf{e}_x, \quad \mathbf{l} = \mathbf{e}_B^{yz}, \\ c_2^e > \frac{1}{2}: & \quad \alpha = \frac{\pi}{2} - \arcsin(|c_2^e|), \\ & \quad \mathbf{n} = \mathbf{e}_x, \quad \mathbf{m} = \mathbf{e}_B^{yz}, \quad \mathbf{l} = \mathbf{e}_A^{yz}. \end{aligned} \quad (155)$$

Analogously, the nematic order parameter $d_4 = d_{2xz}$ becomes

$$\begin{aligned} |c_4^e| \leq \frac{1}{2}: & \quad \alpha = \frac{\pi}{6} + \arcsin(c_4^e), \\ & \quad \mathbf{n} = \mathbf{e}_A^{zx}, \quad \mathbf{m} = \mathbf{e}_B^{zx}, \quad \mathbf{l} = \mathbf{e}_y, \\ c_4^e < -\frac{1}{2}: & \quad \alpha = \arcsin(|c_4^e|) - \frac{\pi}{6}, \\ & \quad \mathbf{n} = \mathbf{e}_A^{zx}, \quad \mathbf{m} = \mathbf{e}_y, \quad \mathbf{l} = \mathbf{e}_B^{zx}, \\ c_4^e > \frac{1}{2}: & \quad \alpha = \frac{\pi}{2} - \arcsin(|c_4^e|), \\ & \quad \mathbf{n} = \mathbf{e}_y, \quad \mathbf{m} = \mathbf{e}_B^{zx}, \quad \mathbf{l} = \mathbf{e}_A^{zx}. \end{aligned} \quad (156)$$

Note that the (nml) representations (155) and (156) are very similar to the in-plane isotropic (nml) representation, Eq. (88). In fact, the latter can be recovered from Eq. (151) by setting $k = 0$ as $c_0^e = d_1/|\mathbf{d}|$, and the three cases support a fine-tuned uniaxial nematic order parameter for $|c_4^e| = |c_2^e| = |c_0^e| = 1/2$. In Figs. 6(e) and 6(f), we show the Fermi surface distortions corresponding, respectively, to the condensation of the nematic order parameters $d_3 = d_{2yz}$ and $d_4 = d_{2xz}$. In the former, one of the nematic in-plane axis always aligns with \mathbf{e}_x while for $d_4 = d_{2xz}$, it aligns with \mathbf{e}_y , in accordance with

Eqs. (155) and (156). In both cases, the twofold degeneracy is associated with the symmetry element C_{2z} , i.e. a 180° rotation about the k_z axis.

We now analyze the case of the monoclinic crystal system, encompassed by the three axial point groups $\{C_{2h}, C_{1h} = C_s, C_2\}$. In all cases, the decomposition of the five nematic components \mathbf{d} (7) is

$$\mathbf{d} \xrightarrow{\text{monoclinic}} (\underline{d_1}, \underline{d_2}, \underline{d_5}, \{d_3, d_4\})^T. \quad (157)$$

As indicated by the underline, the three components $d_1 = d_{\frac{1}{\sqrt{3}}(2z^2 - x^2 - y^2)}$, $d_2 = d_{x^2 - y^2}$, and $d_5 = d_{2xy}$ transform as the trivial IR and are thus always nonzero. On the other hand, the nematic order parameters $d_3 = d_{2yz}$ and $d_4 = d_{2xz}$ transform according to the same one-dimensional IR, as indicated by the curly brackets. Consequently, the analysis of the Landau expansion is analogous to that performed in Appendix G for the tetragonal groups $\{C_{4h}, C_4, S_4\}$. Indeed, we obtain the same form of the nematic action $\mathcal{S} = \mathcal{S}_2 + \mathcal{S}_4$:

$$\mathcal{S}_2 = \int_x \{r_1(d_3)^2 + r_2(d_4)^2 + r_3 d_3 d_4\}, \quad (158)$$

$$\mathcal{S}_4 = \int_x \{u_1(d_3)^4 + u_2(d_4)^4 + u_3(d_3)^2(d_4)^2 + u_4 d_3(d_4)^3 + u_5(d_3)^3 d_4\}. \quad (159)$$

The outcome, as explained in Appendix G, is that a linear combination of d_3 and d_4 , which is enforced by the Landau coefficients, undergoes a Z_2 Ising transition. The visualization of this nematic order parameter in the (nml) representation offers little insight, as the nematic axes $\mathbf{n}, \mathbf{m}, \mathbf{l}$ can point anywhere in space.

The last crystal system is the triclinic one, described by the two axial point groups $\{C_1, C_i = S_2\}$. The symmetry of these crystals is so low that all five nematic components \mathbf{d} transform as the trivial IR, which is a direct consequence of the absence of rotational symmetry axes:

$$\mathbf{d} \xrightarrow{\text{triclinic}} (d_1, d_2, d_3, d_4, d_5)^T. \quad (160)$$

Therefore, nematic phase transitions cannot occur in triclinic crystals.

V. ELECTRONIC NEMATICITY IN QUASICRYSTALLINE AXIAL POINT GROUPS

While a large number of known quasicrystals is described by the icosahedral (i.e., polyhedral) point groups $\{I_h, I\}$, whose electronic nematic properties were analyzed in Sec. III A, there are also quasicrystalline materials with eightfold, tenfold, and twelvefold symmetry [86]. In contrast to the icosahedral quasicrystals, the latter are quasiperiodic in two directions and periodic along an axial direction; consequently, they are described by noncrystallographic axial point groups [88,89,91,105]. In this subsection, we investigate the properties of the electronic nematic order parameter in the class of octagonal, decagonal, and dodecagonal point groups. Importantly, these point groups describe not only quasicrystalline materials, but also artificial quasicrystals obtained from twisting two crystalline 2D materials. The latter will be discussed in more depth in Sec. V D.

In all cases studied here, the symmetry-decomposition of the five nematic components of \mathbf{d} (7) have the same form as that for 2D isotropic systems:

$$\mathbf{d} \xrightarrow{\text{axial quasicrystals}} (\underline{d_1}, \mathbf{d}^{\text{ip}}, \mathbf{d}^{\text{op}})^T. \quad (161)$$

Following the discussion in Sec. IV A for 2D isotropic systems, our goal is to obtain the first invariant in the Landau expansion of \mathbf{d}^α that is not isotropic, i.e. that is not of the form $|\mathbf{d}^\alpha|^{2n}$ with integer n (here, α refers to either ip or op). To accomplish this in a systematic way, we evaluate the symmetrized decomposition of the N th-order product $[\otimes_{j=1}^N E_\Gamma]_s$, where E_Γ is the two-dimensional IR according to which \mathbf{d}^α transforms. The leading-order anisotropic term is obtained from the product with the smallest N for which the decomposition gives either two invariants (if N is even) or one invariant (if N is odd). We note that Ref. [106] performed a related analysis for the d_{2xy} and $d_{x^2-y^2}$ superconducting order parameters in D_n point groups.

A summary of all the results presented in this section, as well as in Sec. III A for the icosahedral quasicrystal, is contained in Table II.

A. Dodecagonal quasicrystals

The noncrystallographic point groups that possess dodecagonal symmetry are $\{D_{12h}, D_{12}, C_{12v}, D_{6d}, C_{12h}, C_{12}, S_{12}\}$. For concreteness, hereafter we consider D_{12h} , for which \mathbf{d}^{ip} and \mathbf{d}^{op} transform as the E_{2g} and E_{1g} IR, respectively. We will discuss later how the results generalize to the other dodecagonal groups.

To derive the Landau expansion of the doublets, we follow the procedure outlined in the beginning of this section. Focusing first on the in-plane doublet \mathbf{d}^{ip} , we compute the symmetrized-product decomposition of the corresponding IR:

$$[\otimes_{j=1}^2 E_{2g}]_s = A_{1g} \oplus E_{4g}, \quad (162)$$

$$[\otimes_{j=1}^3 E_{2g}]_s = B_{1g} \oplus B_{2g} \oplus E_{2g}, \quad (163)$$

$$[\otimes_{j=1}^4 E_{2g}]_s = A_{1g} \oplus 2E_{4g}, \quad (164)$$

$$[\otimes_{j=1}^5 E_{2g}]_s = B_{1g} \oplus B_{2g} \oplus 2E_{2g}, \quad (165)$$

$$[\otimes_{j=1}^6 E_{2g}]_s = 2A_{1g} \oplus A_{2g} \oplus 2E_{4g}. \quad (166)$$

Therefore, since there are two A_{1g} invariants in (166), whereas all other even orders have only one invariant, we conclude that the leading order anisotropic term in the Landau expansion of \mathbf{d}^{ip} appears at sixth order. It can be constructed from the product of the B_{1g} and B_{2g} trilinears,

$$B_{1g}: |\mathbf{d}^{\text{ip}}|^3 \cos(3\gamma_{\text{ip}}), \quad B_{2g}: |\mathbf{d}^{\text{ip}}|^3 \sin(3\gamma_{\text{ip}}), \quad (167)$$

and thus, it becomes $|\mathbf{d}^{\text{ip}}|^6 \cos(6\gamma_{\text{ip}})$, resulting in the action

$$\mathcal{S}_{\text{ip}} = \int_x \{r_0 |\mathbf{d}^{\text{ip}}|^2 + u |\mathbf{d}^{\text{ip}}|^4 + v_6 |\mathbf{d}^{\text{ip}}|^6 \cos(6\gamma_{\text{ip}})\}. \quad (168)$$

The Landau expansion (168) is equivalent to that of the Z_6 clock model, displaying a sixfold-degenerate ground state

$$\gamma_{\text{ip}}^0 = \frac{\pi}{6} \left(\frac{1 + \text{sign} v_6}{2} \right) + \frac{2\pi}{6} n, \quad n \in \{0, 1, \dots, 5\}. \quad (169)$$

As for the out-of-plane doublet \mathbf{d}^{op} , which transforms as the E_{1g} IR, the symmetrized-product decomposition up to sixth-order yields only isotropic invariants of the form $|\mathbf{d}^{\text{op}}|^{2n}$:

$$[\otimes_{j=1}^2 E_{1g}]_s = A_{1g} \oplus E_{2g}, \quad (170)$$

$$[\otimes_{j=1}^3 E_{1g}]_s = E_{1g} \oplus E_{3g}, \quad (171)$$

$$[\otimes_{j=1}^4 E_{1g}]_s = A_{1g} \oplus E_{2g} \oplus E_{4g}, \quad (172)$$

$$[\otimes_{j=1}^5 E_{1g}]_s = E_{1g} \oplus E_{3g} \oplus E_{5g}, \quad (173)$$

$$[\otimes_{j=1}^6 E_{1g}]_s = A_{1g} \oplus B_{1g} \oplus B_{2g} \oplus E_{2g} \oplus E_{4g}. \quad (174)$$

It turns out that an anisotropic invariant can only be constructed at twelfth order, from the product of the B_{1g} and B_{2g} IRs that appear in the sixth-order product decomposition:

$$B_{1g}: |\mathbf{d}^{\text{op}}|^6 \cos(6\gamma_{\text{op}}), \quad B_{2g}: |\mathbf{d}^{\text{op}}|^6 \sin(6\gamma_{\text{op}}). \quad (175)$$

We thus obtain the nematic action:

$$\mathcal{S}_{\text{op}} = \int_{\mathbf{x}} \{r_0 |\mathbf{d}^{\text{op}}|^2 + u |\mathbf{d}^{\text{op}}|^4 + v_{12} |\mathbf{d}^{\text{op}}|^{12} \cos(12\gamma_{\text{op}})\}, \quad (176)$$

which has the same form as the Landau expansion of the Z_{12} clock model. The ground-state is parametrized by

$$\gamma_{\text{op}}^0 = \frac{\pi}{12} \left(\frac{1 + \text{sign} v_{12}}{2} \right) + \frac{2\pi}{12} n, \quad n \in \{0, 1, \dots, 11\}. \quad (177)$$

The in-plane and out-of-plane nematic states given by (169) and (177) can be expressed in the (nml) representation in a straightforward way via the relationships (88) and (89). We show the corresponding Fermi surface distortions in Figs. 7(a) and 7(b). For \mathbf{d}^{ip} , both in-plane nematic axes point along the high-symmetry directions associated with twofold in-plane rotations, whereas the third axis is parallel to the k_z axis. In contrast, for \mathbf{d}^{op} , only the nematic axis l aligns with a high-symmetry direction.

The same results obtained for D_{12h} also hold for the dodecagonal groups $\{D_{12}, C_{12v}, D_{6d}\}$. On the other hand, for $\{C_{12h}, C_{12}, S_{12}\}$, due to the lack of in-plane symmetry axes, the nematic doublets transform as complex IRs, resulting in an offset angle in the clock term of the type (95), similarly to what is shown in Appendixes E–G for crystalline axial point groups.

B. Decagonal quasicrystals

There are seven noncrystallographic point groups that possess tenfold symmetry, $\{D_{10h}, D_{10}, D_{5h}, C_{10v}, C_{10h}, C_{5h}, C_{10}\}$. Similarly to the previous subsection, we need to distinguish the groups $\{D_{10h}, D_{10}, D_{5h}, C_{10v}\}$ from the groups $\{C_{10h}, C_{5h}, C_{10}\}$, as the latter do not have in-plane symmetry axes. The only effect of this lack of in-plane rotational symmetry is that the clock term of the nematic action acquires an offset angle, see Eq. (95).

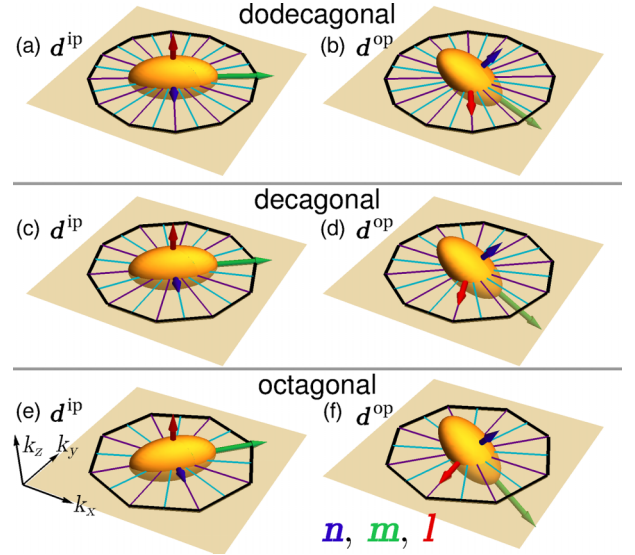


FIG. 7. Distorted Fermi surface in the nematic phase, as given by Eq. (32), plotted together with the nematic axes $\mathbf{n}, \mathbf{m}, \mathbf{l}$ for the cases of dodecagonal in-plane and out-of-plane nematicity (169), (177) [panels (a) and (b)], decagonal in-plane and out-of-plane nematicity (183), (190) [panels (c) and (d)], and octagonal in-plane and out-of-plane nematicity (196), (202) [panels (e) and (f)]. The unit vectors $\{\mathbf{n}, \mathbf{m}, \mathbf{l}\}$ are rescaled by $2.25 k_F$ ($\{\mathbf{n}, \mathbf{m}, \mathbf{l}\}$), respectively. We chose the trivial component such that $d_1/|\mathbf{d}| = 0.1$.

We consider here the case of D_{10h} . Starting with the in-plane doublet \mathbf{d}^{ip} , which transforms as the E_{2g} IR, we obtain the symmetrized-product decomposition:

$$[\otimes_{j=1}^2 E_{2g}]_s = A_{1g} \oplus E_{4g}, \quad (178)$$

$$[\otimes_{j=1}^3 E_{2g}]_s = E_{2g} \oplus E_{4g}, \quad (179)$$

$$[\otimes_{j=1}^4 E_{2g}]_s = A_{1g} \oplus E_{2g} \oplus E_{4g}, \quad (180)$$

$$[\otimes_{j=1}^5 E_{2g}]_s = A_{1g} \oplus A_{2g} \oplus E_{2g} \oplus E_{4g}. \quad (181)$$

According to what was explained in the introduction of this section, the fifth-order invariant must be the leading-order term in the Landau expansion that is not proportional to the square of the doublet. Directly employing a fifth-order transformation condition, as an extension to Eq. (A9), one finds this invariant to be $|\mathbf{d}^{\text{ip}}|^5 \cos(5\gamma_{\text{ip}})$, and thus the nematic action becomes

$$\mathcal{S}_{\text{ip}} = \int_{\mathbf{x}} \{r_0 |\mathbf{d}^{\text{ip}}|^2 + u |\mathbf{d}^{\text{ip}}|^4 + v_5 |\mathbf{d}^{\text{ip}}|^5 \cos(5\gamma_{\text{ip}})\}, \quad (182)$$

which maps onto the Z_5 clock model. Minimization of the clock term gives with the fivefold-degenerate ground state

$$\gamma_{\text{ip}}^0 = \frac{\pi}{5} \left(\frac{1 + \text{sign} v_5}{2} \right) + \frac{2\pi}{5} n, \quad n \in \{0, 1, 2, 3, 4\}. \quad (183)$$

Moving on to the out-of-plane doublet \mathbf{d}^{op} , we note that it transforms as the E_{1g} IR, whose symmetrized product

decomposition is

$$[\otimes_{j=1}^2 E_{1g}]_s = A_{1g} \oplus E_{2g}, \quad (184)$$

$$[\otimes_{j=1}^3 E_{1g}]_s = E_{1g} \oplus E_{3g}, \quad (185)$$

$$[\otimes_{j=1}^4 E_{1g}]_s = A_{1g} \oplus E_{2g} \oplus E_{4g}, \quad (186)$$

$$[\otimes_{j=1}^5 E_{1g}]_s = B_{1g} \oplus B_{2g} \oplus E_{1g} \oplus E_{3g}, \quad (187)$$

$$[\otimes_{j=1}^6 E_{1g}]_s = A_{1g} \oplus E_{2g} \oplus 2E_{4g}. \quad (188)$$

Similarly to the case of the dodecagonal point group D_{12h} , only powers of $|\mathbf{d}^{\text{op}}|^2$ occur up to sixth-order. Following the same steps as in that case, we obtain the clock term from the product of the fifth-order product-decomposition elements B_{1g} and B_{2g} :

$$B_{1g}: |\mathbf{d}^{\text{op}}|^5 \cos(5\gamma_{\text{op}}), \quad B_{2g}: |\mathbf{d}^{\text{op}}|^5 \sin(5\gamma_{\text{op}}),$$

yielding

$$\mathcal{S}_{\text{op}} = \int_{\mathbf{x}} \{r_0 |\mathbf{d}^{\text{op}}|^2 + u |\mathbf{d}^{\text{op}}|^4 + v_{10} |\mathbf{d}^{\text{op}}|^{10} \cos(10\gamma_{\text{op}})\}. \quad (189)$$

We therefore find \mathbf{d}^{op} to be a Z_{10} clock nematic order parameter, whose tenfold degenerate ground states are given by

$$\gamma_{\text{op}}^0 = \frac{\pi}{10} \left(\frac{1 + \text{sign}v_{10}}{2} \right) + \frac{2\pi}{10} n, \quad n \in \{0, 1, \dots, 9\}. \quad (190)$$

In Figs. 7(c) and 7(d), we show the distorted Fermi surfaces obtained from expressing Eqs. (183) and (190) in the (nml) representation. The Fermi surface properties are analogous to the dodecagonal case, except that the in-plane high-symmetry directions are those associated with tenfold rotational symmetry.

C. Octagonal quasicrystals

The analysis of the octagonal point groups $\{D_{8h}, D_8, C_{8v}, D_{4d}, C_{8h}, C_8, S_8\}$ mirrors the analyses of the previous two subsections for the dodecagonal and decagonal quasicrystals. Considering the point group D_{8h} for concreteness, we note that \mathbf{d}^{ip} and \mathbf{d}^{op} transform as E_{2g} and E_{1g} , respectively. Performing the symmetrized product decomposition for E_{2g} gives

$$[\otimes_{j=1}^2 E_{2g}]_s = A_{1g} \oplus B_{1g} \oplus B_{2g}, \quad (191)$$

$$[\otimes_{j=1}^3 E_{2g}]_s = 2E_{2g}, \quad (192)$$

$$[\otimes_{j=1}^4 E_{2g}]_s = 2A_{1g} \oplus A_{2g} \oplus B_{1g} \oplus B_{2g}. \quad (193)$$

Using the bilinears

$$D^{B_{1g}} = |\mathbf{d}^{\text{ip}}|^2 \cos(2\gamma_{\text{ip}}), \quad D^{B_{2g}} = |\mathbf{d}^{\text{ip}}|^2 \sin(2\gamma_{\text{ip}}), \quad (194)$$

it is straightforward to construct the three invariants up to quartic order, $|\mathbf{d}^{\text{ip}}|^2$, $|\mathbf{d}^{\text{ip}}|^4$ and $(D^{B_{1g}})^2 - (D^{B_{2g}})^2$. We therefore obtain the Landau expansion of the Z_4 clock model:

$$\mathcal{S}_{\text{ip}} = \int_{\mathbf{x}} \{r_0 |\mathbf{d}^{\text{ip}}|^2 + u |\mathbf{d}^{\text{ip}}|^4 + v_4 |\mathbf{d}^{\text{ip}}|^4 \cos(4\gamma_{\text{ip}})\}, \quad (195)$$

which has the fourfold-degenerate ground state:

$$\gamma_{\text{ip}}^0 = \frac{\pi}{4} \left(\frac{1 + \text{sign}v_4}{2} \right) + \frac{2\pi}{4} n, \quad n \in \{0, 1, 2, 3\}, \quad (196)$$

see also Eq. (148).

Considering now the out-of-plane doublet \mathbf{d}^{op} , the symmetrized product decomposition of E_{1g} to sixth-order only gives invariants that are powers of $|\mathbf{d}^{\text{op}}|^2$:

$$[\otimes_{j=1}^2 E_{1g}]_s = A_{1g} \oplus E_{2g}, \quad (197)$$

$$[\otimes_{j=1}^3 E_{1g}]_s = E_{1g} \oplus E_{3g}, \quad (198)$$

$$[\otimes_{j=1}^4 E_{1g}]_s = A_{1g} \oplus B_{1g} \oplus B_{2g} \oplus E_{2g}, \quad (199)$$

$$[\otimes_{j=1}^5 E_{1g}]_s = E_{1g} \oplus 2E_{3g}, \quad (200)$$

$$[\otimes_{j=1}^6 E_{1g}]_s = A_{1g} \oplus B_{1g} \oplus B_{2g} \oplus 2E_{2g}. \quad (201)$$

Analogously to the case of the dodecagonal and decagonal quasicrystals, it is straightforward to find the leading-order anisotropic term, this time from the product of the quartic combinations:

$$B_{1g}: |\mathbf{d}^{\text{op}}|^4 \cos(4\gamma_{\text{op}}), \quad B_{2g}: |\mathbf{d}^{\text{op}}|^4 \sin(4\gamma_{\text{op}}).$$

Hence, we find the nematic action

$$\mathcal{S}_{\text{op}} = \int_{\mathbf{x}} \{r_0 |\mathbf{d}^{\text{op}}|^2 + u |\mathbf{d}^{\text{op}}|^4 + v_8 |\mathbf{d}^{\text{op}}|^8 \cos(8\gamma_{\text{op}})\}, \quad (202)$$

corresponding to the Z_8 clock model. The directions of \mathbf{d}^{op} that minimize the action are eightfold degenerate:

$$\gamma_{\text{op}}^0 = \frac{\pi}{8} \left(\frac{1 + \text{sign}v_8}{2} \right) + \frac{2\pi}{8} n, \quad n \in \{0, 1, \dots, 7\}. \quad (203)$$

The same results hold for $\{D_8, C_{8v}, D_{4d}\}$, whereas in the groups $\{C_{8h}, C_8, S_8\}$, the clock terms in the nematic actions of \mathbf{d}^{ip} and \mathbf{d}^{op} acquire an offset angle of the form (95).

The (nml) representation of the in-plane and out-of-plane nematic doublets (196) and (203) is represented in Figs. 7(e) and 7(f) via the corresponding distortions of the Fermi surface. The high-symmetry in-plane directions associated with the eightfold symmetry of the quasicrystal are highlighted in the figure.

D. Twisted quasicrystals

The rapid advances in the field of twistronics opened a new path to investigate the properties of emergent quasicrystals created by twisting 2D materials. In some cases, the twisted structure is an incommensurate lattice that, however, retains a crystallographic point group. This is the case of twisted bilayer graphene with a noncommensurate twist angle, although the effects of quasiperiodicity are dramatically enhanced when three graphene layers are twisted by two different angles, as shown recently in Ref. [85]. Interestingly, this work reported the emergence of robust superconductivity in this quasiperiodic structure. Most recently, three-fold rotational symmetry breaking consistent with nematicity was observed in similar moiré of moiré structures in Ref. [117]. In what concerns electronic nematicity, as long as the point

group is the same as a crystallographic one, the results derived in Sec. IV can be directly applied.

An alternative route to realize twisted quasicrystals, as shown in Refs. [94,95], is to start with two identical 2D materials described by the (planar) crystallographic point group D_n (with $n = 2, 3, 4, 6$). Upon twisting the two crystals by a relative angle of π/n with respect to their common z axis, the resulting structure becomes invariant under an n -fold rotation about z followed by a horizontal mirror reflection (which maps one layer onto the other). This is nothing but the improper rotation element S_{2nz} . Comparing Eqs. (74) and (77), we conclude that the twisted bilayer is actually a quasiperiodic “lattice” with point group D_{nd} , i.e. $D_n \xrightarrow{\text{twist}} D_{nd}$. Experimentally, both twisted bilayer graphene with a twist angle of 30° and twisted bilayer cuprate with a twist angle of 45° have been realized [92,96].

While much of the recent interest in these constructions have focused on realizing time-reversal symmetry-breaking superconductivity [93–95], it has been recently pointed out that electronic nematicity can be strongly impacted by the enhanced symmetry of the twisted bilayer [59]. Here, we further explore this idea by discussing the properties of the in-plane nematic order parameter \mathbf{d}^{ip} in the four cases of π/n twisted bilayers ($n = 2, 3, 4, 6$).

The point group in the cases $n = 2$ and $n = 3$ remain crystallographic, $D_2 \xrightarrow{\text{twist}} D_{2d}$ and $D_3 \xrightarrow{\text{twist}} D_{3d}$. There is, however, one important difference. While D_3 and D_{3d} both belong to the trigonal crystal system, D_2 and D_{2d} belong to different systems—monoclinic and orthorhombic, respectively. In terms of the components of $\mathbf{d}^{\text{ip}} = (d_2, d_5)^T$, this means that while in D_2 only the shear component d_5 transforms nontrivially, in D_{2d} both components transform nontrivially as two different one-dimensional IRs—see Table I. Therefore, twisting two monoclinic layers by 90° opens up a new nematic instability channel.

For two tetragonal layers twisted by 45° ($n = 4$), the twisted bilayer has a noncrystallographic octagonal point group, $D_4 \xrightarrow{\text{twist}} D_{4d}$ [93]. Using the results above, we see that the two components of the in-plane nematic doublet \mathbf{d}^{ip} change from transforming as the one-dimensional IRs B_1 and B_2 of D_4 in each layer to transforming as a single two-dimensional IR E_2 of D_{4d} in the twisted bilayer. Therefore, the character of the nematic transition changes from Z_2 Ising for the individual tetragonal layers to Z_4 clock for the coupled 45° twisted bilayer. As discussed in the end of Sec. IV A, the 2D four-state clock model (which has the same properties as the 2D Ashkin-Teller model) undergoes a transition from the disordered to the ordered phase that can be understood as the merging of the two BKT transitions of the q -state clock model as $q \rightarrow 4^+$. Because of its unique character, the exponents of this transition are nonuniversal and depend on g_{ip} , except for the anomalous exponent $\eta = 1/4$. Since electronic nematicity is observed in tetragonal cuprates and iron pnictides or chalcogenides [43,44], this setting offers an interesting path to realize Ashkin-Teller nematicity.

Finally, the case of two hexagonal layers twisted by 30° ($n = 6$) corresponds to $D_6 \xrightarrow{\text{twist}} D_{6d}$ and was investigated in Ref. [59]. The outcome, which follows from the nematic properties of dodecagonal quasicrystals, is that while the

uncoupled layers undergo a second-order nematic transition in the 2D three-state Z_3 Potts (which is equivalent to the Z_3 clock) universality class (see Table I), the coupled 30° twisted bilayer undergoes two BKT transitions: the higher one from the disordered to the critical phase (where there is only quasi-long-range nematic order) and the lower one from the critical phase to the long-range ordered nematic phase.

VI. DISCUSSION AND SUMMARY

In summary, in this paper we derived the properties of electronic nematic order in all 32 crystallographic point groups and in the noncrystallographic point groups associated with quasicrystals. We expressed the Fermi surface distortion patterns caused by nematic order in terms of a general three-dimensional nematic order parameter expressed in tensorial form in Eq. (11) and in five-component vectorial form in Eq. (14). We also established the critical properties of the allowed nematic transitions in these point groups. These latter results are summarized in two tables: Table I, for crystallographic point groups, and Table II, for the point groups of quasicrystals.

The crystallographic point groups shown in Table I are organized in six blocks corresponding to the cubic, hexagonal, trigonal, tetragonal, orthorhombic and monoclinic crystal systems; we do not show the triclinic crystal system since it does not support any nematic transition. For each point group in the first column, we list all nematic order parameters that transform as a nontrivial irreducible representation (IR, second column), together with the corresponding basis for that order parameter (third column). The possible basis are: the full five-component nematic order parameter $\mathbf{d} = (d_1, d_2, d_3, d_4, d_5)^T$, whose elements correspond, respectively, to the usual charge quadrupolar order parameters $d_{\frac{1}{\sqrt{3}}(2z^2-x^2-y^2)}$, $d_{x^2-y^2}$, d_{2yz} , d_{2xz} , and d_{2xy} ; the E_g and T_{2g} cubic bases $\mathbf{d}^e = (d_1, d_2)^T$ and $\mathbf{d}^t = (d_3, d_4, d_5)^T$; and the in-plane and out-of-plane axial bases $\mathbf{d}^{\text{ip}} = (d_2, d_5)^T$, and $\mathbf{d}^{\text{op}} = (d_3, d_4)^T$. Curly brackets indicate that the enclosed nematic order parameters transform as the same IR. The fourth column lists the universality class of the respective nematic Landau expansion: Z_2 Ising [e.g., Eq. (141)]; Z_3 clock, which is equivalent to Z_3 Potts [e.g., Eq. (68) and (102)]; Z_4 Potts [e.g., Eq. (60)]; Z_4 clock [e.g., Eq. (148)]; and Z_6 clock [e.g., Eq. (110)]. The asterisk notation in Z_q^* clock indicates that the clock term has an offset angle [e.g., Eq. (E5)], which is always the case when the group lacks twofold in-plane rotation axes and the nematic order parameter transforms as a complex IR (which is indicated by an overbar in the second column). The fifth column shows the residual point group (PG) after the onset of nematic order, which indicates the set of symmetry elements that remain intact after nematicity is established.

Finally, in the last column of Table I, we list the transformation matrices of the nematic order parameters expressed in terms of the transformation matrices of the coordinate vector. To understand what this entails, consider first the five-component nematic order parameter \mathbf{d} . It transforms according to the IR $\Gamma_{j=2}^+$ of the fully-isotropic orthogonal group $O(3)$, and therefore transforms with the 5×5 matrices $\mathcal{R}_{+,j=2}(g) = \mathcal{R}_{j=2}(\vartheta, \hat{\ell}) = \exp(-i\vartheta \mathbf{J}^{(2)} \cdot \hat{\ell})$, where

TABLE I. Symmetry properties of the allowed nematic order parameters in all crystallographic point groups (PG). The columns list the corresponding irreducible representation (IR), the relevant nematic basis vector (see main text for the definition), the universality class of the corresponding Landau expansion, the residual PG, and the transformation matrices (see main text). Note that the Z_3 clock and Z_3 Potts models have the same properties. The Z_q^* clock model has the same form as the Z_q clock model, except that the clock term has a nonuniversal offset angle. The overbar over the IR denotes a complex IR.

cubic						tetragonal					
IR	nem. basis	universality	res. PG	transf. matrix		IR	nem. basis	universality	res. PG	transf. matrix	
O_h	E_g	d^e	Z_3 -Potts	D_{4h}		D_{4h}	B_{1g}	$d_{x^2-y^2}$	Z_2 -Ising	D_{2h}	
	T_{2g}	d^t	Z_4 -Potts	D_{3d}	$\mathcal{R}_g^{A_{2u}}\mathcal{R}_g^{(3)}$		B_{2g}	d_{2xy}	Z_2 -Ising	D_{2h}	
O	E	d^e	Z_3 -Potts	D_4			E_g	d^{op}	Z_4 -clock	C_{2h}	$\mathcal{R}_g^{A_{1u}}\sigma^z\mathcal{R}_g^{(2)}\sigma^z$
	T_2	d^t	Z_4 -Potts	D_3	$\mathcal{R}_g^{A_2}\mathcal{R}_g^{(3)}$	D_4	B_1	$d_{x^2-y^2}$	Z_2 -Ising	D_2	
T_d	E	d^e	Z_3 -Potts	D_{2d}			B_2	d_{2xy}	Z_2 -Ising	D_2	
	T_2	d^t	Z_4 -Potts	C_{3v}	$\mathcal{R}_g^{(3)}$		E	d^{op}	Z_4 -clock	C_2	$\sigma^z\mathcal{R}_g^{(2)}\sigma^z$
T_h	\bar{E}_g	d^e	Z_3^* -Potts	D_{2h}		C_{4v}	B_1	$d_{x^2-y^2}$	Z_2 -Ising	C_{2v}	
	T_g	d^t	Z_4 -Potts	S_6	$\mathcal{R}_g^{A_u}\mathcal{R}_g^{(3)}$		B_2	d_{2xy}	Z_2 -Ising	C_{2v}	
T	\bar{E}	d^e	Z_3^* -Potts	D_2			E	d^{op}	Z_4 -clock	C_s	$\sigma^x\mathcal{R}_g^{(2)}\sigma^x$
	T	d^t	Z_4 -Potts	C_3	$\mathcal{R}_g^{(3)}$	D_{2d}	B_1	$d_{x^2-y^2}$	Z_2 -Ising	D_2	
hexagonal							B_2	d_{2xy}	Z_2 -Ising	C_{2v}	
D_{6h}	E_{2g}	d^{ip}	Z_3 -clock	D_{2h}	$\mathcal{R}_g^{B_{1u}}\sigma^z\mathcal{R}_g^{(2)}\sigma^z$		E	d^{op}	Z_4 -clock	C_2/C_s	$\mathcal{R}_g^{(2)}$
	E_{1g}	d^{op}	Z_6 -clock	C_{2h}	$\mathcal{R}_g^{A_{1u}}\sigma^z\mathcal{R}_g^{(2)}\sigma^z$	C_{4h}	B_g	$\{d_{x^2-y^2}, d_{2xy}\}$	Z_2^* -Ising	C_{2h}	
D_6	E_2	d^{ip}	Z_3 -clock	D_2	$\mathcal{R}_g^{B_1}\sigma^z\mathcal{R}_g^{(2)}\sigma^z$		\bar{E}_g	d^{op}	Z_4^* -clock	C_i	$\mathcal{R}_g^{A_u}\sigma^x\mathcal{R}_g^{(2)}\sigma^x$
	E_1	d^{op}	Z_6 -clock	C_2	$\sigma^z\mathcal{R}_g^{(2)}\sigma^z$		C_4	B	$\{d_{x^2-y^2}, d_{2xy}\}$	C_2	
D_{3h}	E'	d^{ip}	Z_3 -clock	C_{2v}	$\sigma^z\mathcal{R}_g^{(2)}\sigma^z$		\bar{E}	d^{op}	Z_4^* -clock	C_1	$\sigma^x\mathcal{R}_g^{(2)}\sigma^x$
	E''	d^{op}	Z_6 -clock	C_2	$\mathcal{R}_g^{A_1''}\sigma^z\mathcal{R}_g^{(2)}\sigma^z$		S_4	B	$\{d_{x^2-y^2}, d_{2xy}\}$	C_2	
C_{6v}	E_2	d^{ip}	Z_3 -clock	C_{2v}	$\mathcal{R}_g^{B_2}\sigma^x\mathcal{R}_g^{(2)}\sigma^x$		\bar{E}	d^{op}	Z_4^* -clock	C_1	$\mathcal{R}_g^{(2)}$
	E_1	d^{op}	Z_6 -clock	C_s	$\sigma^x\mathcal{R}_g^{(2)}\sigma^x$	orthorhombic					
C_{6h}	\bar{E}_{2g}	d^{ip}	Z_3^* -clock	C_{2h}	$\mathcal{R}_g^{B_u}\sigma^z\mathcal{R}_g^{(2)}\sigma^z$	D_{2h}	B_{1g}	d_{2xy}	Z_2 -Ising	C_{2h}	
	\bar{E}_{1g}	d^{op}	Z_6^* -clock	C_i	$\mathcal{R}_g^{A_u}\sigma^z\mathcal{R}_g^{(2)}\sigma^z$		B_{2g}	d_{2xz}	Z_2 -Ising	C_{2h}	
C_{3h}	\bar{E}'	d^{ip}	Z_3^* -clock	C_s	$\sigma^z\mathcal{R}_g^{(2)}\sigma^z$		B_{3g}	d_{2yz}	Z_2 -Ising	C_{2h}	
	\bar{E}''	d^{op}	Z_6^* -clock	C_1	$\mathcal{R}_g^{A''}\sigma^z\mathcal{R}_g^{(2)}\sigma^z$	D_2	B_1	d_{2xy}	Z_2 -Ising	C_2	
C_6	\bar{E}_2	d^{ip}	Z_3 -clock	C_2	$\mathcal{R}_g^B\sigma^z\mathcal{R}_g^{(2)}\sigma^z$		B_2	d_{2xz}	Z_2 -Ising	C_2	
	\bar{E}_1	d^{op}	Z_6^* -clock	C_1	$\sigma^z\mathcal{R}_g^{(2)}\sigma^z$		B_3	d_{2yz}	Z_2 -Ising	C_2	
trigonal						C_{2v}	A_2	d_{2xy}	Z_2 -Ising	C_2	
D_{3d}	E_g	$\{d^{ip}, d^{op}\}$	Z_3 -clock	C_{2h}	$\mathcal{R}_g^{A_{1u}}\sigma^z\mathcal{R}_g^{(2)}\sigma^z$		B_1	d_{2xz}	Z_2 -Ising	C_s	
	D_3	E	$\{d^{ip}, d^{op}\}$	Z_3 -clock	$\sigma^z\mathcal{R}_g^{(2)}\sigma^z$		B_2	d_{2yz}	Z_2 -Ising	C_s	
C_{3v}	E	$\{d^{ip}, d^{op}\}$	Z_3 -clock	C_s	$\sigma^x\mathcal{R}_g^{(2)}\sigma^x$	monoclinic					
	S_6	\bar{E}_g	$\{d^{ip}, d^{op}\}$	Z_3^* -clock	$\mathcal{R}_g^{A_u}\sigma^z\mathcal{R}_g^{(2)}\sigma^z$	C_{2h}	B_g	$\{d_{2xz}, d_{2yz}\}$	Z_2 -Ising	C_i	
	C_3	\bar{E}	$\{d^{ip}, d^{op}\}$	Z_3^* -clock	$\sigma^z\mathcal{R}_g^{(2)}\sigma^z$	$C_{1h} \equiv C_s$	A''	$\{d_{2xz}, d_{2yz}\}$	Z_2 -Ising	C_1	
						C_2	B	$\{d_{2xz}, d_{2yz}\}$	Z_2 -Ising	C_1	

TABLE II. Symmetry properties of the allowed nematic order parameters in noncrystallographic point groups (PGs) describing quasicrystals. The columns represent the same quantities as those in Table I.

octagonal	IR	nem. basis	universality	res. PG	transf. matrix
D _{8h}	E _{2g}	d ^{ip}	Z ₄ -clock	D _{2h}	
	E _{1g}	d ^{op}	Z ₈ -clock	C _{2h}	$\mathcal{R}_g^{A_{1u}} \sigma^z \mathcal{R}_g^{(2)} \sigma^z$
D ₈	E ₂	d ^{ip}	Z ₄ -clock	D ₂	
	E ₁	d ^{op}	Z ₈ -clock	C ₂	$\sigma^z \mathcal{R}_g^{(2)} \sigma^z$
C _{8v}	E ₂	d ^{ip}	Z ₄ -clock	C _{2v}	
	E ₁	d ^{op}	Z ₈ -clock	C _s	$\sigma^x \mathcal{R}_g^{(2)} \sigma^x$
D _{4d}	E ₂	d ^{ip}	Z ₄ -clock	D ₂ /C _{2v}	
	E ₃	d ^{op}	Z ₈ -clock	C ₂ /C _s	$\mathcal{R}_g^{B_1} \sigma^z \mathcal{R}_g^{(2)} \sigma^z$
C _{8h}	\bar{E}_{2g}	d ^{ip}	Z ₄ [*] -clock	C _{2h}	
	\bar{E}_{1g}	d ^{op}	Z ₈ [*] -clock	C _i	$\mathcal{R}_g^{A_u} \sigma^z \mathcal{R}_g^{(2)} \sigma^z$
C ₈	\bar{E}_2	d ^{ip}	Z ₄ [*] -clock	C ₂	
	\bar{E}_1	d ^{op}	Z ₈ [*] -clock	C ₁	$\sigma^z \mathcal{R}_g^{(2)} \sigma^z$
S ₈	\bar{E}_2	d ^{ip}	Z ₄ [*] -clock	C ₂	
	\bar{E}_3	d ^{op}	Z ₈ [*] -clock	C ₁	$\mathcal{R}_g^B \sigma^z \mathcal{R}_g^{(2)} \sigma^z$
decagonal	IR	nem. basis	universality	res. PG	transf. matrix
D _{10h}	E _{2g}	d ^{ip}	Z ₅ -clock	D _{2h}	
	E _{1g}	d ^{op}	Z ₁₀ -clock	C _{2h}	$\mathcal{R}_g^{A_{1u}} \sigma^z \mathcal{R}_g^{(2)} \sigma^z$
D ₁₀	E ₂	d ^{ip}	Z ₅ -clock	D ₂	
	E ₁	d ^{op}	Z ₁₀ -clock	C ₂	$\sigma^z \mathcal{R}_g^{(2)} \sigma^z$
D _{5h}	E _{2'}	d ^{ip}	Z ₅ -clock	C _{2v}	
	E _{1''}	d ^{op}	Z ₁₀ -clock	C ₂ /C _s	$\mathcal{R}_g^{A_1'} \sigma^z \mathcal{R}_g^{(2)} \sigma^z$
C _{10v}	E ₂	d ^{ip}	Z ₅ -clock	C _{2v}	
	E ₁	d ^{op}	Z ₁₀ -clock	C _s	$\sigma^x \mathcal{R}_g^{(2)} \sigma^x$
dodecagonal	IR	nem. basis	universality	res. PG	transf. matrix
D _{12h}	E _{2g}	d ^{ip}	Z ₆ -clock	D _{2h}	
	E _{1g}	d ^{op}	Z ₁₂ -clock	C _{2h}	$\mathcal{R}_g^{A_{1u}} \sigma^z \mathcal{R}_g^{(2)} \sigma^z$
D ₁₂	E ₂	d ^{ip}	Z ₆ -clock	D ₂	
	E ₁	d ^{op}	Z ₁₂ -clock	C ₂	$\sigma^z \mathcal{R}_g^{(2)} \sigma^z$
C _{12v}	E ₂	d ^{ip}	Z ₆ -clock	C _{2v}	
	E ₁	d ^{op}	Z ₁₂ -clock	C _s	$\sigma^x \mathcal{R}_g^{(2)} \sigma^x$
D _{6d}	E ₂	d ^{ip}	Z ₆ -clock	D ₂ /C _{2v}	
	E ₅	d ^{op}	Z ₁₂ -clock	C ₂ /C _s	$\mathcal{R}_g^{B_1} \sigma^z \mathcal{R}_g^{(2)} \sigma^z$
C _{12h}	\bar{E}_{2g}	d ^{ip}	Z ₆ [*] -clock	C _{2h}	
	\bar{E}_{1g}	d ^{op}	Z ₁₂ [*] -clock	C _i	$\mathcal{R}_g^{A_u} \sigma^z \mathcal{R}_g^{(2)} \sigma^z$
C ₁₂	\bar{E}_2	d ^{ip}	Z ₆ [*] -clock	C ₂	
	\bar{E}_1	d ^{op}	Z ₁₂ [*] -clock	C ₁	$\sigma^z \mathcal{R}_g^{(2)} \sigma^z$
S ₁₂	\bar{E}_2	d ^{ip}	Z ₆ [*] -clock	C ₂	
	\bar{E}_5	d ^{op}	Z ₁₂ [*] -clock	C ₁	$\mathcal{R}_g^B \sigma^z \mathcal{R}_g^{(2)} \sigma^z$
icosahedral	IR	nem. basis	universality	res. PG	transf. matrix
I _h	H _g	d		D _{3d} /D _{5d}	
I	H	d		D ₃ /D ₅	

$g = (\vartheta, \hat{\ell}, \mathcal{I})$ are the symmetry elements of O(3), see Appendix A for more details. Moving from isotropic space to point groups has two effects: first, it restricts the symmetry elements g to the discrete set of operations that characterize the group. Second, it causes the nematic order parameter to be decomposed into different irreducible channels. Accordingly, in the point groups, the 5×5 matrices $\mathcal{R}_{+,j=2}(g)$ assume a block-diagonal form, where each block is labeled by the IR characterizing the nematic order parameter. For one-dimensional IRs, one simply recovers the characters of the respective IR. For multidimensional IRs, the transformation matrices appear as blocks constructed from $\mathcal{R}_{+,j=2}(g)$. In

particular, for the four multicomponent nematic bases \mathbf{d}^e , \mathbf{d}^i , \mathbf{d}^{ip} , and \mathbf{d}^{op} used here, we have:

$$\mathcal{R}_{\mathbf{d}^e}(g) = \begin{pmatrix} [\mathcal{R}_{+,j=2}(g)]_{11} & [\mathcal{R}_{+,j=2}(g)]_{12} \\ [\mathcal{R}_{+,j=2}(g)]_{21} & [\mathcal{R}_{+,j=2}(g)]_{22} \end{pmatrix}, \quad (204)$$

$$\mathcal{R}_{\mathbf{d}^i}(g) = \begin{pmatrix} [\mathcal{R}_{+,j=2}(g)]_{33} & [\mathcal{R}_{+,j=2}(g)]_{34} & [\mathcal{R}_{+,j=2}(g)]_{35} \\ [\mathcal{R}_{+,j=2}(g)]_{43} & [\mathcal{R}_{+,j=2}(g)]_{44} & [\mathcal{R}_{+,j=2}(g)]_{45} \\ [\mathcal{R}_{+,j=2}(g)]_{53} & [\mathcal{R}_{+,j=2}(g)]_{54} & [\mathcal{R}_{+,j=2}(g)]_{55} \end{pmatrix}, \quad (205)$$

$$\mathcal{R}_{\mathbf{d}^{ip}}(g) = \begin{pmatrix} [\mathcal{R}_{+,j=2}(g)]_{22} & [\mathcal{R}_{+,j=2}(g)]_{25} \\ [\mathcal{R}_{+,j=2}(g)]_{52} & [\mathcal{R}_{+,j=2}(g)]_{55} \end{pmatrix}, \quad (206)$$

$$\mathcal{R}_{d^{\text{op}}}(g) = \begin{pmatrix} [\mathcal{R}_{+,j=2}(g)]_{33} & [\mathcal{R}_{+,j=2}(g)]_{34} \\ [\mathcal{R}_{+,j=2}(g)]_{43} & [\mathcal{R}_{+,j=2}(g)]_{44} \end{pmatrix}. \quad (207)$$

In principle, we could simply use these matrices to define the transformation properties of the nematic order parameters listed in the table. However, to construct invariants involving the coupling between the nematic order parameter and other physical quantities, it is often more convenient to express these four nematic transformation matrices (204)–(207) in terms of transformation matrices of the coordinate vector. The latter transforms according to the IR $\Gamma_{j=1}^-$ of $O(3)$. As a result, its transformation matrices for any symmetry element $g = (\vartheta, \hat{\ell}, \mathcal{I})$ of $O(3)$ are given by

$$\mathcal{R}_g^{(3)} = \mathcal{R}_{-,j=1}(g), \quad (208)$$

$$\mathcal{R}_g^{(2)} = \begin{pmatrix} [\mathcal{R}_{-,j=1}(g)]_{11} & [\mathcal{R}_{-,j=1}(g)]_{12} \\ [\mathcal{R}_{-,j=1}(g)]_{21} & [\mathcal{R}_{-,j=1}(g)]_{22} \end{pmatrix}, \quad (209)$$

where $\mathcal{R}_{-,j=1}(g) = \mathcal{I}\mathcal{R}_{j=1}(\vartheta, \hat{\ell})$ and $\mathcal{R}_{j=1}(\vartheta, \hat{\ell}) = \exp(-i\vartheta \mathbf{J}^{(1)} \cdot \hat{\ell})$, see Eq. (A4) in Appendix A. Here, we introduced two different matrices to distinguish between the cases of a 3D vector, which transforms with $\mathcal{R}_g^{(3)}$ (208) and is relevant for the polyhedral point groups, and a 2D in-plane vector, which transforms with $\mathcal{R}_g^{(2)}$ (209) and is relevant for the axial point groups. The key point illustrated by the last column of Table I is that, for most of the nematic order parameters, the transformation matrices (204)–(207) can be directly related to either $\mathcal{R}_g^{(3)}$ or $\mathcal{R}_g^{(2)}$. For instance, for the nematic order parameter that transforms as the T_{2g} IR of O_h , the last entry on the row means that $\mathcal{R}_{d^i}(g) = \mathcal{R}_g^{A_{2u}} \mathcal{R}_g^{(3)}$, where $\mathcal{R}_g^{A_{2u}}$ are the characters of the A_{2u} IR. Similarly, for the nematic order parameter transforming as the E IR of C_{4v} , we have $\mathcal{R}_{d^{\text{op}}}(g) = \sigma^x \mathcal{R}_g^{(2)} \sigma^x$, where σ^j are Pauli matrices.

To illustrate the usefulness of this representation of the transformation matrices, let us construct invariants involving the coupling between the nematic order parameters and the electric polarization \mathbf{P} , which transforms like a vector. To make the example more transparent, we consider the hexagonal point group C_{3h} and the nematic in-plane order parameter d^{ip} . This doublet transforms according to the IR E' and via the transformation matrix $\mathcal{R}_{d^{\text{ip}}}(g) = \sigma^z \mathcal{R}_g^{(2)} \sigma^z$, as shown in Table I. The in-plane polarization $\mathbf{P}_{\text{ip}} = (P_x, P_y)$, on the other hand, transforms according to the same IR E' , but via the matrices $\mathcal{R}^{\mathbf{P}_{\text{ip}}}(g) = \mathcal{R}_g^{(2)}$ that characterize a vector. Indeed, $\mathcal{R}^{\mathbf{P}_{\text{ip}}}(g)$ is related to $\mathcal{R}_{d^{\text{ip}}}(g)$ through a similarity transformation, the Pauli matrix σ^z . Since both d^{ip} and \mathbf{P}_{ip} transform as E' , there must exist a bilinear invariant. However, due to the difference in transformation matrices, this invariant is not simply $(d^{\text{ip}})^T \cdot \mathbf{P}_{\text{ip}}$, but instead it is $(d^{\text{ip}})^T \sigma^z \mathbf{P}_{\text{ip}}$, where the additional Pauli matrix σ^z is needed to compensate for the similarity transformation relating $\mathcal{R}^{\mathbf{P}_{\text{ip}}}(g)$ and $\mathcal{R}_{d^{\text{ip}}}(g)$. As a second example, consider the coupling between the nematic out-of-plane doublet d^{op} and the out-of-plane polarization P_z within the same point group C_{3h} . The nematic order parameter transforms according to the IR E'' and via the transformation matrix $\mathcal{R}_{d^{\text{op}}}(g) = \mathcal{R}_g^{A''} (\sigma^z \mathcal{R}_g^{(2)} \sigma^z)$, see Table I. The out-of-plane polarization P_z , on the other hand, transforms as A'' and via the 1×1 “matrix” $\mathcal{R}^{P_z}(g) = \mathcal{R}_g^{A''}$. Using the fact that \mathbf{P}_{ip}

transforms according to $\mathcal{R}_g^{(2)}$, we can readily construct the invariant $P_z (d^{\text{op}})^T \sigma^z \mathbf{P}_{\text{ip}}$.

Table II has the same layout as Table I, but refers to the quasicrystalline point groups considered in this work. They correspond to octagonal, decagonal, dodecagonal, and icosahedral quasicrystals.

The group-theoretical classification presented here can be valuable in searching for new nematic systems in material databases. More broadly, our results offer interesting insights into which types of lattice may realize exotic electronic nematic phenomena. Indeed, for any of the nematic doublets that behave as a Z_q clock order parameter with $q \geq 4$, the nematic transition in 3D belongs to the XY universality class, which in turn also describes the nematic transition of a 2D isotropic model. On the other hand, in a 2D system with a Z_q clock nematic order parameter, a critical nematic phase with quasi-long-range order precedes the onset of long-range order for $q \geq 5$, whereas for $q = 4$ one obtains an Ashkin-Teller nematic model, whose critical properties are described by nonuniversal critical exponents. From Tables I and II, we see that this condition is satisfied by (d_{2yz}, d_{2xz}) nematicity in hexagonal and tetragonal crystals, as well as (d_{2yz}, d_{2xz}) and $(d_{x^2-y^2}, d_{2xy})$ nematicity in octagonal, decagonal, and dodecagonal quasicrystals. In this regard, it will be interesting to investigate the properties of the Landau expansion (48) of the icosahedral nematic order parameter, since the mean-field ground states are either sixfold or tenfold degenerate.

Experimentally, these properties should be directly accessible via probes that measure the nematic susceptibility in different channels, such as elasto-resistance [9] and Raman spectroscopy [118]. Theoretically, one expects that nematic fluctuations will be enhanced near the 3D XY nematic transition, since there will be not only soft longitudinal (i.e., amplitude) fluctuations but also soft transverse (i.e., phase) fluctuations associated with the emergent continuous symmetry. Given that nematic fluctuations have been proposed as potential drivers of non-Fermi liquid behavior [49–51,69] and pairing [119,120], the investigation of emergent XY -nematicity could provide further insights into these problems as well. As for the exotic 2D behavior associated with $q \geq 4$ clock in-plane nematicity, the most promising realizations would be in 30° twisted hexagonal bilayers (Z_6 clock) and 45° twisted tetragonal bilayers (Z_4 clock). Both settings have been recently realized experimentally by twisting graphene [92] and monolayers of cuprate BSCCO [96]. Interestingly, nematic order has been observed in underdoped BSCCO [2].

One important ingredient that was not included in this paper and that deserves further investigation is the role of strain, both extrinsic and intrinsic. For instance, it was recently shown that the impact of uniaxial strain on in-plane Z_3 Potts (which is equivalent to the Z_3 clock) nematics is fundamentally different from the well-studied case of Ising-nematics [81]. This raises the broader question of how external strain can be used to probe and modify the behavior of Z_q clock nematic order parameters. Moreover, long-wavelength quantized strain fluctuations, which are manifested as acoustic phonons, are known to significantly change the critical properties of Z_2 and Z_3 electronic nematic transitions in tetragonal, hexagonal, and trigonal crystals by

promoting long-range nematic interactions [74,107,121–124]. It will be important to perform similar analyses in cubic crystals as well as quasicrystals, which also host phason modes on top of phonon modes [125,126]. Finally, crystalline defects such as dislocations, vacancies, and interstitials create inhomogeneous strain distributions, which act as random nematic conjugate fields [64,127,128]. While most studies have focused on a random-field Ising-model description of this rich phenomenon, it will be important to develop models that can capture the long-range and correlated nature of the various components of the strain fields generated by these defects.

ACKNOWLEDGMENTS

We thank T. Birol and J. Viñals for fruitful discussions. This work was primarily supported by the U. S. Department of Energy, Office of Science, Basic Energy Sciences, Materials Sciences and Engineering Division, under Award No. DE-SC0020045 (M.H., A.R., and R.M.F.). D.F.A. was supported by Department of Energy, Office of Basic Energy Science, Division of Materials Sciences and Engineering under Award No. DE-SC0021971.

APPENDIX A: GENERATORS OF SO(3) AND PARAMETRIZATION OF d

In this Appendix, we give further details about the generators of SO(3). Within the full rotation group SO(3), the transformation matrices associated with an irreducible representation (IR) Γ_j are given by $\mathcal{R}_j(\vartheta, \hat{\ell}) = \exp(-i\vartheta \mathbf{J}^{(j)} \cdot \hat{\ell})$, parametrized by a rotation angle ϑ around a unit-length

which can also be expressed in terms of the antisymmetric Levi-Civita tensor $(J_{\mu_1}^{(1)})_{\mu_2\mu_3} = -i\epsilon_{\mu_1\mu_2\mu_3}$. The three generators for $j = 2$ are given by

$$J_x^{(2)} = i \begin{pmatrix} 0 & 0 & \sqrt{3} & 0 & 0 \\ 0 & 0 & 1 & 0 & 0 \\ -\sqrt{3} & -1 & 0 & 0 & 0 \\ 0 & 0 & 0 & 0 & 1 \\ 0 & 0 & 0 & -1 & 0 \end{pmatrix}, \quad J_y^{(2)} = i \begin{pmatrix} 0 & 0 & 0 & -\sqrt{3} & 0 \\ 0 & 0 & 0 & 1 & 0 \\ 0 & 0 & 0 & 0 & -1 \\ \sqrt{3} & -1 & 0 & 0 & 0 \\ 0 & 0 & 1 & 0 & 0 \end{pmatrix}, \quad J_z^{(2)} = i \begin{pmatrix} 0 & 0 & 0 & 0 & 0 \\ 0 & 0 & 0 & 0 & -2 \\ 0 & 0 & 0 & 1 & 0 \\ 0 & 0 & -1 & 0 & 0 \\ 0 & 2 & 0 & 0 & 0 \end{pmatrix}, \quad (\text{A5})$$

and those for $j = 4$ are

$$J_x^{(4)} = \frac{i}{\sqrt{2}} \begin{pmatrix} 0 & 0 & 0 & 0 & 2\sqrt{5} & 0 & 0 & 0 & 0 \\ 0 & 0 & 2 & 0 & 0 & 0 & 0 & 0 & 0 \\ 0 & -2 & 0 & -\sqrt{7} & 0 & 0 & 0 & 0 & 0 \\ 0 & 0 & \sqrt{7} & 0 & 3 & 0 & 0 & 0 & 0 \\ -2\sqrt{5} & 0 & 0 & -3 & 0 & 0 & 0 & 0 & 0 \\ 0 & 0 & 0 & 0 & 0 & 0 & 3 & 0 & 0 \\ 0 & 0 & 0 & 0 & 0 & -3 & 0 & -\sqrt{7} & 0 \\ 0 & 0 & 0 & 0 & 0 & 0 & \sqrt{7} & 0 & 2 \\ 0 & 0 & 0 & 0 & 0 & 0 & 0 & -2 & 0 \end{pmatrix}, \quad (\text{A6})$$

rotation axis $\hat{\ell}$. The three generators $J_{\mu}^{(j)}$ satisfy the Lie algebra

$$[J_{\mu_1}^{(j)}, J_{\mu_2}^{(j)}] = i\epsilon_{\mu_1\mu_2\mu_3} J_{\mu_3}^{(j)}, \quad (\text{A1})$$

with the antisymmetric Levi-Civita tensor $\epsilon_{\mu_1\mu_2\mu_3}$. In principle, the matrices $J_{\mu}^{(j)}$ can be defined in the ‘‘Lie basis’’ using the standard relationships

$$\hat{J}_z^{(j)} |j, m\rangle = m |j, m\rangle, \quad (\text{A2})$$

$$\hat{J}_{\pm}^{(j)} |j, m\rangle = \sqrt{j(j+1) - m(m \pm 1)} |j, m \pm 1\rangle, \quad (\text{A3})$$

where $\hat{J}_{\pm}^{(j)} = \hat{J}_x^{(j)} \pm i\hat{J}_y^{(j)}$. However, for the transformation matrices to be orthogonal, i.e., $\mathcal{R}_j^T(\vartheta, \hat{\ell}) = \mathcal{R}_j(-\vartheta, \hat{\ell}) = \mathcal{R}_j^{-1}(\vartheta, \hat{\ell})$, one needs to impose the requirement $(J_{\mu}^{(j)})^T = (J_{\mu}^{(j)})^* = -J_{\mu}^{(j)}$, i.e., the generators need to be antisymmetric, and thus, a similarity transformation has to be applied on Eqs. (A2) and (A3). We now list the resulting generators. For $j = 0$ the three generators are $J_x^{(0)} = J_y^{(0)} = J_z^{(0)} = 0$, which ensures that a $\Gamma_{j=0}$ scalar is invariant under all rotations. For $j = 1$ the three generators are the well-known antisymmetric Gell-Mann matrices

$$J_x^{(1)} = i \begin{pmatrix} 0 & 0 & 0 \\ 0 & 0 & -1 \\ 0 & 1 & 0 \end{pmatrix}, \quad J_y^{(1)} = i \begin{pmatrix} 0 & 0 & 1 \\ 0 & 0 & 0 \\ -1 & 0 & 0 \end{pmatrix},$$

$$J_z^{(1)} = i \begin{pmatrix} 0 & -1 & 0 \\ 1 & 0 & 0 \\ 0 & 0 & 0 \end{pmatrix}, \quad (\text{A4})$$

$$J_y^{(4)} = \frac{i}{\sqrt{2}} \begin{pmatrix} 0 & 0 & 0 & 0 & 0 & -2\sqrt{5} & 0 & 0 & 0 \\ 0 & 0 & 0 & 0 & 0 & 0 & 0 & 2 & 0 \\ 0 & 0 & 0 & 0 & 0 & 0 & \sqrt{7} & 0 & -2 \\ 0 & 0 & 0 & 0 & 0 & 3 & 0 & -\sqrt{7} & 0 \\ 0 & 0 & 0 & 0 & 0 & 0 & -3 & 0 & 0 \\ 2\sqrt{5} & 0 & 0 & -3 & 0 & 0 & 0 & 0 & 0 \\ 0 & 0 & -\sqrt{7} & 0 & 3 & 0 & 0 & 0 & 0 \\ 0 & -2 & 0 & \sqrt{7} & 0 & 0 & 0 & 0 & 0 \\ 0 & 0 & 2 & 0 & 0 & 0 & 0 & 0 & 0 \end{pmatrix}, \quad (\text{A7})$$

$$J_z^{(4)} = i \begin{pmatrix} 0 & 0 & 0 & 0 & 0 & 0 & 0 & 0 & 0 \\ 0 & 0 & 0 & 0 & 0 & 0 & 0 & 0 & -4 \\ 0 & 0 & 0 & 0 & 0 & 0 & 0 & 3 & 0 \\ 0 & 0 & 0 & 0 & 0 & 0 & -2 & 0 & 0 \\ 0 & 0 & 0 & 0 & 0 & 1 & 0 & 0 & 0 \\ 0 & 0 & 0 & 0 & -1 & 0 & 0 & 0 & 0 \\ 0 & 0 & 0 & 2 & 0 & 0 & 0 & 0 & 0 \\ 0 & 0 & -3 & 0 & 0 & 0 & 0 & 0 & 0 \\ 0 & 4 & 0 & 0 & 0 & 0 & 0 & 0 & 0 \end{pmatrix}. \quad (\text{A8})$$

Clearly, the generators are never unique in the sense that they can always be rotated via an orthogonal matrix $O^{(j)}$ according to $[O^{(j)}]^T J^{(j)} O^{(j)}$, which corresponds to a basis rotation. Throughout this work, the generators are fixed according to Eqs. (A4)–(A8).

Next, we determine the bilinears $D^{j=2}$ and $D^{j=4}$ that occur in the decomposition (16) and which were used in the derivation of the Landau expansion of the 3D isotropic nematic system. The transformation conditions are structurally similar to Eq. (5). For example, for the $\Gamma_{j=4}^+$ bilinear $D^{j=4,v} = d_i \Lambda_{i,i'}^{j=4,v} d_{i'}$, one needs to solve the equation

$$\mathcal{R}_{+,j=2}^T(g) \Lambda^{j=4,v} \mathcal{R}_{+,j=2}(g) = \mathcal{R}_{+,j=4}(g)_{vv'} \Lambda^{j=4,v'}, \quad (\text{A9})$$

where $\Lambda^{j=4,v}$ are 5×5 -dimensional matrices with $i, i' = 1, \dots, 5$ and $v, v' = 1, \dots, 9$. Recall that the $\Gamma_{j=2}^+$ nematic order parameter \mathbf{d} transforms via the matrices $\mathcal{R}_{+,j=2}(g) = \mathcal{R}_{j=2}(\vartheta, \hat{\ell})$ for each element $g = (\vartheta, \hat{\ell}, \mathcal{I})$.

A straightforward but tedious calculation then yields $D^{j=0} = |\mathbf{d}|^2$, $D^{j=2}$ given by Eq. (19), and

$$D^{j=4} = \frac{\sqrt{5}}{6} \begin{pmatrix} \frac{1}{\sqrt{5}} [6d_1^2 - 4(d_3^2 + d_4^2) + (d_2^2 + d_5^2)] \\ \sqrt{7}(d_2^2 - d_5^2) \\ \sqrt{14}(d_2d_3 + d_4d_5) \\ 2\sqrt{3}d_1d_2 - 2(d_3^2 - d_4^2) \\ \sqrt{2}[(2\sqrt{3}d_1 + d_2)d_3 - d_4d_5] \\ \sqrt{2}[(2\sqrt{3}d_1 - d_2)d_4 - d_3d_5] \\ 2\sqrt{3}d_1d_5 + 4d_3d_4 \\ \sqrt{14}(d_2d_4 - d_3d_5) \\ 2\sqrt{7}d_2d_5 \end{pmatrix}. \quad (\text{A10})$$

Importantly, all three bilinears have the same magnitude, $(D^{j=0})^2 = (D^{j=2})^2 = (D^{j=4})^2 = |\mathbf{d}|^4$. From the condition (A9) we see that a basis rotation $O^{(j=4)}$ on the

generators $J^{(j=4)}$ would rotate the basis state $D^{j=4}$ (A10) into $O^{(j=4)} D^{j=4}$.

To finish this Appendix, we further discuss the parametrization of the five-component nematic order parameter within the (nml) representation (14). Recall that:

$$\mathbf{d} = \frac{|\mathbf{d}|}{\sqrt{3}} \left\{ \cos(\alpha) (n_\mu \lambda_{\mu\mu'}^{j=2} n_{\mu'}) + \cos\left(\alpha + \frac{2\pi}{3}\right) (m_\mu \lambda_{\mu\mu'}^{j=2} m_{\mu'}) \right. \\ \left. + \cos\left(\alpha + \frac{4\pi}{3}\right) (l_\mu \lambda_{\mu\mu'}^{j=2} l_{\mu'}) \right\}. \quad (\text{A11})$$

The three angles describing the three orthonormal eigenvectors $\mathbf{n}, \mathbf{m}, \mathbf{l}$ can be chosen in several ways. The parametrization employed in this work makes use of the spherical unit vectors

$$\hat{\mathbf{e}}_r = \begin{pmatrix} \cos \varphi \sin \theta \\ \sin \varphi \sin \theta \\ \cos \theta \end{pmatrix}, \quad \hat{\mathbf{e}}_\varphi = \begin{pmatrix} \sin \varphi \\ -\cos \varphi \\ 0 \end{pmatrix}, \quad \hat{\mathbf{e}}_\theta = \begin{pmatrix} \cos \varphi \cos \theta \\ \sin \varphi \cos \theta \\ -\sin \theta \end{pmatrix}. \quad (\text{A12})$$

One of the eigenvectors, e.g., \mathbf{l} , can always be chosen to be aligned with the radial vector $\hat{\mathbf{e}}_r$, i.e., $\mathbf{l} = \hat{\mathbf{e}}_r$. Conversely, the remaining two vectors can be arbitrarily rotated about this axis by an angle η :

$$\mathbf{l} = \hat{\mathbf{e}}_r, \quad \mathbf{n} = \cos \eta \hat{\mathbf{e}}_\varphi + \sin \eta \hat{\mathbf{e}}_\theta, \\ \mathbf{m} = -\sin \eta \hat{\mathbf{e}}_\varphi + \cos \eta \hat{\mathbf{e}}_\theta. \quad (\text{A13})$$

Thus, within the (nml) representation the five degrees of freedom are encoded in the magnitude $|\mathbf{d}|$ and the four angles $\alpha, \varphi, \theta, \eta$. To ensure a one-to-one mapping between the two representations, (9) and (11), the parameter ranges have to be

restricted according to¹

$$\begin{aligned} |\mathbf{d}| \geq 0, \quad \alpha \in \left[0, \frac{\pi}{3}\right], \quad \theta \in \left[0, \frac{\pi}{2}\right], \\ \varphi \in [0, 2\pi], \quad \eta \in [0, \pi]. \end{aligned} \quad (\text{A14})$$

APPENDIX B: SYMMETRIZED PRODUCTS

In this Appendix, we discuss in more detail the product decomposition associated with a generic order parameter $\boldsymbol{\eta} = (\eta_1, \dots, \eta_{\dim n})$ that transforms according to an IR n of some group. Because the order parameter components commute, i.e., $\eta_i \eta_j = \eta_j \eta_i$, the number of product components is reduced. For example, for a two-component order parameter $\boldsymbol{\eta} = (\eta_1, \eta_2)$ one would naively expect $2 \times 2 = 4$ product components, while in fact, there are only three: η_1^2 , η_2^2 , and $\eta_1 \eta_2$, since the antisymmetric combination $\eta_1 \eta_2 - \eta_2 \eta_1$ vanishes. Here, we use group theory to derive expressions for the product decompositions in the symmetric channel, see, e.g., Ref. [129]. Doing so automatically excludes vanishing contributions, such as the antisymmetric combination $\eta_1 \eta_2 - \eta_2 \eta_1$ in the above example, and removes redundancies associated with double counting. To illustrate the last point, consider the symmetrized bilinears in the above example: $N_1 = \eta_1^2 + \eta_2^2$ and $N_2 = (\eta_1^2 - \eta_2^2, 2\eta_1 \eta_2)$. Then, a straightforward decomposition would suggest that two invariants exist in fourth order, N_1^2 and $N_2 \cdot N_2$, while in fact they are identical since $N_1^2 = N_2 \cdot N_2 = (\eta_1^2 + \eta_2^2)^2$. Such double-countings are removed by using the symmetrized decomposition. As we are interested in Landau expansions, we consider products up to sixth order, but extension to higher orders is straightforward.

Let us begin with the second-order product $P_{2,ij} = \eta_i \eta_j$. Using the order-parameter transformation $\eta'_i = \mathcal{R}_n(g)_{ii'} \eta_{i'}$ under a symmetry element g , one finds the product to transform as

$$P'_{2,ij} = \mathcal{R}^{\eta^2}(g)_{ij,i'j'} P_{2,i'j'}, \quad (\text{B1})$$

where $\mathcal{R}^{\eta^2}(g)_{ij,i'j'} = \mathcal{R}_n(g)_{ii'} \mathcal{R}_n(g)_{jj'}$. The transformation matrices $\mathcal{R}^{\eta^2}(g)$ themselves form a representation of the group, i.e., it holds that $\mathcal{R}^{\eta^2}(g_1 g_2) = \mathcal{R}^{\eta^2}(g_1) \mathcal{R}^{\eta^2}(g_2)$, see, e.g., Ref. [129] for details. Correspondingly, the characters of this representation result from the trace,

$$\chi^{\eta^2}(g) = \sum_{i,j} \mathcal{R}^{\eta^2}(g)_{ij,ij} = \sum_{i,j} \mathcal{R}_n(g)_{ii} \mathcal{R}_n(g)_{jj} = \chi_n^2(g). \quad (\text{B2})$$

The formula (B2) contains all symmetry channels, including those that eventually vanish due to the commutativity of the components of $\boldsymbol{\eta}$. To have these removed, we symmetrize the transformation matrix $\mathcal{R}^{\eta^2}(g)$ before computing its character. Symmetrization involves the addition of all permutations in Eq. (B1) with respect to (i', j') , divided by the number of permutations, i.e.,

$$\mathcal{R}_s^{\eta^2}(g)_{ij,i'j'} = \frac{1}{2!} [\mathcal{R}^{\eta^2}(g)_{ij,i'j'} + \mathcal{R}^{\eta^2}(g)_{ij,j'i'}]. \quad (\text{B3})$$

¹For the limiting values of θ the rotation angles are actually more restricted: For $\theta = 0$ we constrain $\varphi \in [0, 0]$ and $\eta \in [0, \pi]$, and for $\theta = \pi/2$ we constrain $\varphi \in [0, 2\pi]$ and $\eta \in [0, \pi/2]$.

Then, the characters for the symmetrized product (B3) become

$$\chi_s^{\eta^2}(g) = \sum_{i,j} \mathcal{R}_s^{\eta^2}(g)_{ij,ij} = \frac{1}{2} [\chi_n^2(g) + \chi_n(g^2)]. \quad (\text{B4})$$

Thus, the decomposition of a symmetrized product (B4) only contains a subset of the original symmetry channels associated with the bare product (B2). The symmetrized decomposition is accomplished by using $\mathcal{R}_s^{\eta^2}(g)$ rather than $\mathcal{R}^{\eta^2}(g)$.

For the higher-order products such as $P_{3,ijk} = \eta_i \eta_j \eta_k$ and $P_{4,ijkl} = \eta_i \eta_j \eta_k \eta_l$, one proceeds analogously. As in the case above, the corresponding transformation matrices

$$\mathcal{R}^{\eta^3}(g)_{ijk,i'j'k'} = \mathcal{R}_n(g)_{ii'} \mathcal{R}_n(g)_{jj'} \mathcal{R}_n(g)_{kk'}, \quad (\text{B5})$$

$$\mathcal{R}^{\eta^4}(g)_{ijkl,i'j'k'l'} = \mathcal{R}_n(g)_{ii'} \mathcal{R}_n(g)_{jj'} \mathcal{R}_n(g)_{kk'} \mathcal{R}_n(g)_{ll'}, \quad (\text{B6})$$

form representations of the group with characters

$$\chi^{\eta^3}(g) = \sum_{ijk} \mathcal{R}^{\eta^3}(g)_{ijk,ijk} = \chi_n^3(g), \quad (\text{B7})$$

$$\chi^{\eta^4}(g) = \sum_{ijkl} \mathcal{R}^{\eta^4}(g)_{ijkl,ijkl} = \chi_n^4(g). \quad (\text{B8})$$

The symmetrized transformation matrices are

$$\mathcal{R}_s^{\eta^3}(g)_{ijk,i'j'k'} = \frac{1}{3!} [\mathcal{R}^{\eta^3}(g)_{ijk,i'j'k'} + 5(i' \leftrightarrow j' \leftrightarrow k')], \quad (\text{B9})$$

$$\begin{aligned} \mathcal{R}_s^{\eta^4}(g)_{ijkl,i'j'k'l'} \\ = \frac{1}{4!} [\mathcal{R}^{\eta^4}(g)_{ijkl,i'j'k'l'} + 23(i' \leftrightarrow j' \leftrightarrow k' \leftrightarrow l')], \end{aligned} \quad (\text{B10})$$

with the number of added permutation terms indicated explicitly [cf. Eq. (B3)]. One finds the characters associated with these symmetrized products to be

$$\begin{aligned} \chi_s^{\eta^3}(g) &= \sum_{ijk} \mathcal{R}_s^{\eta^3}(g)_{ijk,ijk} \\ &= [\chi_n^3(g) + 2\chi_n(g^3) + 3\chi_n(g)\chi_n(g^2)]/6, \end{aligned} \quad (\text{B11})$$

$$\begin{aligned} \chi_s^{\eta^4}(g) &= \sum_{ijkl} \mathcal{R}_s^{\eta^4}(g)_{ijkl,ijkl} = \frac{1}{24} [\chi_n^4(g) + 6\chi_n^2(g)\chi_n(g^2) \\ &+ 8\chi_n(g)\chi_n(g^3) + 3\chi_n^2(g^2) + 6\chi_n(g^4)]. \end{aligned} \quad (\text{B12})$$

Similarly, one finds the fifth- and sixth-order expressions

$$\begin{aligned} \chi_s^{\eta^5}(g) &= \frac{1}{5!} [\chi_n^5(g) + 10\chi_n^3(g)\chi_n(g^2) + 20\chi_n^2(g)\chi_n(g^3) \\ &+ 24\chi_n(g^5) + 30\chi_n(g)\chi_n(g^4) + 20\chi_n(g^2)\chi_n(g^3) \\ &+ 15\chi_n(g)\chi_n^2(g^2)], \end{aligned} \quad (\text{B13})$$

$$\begin{aligned} \chi_s^{\eta^6}(g) &= \frac{1}{6!} [15\chi_n^4(g)\chi_n(g^2) + 120\chi_n(g)\chi_n(g^2)\chi_n(g^3) \\ &+ \chi_n^6(g) + 15\chi_n^3(g^2) + 40\chi_n^2(g^3) + 45\chi_n^2(g)\chi_n^2(g^2) \\ &+ 144\chi_n(g)\chi_n(g^5) + 40\chi_n^3(g)\chi_n(g^3) + 120\chi_n(g^6) \\ &+ 90\chi_n(g^2)\chi_n(g^4) + 90\chi_n^2(g)\chi_n(g^4)]. \end{aligned} \quad (\text{B14})$$

The presented derivation is not restricted to $\boldsymbol{\eta}$ transforming according to a single IR. In fact, we can equally assume

that η transforms according to the representation $n_1 + n_2 + \dots + n_v$. For example, in the case of a complex IR, we choose $n_1 = E$ and $n_2 = \bar{E}$; in the case of a degeneracy such as in a trigonal system, we have $n_1 = E_g$ and $n_2 = E_g$, or even combinations thereof such as in C_3 with $n_1 = n_3 = E$ and $n_2 = n_4 = \bar{E}$. For clarity, we let $\tilde{\mathcal{R}}_n(g)$ be the transformation matrices associates with the IR n , and $\tilde{\chi}_n(g)$ the corresponding character. The nematic order parameter $\boldsymbol{\eta} = (\eta_1, \eta_2, \dots, \eta_{\dim n_1 + \dots + \dim n_v})$, on the other hand, transforms with the matrices $\mathcal{R}_n(g) = \tilde{\mathcal{R}}_{n_1}(g) \oplus \dots \oplus \tilde{\mathcal{R}}_{n_v}(g)$. Clearly, its characters are given by $\chi_n(g) = \tilde{\chi}_{n_1}(g) + \dots + \tilde{\chi}_{n_v}(g)$. More importantly, since the transformation matrices $\mathcal{R}_n(g)$ are block diagonal, we find

$$[\mathcal{R}_n(g)]^\ell = [\tilde{\mathcal{R}}_{n_1}(g)]^\ell \oplus \dots \oplus [\tilde{\mathcal{R}}_{n_v}(g)]^\ell, \quad (\text{B15})$$

with $\ell = \{0, 1, 2, \dots\}$. As a result, the characters for any power ℓ become

$$\chi_n(g^\ell) = \tilde{\chi}_{n_1}(g^\ell) + \dots + \tilde{\chi}_{n_v}(g^\ell). \quad (\text{B16})$$

We now note that the above formalism equally applies to the ‘‘mixed’’ $\boldsymbol{\eta} = (\eta_1, \eta_2, \dots, \eta_{\dim n_1 + \dots + \dim n_v})$ with transformation matrices $\mathcal{R}_n(g)$. The only difference is that the characters (B16) have to be inserted into the formulas (B4)–(B14).

APPENDIX C: MINIMIZATION OF THE ICOSAHEDRAL NEMATIC LANDAU EXPANSION

In this Appendix, we derive the mean-field phase diagram of the nematic instability in an icosahedral group, which is presented in Fig. 3. Starting from the symmetrized product decomposition (43)–(45) we first determine the three bilinear combinations D^{A_g} , $D^{H_g,1}$, and $D^{H_g,2}$. The trivial one is given by $D^{A_g} = |\mathbf{d}|^2$. For the two degenerate H_g bilinears we choose a representation where both bilinears have equal amplitude $|D^{H_g,1}| = |D^{H_g,2}| = |\mathbf{d}|^2$. This condition indeed fixes the two bilinears and one finds $D^{H_g,1} = D^{j=2}$ to be identical to the $O(3)$ bilinear (19). With the amplitudes being equal, it is clear that the obtained $D^{H_g,2}$ must be related to $D^{H_g,1}$ through a rotation of the kind $D^{H_g,2} = \mathcal{R}^A \tilde{D}^{H_g,1}$ where $\tilde{D}^{H_g,1} = D^{H_g,1}|_{\mathbf{d} \rightarrow \tilde{\mathbf{d}} = \mathcal{R}^B \mathbf{d}}$ with rotation matrices $\mathcal{R}^{A,B}$. Clearly, this choice preserves the magnitude as $(D^{H_g,2})^T D^{H_g,2} = (\tilde{D}^{H_g,1})^T \tilde{D}^{H_g,1} = [(\tilde{\mathbf{d}})^T \tilde{\mathbf{d}}]^2 = [(\mathbf{d})^T \mathbf{d}]^2$. We find this relation to be satisfied for $\mathcal{R}^A = \mathcal{R}_5(-\phi_0)$ and $\mathcal{R}^B = \mathcal{R}_5(\phi_0)$, as presented in the main text in Eqs. (46) and (47). Introducing the unit vectors $\hat{\mathbf{d}} = \mathbf{d}/|\mathbf{d}|$ and $\hat{D}^{H_g,1/2} = D^{H_g,1/2}/|\mathbf{d}|^2$, we rewrite the Landau expansion (48) as

$$\mathcal{S} = \int_x |\mathbf{d}|^2 \{r_0 + |\mathbf{d}| f_{\alpha,n,m,l}^{(3)} + |\mathbf{d}|^2 f_{\alpha,n,m,l}^{(4)}\}, \quad (\text{C1})$$

with the direction-dependent functions

$$f_{\alpha,n,m,l}^{(3)} = g_1 \hat{\mathbf{d}} \cdot \hat{D}^{H_g,1} + g_2 \hat{\mathbf{d}} \cdot \hat{D}^{H_g,2}, \quad (\text{C2})$$

$$f_{\alpha,n,m,l}^{(4)} = u_1 + u_2 \hat{D}^{H_g,1} \cdot \hat{D}^{H_g,2}. \quad (\text{C3})$$

Within a mean-field analysis, the cubic term in the action (C1) triggers a first-order transition at a reduced temperature $r_0 > 0$. To derive this solution, one first solves the

Landau equations for $|\mathbf{d}|$:

$$|\mathbf{d}|_0 = \frac{3|f_{\alpha,n,m,l}^{(3)}|}{8f_{\alpha,n,m,l}^{(4)}} \left[1 + \sqrt{1 - \frac{32r_0 f_{\alpha,n,m,l}^{(4)}}{9[f_{\alpha,n,m,l}^{(3)}]^2}} \right], \quad (\text{C4})$$

where we implicitly assumed that $f_{\alpha,n,m,l}^{(3)} < 0$; we later verified that this is indeed the case for the mean-field solution. The first-order phase transition occurs at the reduced temperature r_0^c where the expansion (C1) evaluated at the solution (C4) vanishes. We find

$$r_0^c = \max_{\alpha,n,m,l} \frac{[f_{\alpha,n,m,l}^{(3)}]^2}{4f_{\alpha,n,m,l}^{(4)}}, \quad (\text{C5})$$

where the maximum function determines the optimal direction of the nematic direction parameters α, n, m, l . This optimization with respect to the four degrees of freedom has been conducted numerically to derive the phase diagram in Fig. 3.

An analytical solution is readily available in two regions of the $(g_2/g_1, u_2/u_1)$ parameter-space. First, it is convenient to parametrize the rotated nematic vector $\tilde{\mathbf{d}} = \mathcal{R}_5(\phi_0) \mathbf{d}$ as

$$\tilde{\mathbf{d}} = \frac{|\mathbf{d}|}{\sqrt{3}} \left\{ \cos(\tilde{\alpha}) (\tilde{n}_\mu \lambda_{\mu\mu}^{j=2} \tilde{n}_{\mu'}) + \cos\left(\tilde{\alpha} + \frac{2\pi}{3}\right) (\tilde{m}_\mu \lambda_{\mu\mu}^{j=2} \tilde{m}_{\mu'}) \right. \\ \left. + \cos\left(\tilde{\alpha} + \frac{4\pi}{3}\right) (\tilde{l}_\mu \lambda_{\mu\mu}^{j=2} \tilde{l}_{\mu'}) \right\}, \quad (\text{C6})$$

similar to the (nml) representation (14). Here, $(\tilde{\alpha}, \tilde{n}, \tilde{m}, \tilde{l})$ are functions of (α, n, m, l) defined implicitly through $\tilde{\mathbf{d}} = \mathcal{R}_5(\phi_0) \mathbf{d}$. This allows us to rewrite the cubic terms in Eq. (C1) as

$$\mathbf{d} \cdot D^{H_g,1} = |\mathbf{d}|^3 \cos(3\alpha), \quad (\text{C7})$$

$$\mathbf{d} \cdot D^{H_g,2} = \tilde{\mathbf{d}} \cdot \tilde{D}^{H_g,1} = |\mathbf{d}|^3 \cos(3\tilde{\alpha}). \quad (\text{C8})$$

The two parameter regimes where we can analytically derive the nematic ground state are spanned by (i) $\text{sign} g_1 = \text{sign} g_2$ and $u_2 < 0$; and by (ii) $\text{sign} g_1 = -\text{sign} g_2$ and $u_2 > 0$. In both regimes, all direction-dependent terms in the expansion (C1) can be simultaneously minimized.

In the first parameter regime (i), the cubic terms are minimized by $\hat{\mathbf{d}} \cdot \hat{D}^{H_g,1} = \hat{\mathbf{d}} \cdot \hat{D}^{H_g,2} = -\text{sign} g_1$, which corresponds to $\cos(3\alpha) = \cos(3\tilde{\alpha}) = -\text{sign} g_1$, see Eqs. (C7) and (C8). For concreteness, we choose $g_1 < 0$, such that the minimization gives $\alpha = \tilde{\alpha} = 0$; a similar procedure can be carried out for $g_1 > 0$. Technically, one still needs to demonstrate that eigenvectors n, m, l exist for these values. Setting $\alpha = \tilde{\alpha} = 0$ in the definition $\tilde{\mathbf{d}} = \mathcal{R}_5(\phi_0) \mathbf{d}$ and in expression (C6), we find two equations

$$\tilde{\mathbf{d}} = |\mathbf{d}| \frac{\sqrt{3}}{2} n_\mu (\mathcal{R}_5(\phi_0) \lambda^{j=2})_{\mu\mu'} n_{\mu'}, \quad (\text{C9})$$

$$\tilde{\mathbf{d}} = |\mathbf{d}| \frac{\sqrt{3}}{2} \tilde{n}_\mu \lambda_{\mu\mu}^{j=2} \tilde{n}_{\mu'}, \quad (\text{C10})$$

which have to be identical. Equating the two lines (C9) and (C10) leads to the five equations

$$2\tilde{n}_z^2 - \tilde{n}_x^2 - \tilde{n}_y^2 = \frac{1 + 3\sqrt{5}}{4} n_x^2 + \frac{1 - 3\sqrt{5}}{4} n_y^2 - \frac{1}{2} n_z^2, \quad (\text{C11})$$

$$\tilde{n}_x^2 - \tilde{n}_y^2 = \frac{-1 + \sqrt{5}}{4} n_x^2 + \frac{1 + \sqrt{5}}{4} n_y^2 - \frac{2\sqrt{5}}{4} n_z^2, \quad (\text{C12})$$

$$\tilde{n}_x \tilde{n}_z = n_x n_z, \quad (\text{C13})$$

$$\tilde{n}_y \tilde{n}_z = n_y n_z, \quad (\text{C14})$$

$$\tilde{n}_x \tilde{n}_y = n_x n_y, \quad (\text{C15})$$

that need to be simultaneously satisfied by the four degrees of freedom comprised in \mathbf{n} and $\tilde{\mathbf{n}}$ (recall that each unit vector has two independent degrees of freedom). The set of equations (C11)–(C15) has a total of 10 solutions. The first four solutions correspond to the equal amplitude condition $|n_\mu| = |\tilde{n}_\mu| = 1/\sqrt{3}$, which automatically satisfies Eqs. (C11) and (C12). Equations (C13)–(C15) are solved by appropriately choosing the relative signs between the components of each vector, yielding $\mathbf{n}_i = \tilde{\mathbf{n}}_i = \mathcal{V}_i^{111}$ with \mathcal{V}^{111} given by Eq. (35) and $i = 1, 2, 3, 4$. Recall that changing the sign of \mathbf{n}_i or $\tilde{\mathbf{n}}_i$ does not change the corresponding nematic order parameter \mathbf{d} , which allows us to discard the solutions $\mathbf{n}_i = -\tilde{\mathbf{n}}_i$.

The other six solutions are obtained upon setting one component $n_\mu = 0$ to zero. This necessarily requires $\tilde{n}_\mu = 0$ in order to solve two of Eqs. (C13)–(C15). The remaining three equations can then be solved in a straightforward way. For example, for $n_z = 0$ we find the two solutions

$$\mathbf{n}_5 = (\alpha_-^{(3)}, \alpha_+^{(3)}, 0), \quad \tilde{\mathbf{n}}_5 = (\alpha_+^{(3)}, \alpha_-^{(3)}, 0), \quad (\text{C16})$$

$$\mathbf{n}_6 = (\alpha_-^{(3)}, -\alpha_+^{(3)}, 0), \quad \tilde{\mathbf{n}}_6 = (\alpha_+^{(3)}, -\alpha_-^{(3)}, 0), \quad (\text{C17})$$

with $\alpha_\pm^{(3)} = \frac{1}{\sqrt{6}}(3 \pm \sqrt{5})^{1/2}$. The other four solutions are found analogously and are presented in Eqs. (50) and (34). Note that the $\tilde{\mathbf{n}}$ directions in Eqs. (C16) and (C17) do not carry any information, they are merely a mathematical construct used to find the solution.

In the second parameter regime (ii), the cubic terms are minimized by $\hat{\mathbf{d}} \cdot \hat{\mathbf{D}}^{H_g,1} = -\hat{\mathbf{d}} \cdot \hat{\mathbf{D}}^{H_g,1} = -\text{sign}g_1$ or, equivalently, $\cos(3\alpha) = -\cos(3\tilde{\alpha}) = -\text{sign}g_1$. Setting again $g_1 < 0$ for concreteness, we search for solutions with $\alpha = 0$ and $\tilde{\alpha} = \pi/3$. As a result, one obtains Eq. (C9) while the second equation (C10) is replaced by

$$\tilde{\mathbf{d}} = -\frac{\sqrt{3}}{2} |\mathbf{d}| \tilde{m}_\mu \lambda_{\mu\mu}^{j=2} \tilde{m}_\mu. \quad (\text{C18})$$

Equating Eqs. (C18) and (C9) gives once again five equations:

$$\tilde{m}_x^2 + \tilde{m}_y^2 - 2\tilde{m}_z^2 = \frac{1 + 3\sqrt{5}}{4} n_x^2 + \frac{1 - 3\sqrt{5}}{4} n_y^2 - \frac{1}{2} n_z^2, \quad (\text{C19})$$

$$-\tilde{m}_x^2 + \tilde{m}_y^2 = \frac{-1 + \sqrt{5}}{4} n_x^2 + \frac{1 + \sqrt{5}}{4} n_y^2 - \frac{2\sqrt{5}}{4} n_z^2, \quad (\text{C20})$$

$$-\tilde{m}_x \tilde{m}_z = n_x n_z, \quad (\text{C21})$$

$$-\tilde{m}_y \tilde{m}_z = n_y n_z, \quad (\text{C22})$$

$$-\tilde{m}_x \tilde{m}_y = n_x n_y. \quad (\text{C23})$$

In contrast with the previous case, Eqs. (C19)–(C23) do not allow for solutions with equal amplitudes due to the relative minus signs in Eqs. (C21)–(C23). The six existing solutions are obtained by imposing a vanishing component $n_\mu = 0$, which directly implies $\tilde{m}_\mu = 0$, leading to three remaining

equations. Those can be solved in a similar fashion as the previous case. For instance, for $n_z = 0$, we find the two solutions

$$\mathbf{n}_1 = (\alpha_+^{(5)}, -\alpha_-^{(5)}, 0), \quad \tilde{\mathbf{m}}_1 = (\alpha_-^{(5)}, \alpha_+^{(5)}, 0), \quad (\text{C24})$$

$$\mathbf{n}_2 = (\alpha_+^{(5)}, \alpha_-^{(5)}, 0), \quad \tilde{\mathbf{m}}_2 = (\alpha_-^{(5)}, -\alpha_+^{(5)}, 0). \quad (\text{C25})$$

A similar procedure can be applied for $n_x = 0$ and $n_y = 0$, resulting in the solutions presented in Eqs. (52) and (33).

APPENDIX D: LANDAU EXPANSION FOR THE TETRAHEDRAL GROUPS T_h and T

In this Appendix, we derive the Landau expansion of the nematic doublet order parameter \mathbf{d}^e in the case of the cubic point groups $\{T_h, T\}$. The main difference with respect to the derivation presented in Sec. III B, which applied to the cubic point groups $\{O_h, O, T_d\}$, is that here the nematic doublet \mathbf{d}^e transforms according to a complex IR. We emphasize that, for the $\{T_h, T\}$ point groups, the nematic triplet order parameter \mathbf{d}^t still transforms as a real IR, so the results in Sec. III B apply directly to those groups as well.

To keep the notation transparent, we focus on the point group T_h ; the results apply equally to the group T . Within T_h , the complex combination $\Delta^e = |\mathbf{d}^e| e^{i\gamma_e}$ transforms as the E_g IR while its complex conjugate $\bar{\Delta}^e$ transforms as the \bar{E}_g IR, such that the two-component doublet \mathbf{d}^e transforms according to the representation $(E_g \oplus \bar{E}_g)$. To derive the corresponding Landau expansion, we first compute the decomposition of the symmetrized product for each expansion order, following the procedure outlined in Appendix B:

$$[\otimes_{j=1}^2 (E_g \oplus \bar{E}_g)]_s = A_g \oplus (E_g \oplus \bar{E}_g), \quad (\text{D1})$$

$$[\otimes_{j=1}^3 (E_g \oplus \bar{E}_g)]_s = 2A_g \oplus (E_g \oplus \bar{E}_g), \quad (\text{D2})$$

$$[\otimes_{j=1}^4 (E_g \oplus \bar{E}_g)]_s = A_g \oplus 2(E_g \oplus \bar{E}_g). \quad (\text{D3})$$

We note the existence of one additional cubic invariant in this case, when compared with the cases in which \mathbf{d}^e transforms as a real IR, see Eq. (65). To construct the four A_g invariants in (D1)–(D3), we first determine the bilinears associated with Eq. (D1):

$$D^{A_g} = |\mathbf{d}^e|^2, \quad D^{E_g} = |\mathbf{d}^e|^2 e^{-i2\gamma_e}, \quad D^{\bar{E}_g} = |\mathbf{d}^e|^2 e^{i2\gamma_e}. \quad (\text{D4})$$

Then, the four invariants can be written as $|\mathbf{d}^e|^2$, $|\mathbf{d}^e|^4$, $\bar{\Delta}^e D^{E_g}$, and $\Delta^e D^{\bar{E}_g}$. From the latter two, we construct two real combinations $(\bar{\Delta}^e D^{E_g} + \Delta^e D^{\bar{E}_g})$ and $i(\bar{\Delta}^e D^{E_g} - \Delta^e D^{\bar{E}_g})$, such that the Landau expansion becomes

$$\mathcal{S} = \int_{\mathbf{x}} \{r_0 |\mathbf{d}^e|^2 + |\mathbf{d}^e|^3 [g^c \cos(3\gamma_e) + g^s \sin(3\gamma_e)] + u |\mathbf{d}^e|^4\}. \quad (\text{D5})$$

The presence of the second cubic term proportional to $\sin(3\gamma_e)$ can be traced back to the fact that the cubic groups $\{T_h, T\}$ lack an axis of (proper or improper) fourfold rotational symmetry compared with the cubic groups $\{O_h, O, T_d\}$. To proceed, it is instructive to rewrite the cubic terms as

$$g^c \cos(3\gamma_e) + g^s \sin(3\gamma_e) = g \cos(3\gamma_e - \delta_0), \quad (\text{D6})$$

with

$$g = \text{sign}(g^c) \sqrt{(g^c)^2 + (g^s)^2}, \quad \delta_0 = \arctan(g^s/g^c). \quad (\text{D7})$$

Then, the action (D5) becomes

$$S = \int_{\mathbf{x}} \{r_0 |\mathbf{d}^e|^2 + g |\mathbf{d}^e|^3 \cos(3\gamma_e - \delta_0) + u |\mathbf{d}^e|^4\}, \quad (\text{D8})$$

illustrating the emergence of an offset angle δ_0 for the nematic director that is nonuniversal, i.e., it is determined by the Landau coefficients, which in turn depend on the microscopic model. As discussed above, this is due to the lack of proper or improper fourfold rotational symmetry. This Landau expansion thus behaves effectively as a Z_3 Potts model whose threefold-degenerate ground-state directions

$$\gamma_e^0 = \frac{1}{3}\delta_0 + \frac{m\pi}{3} \quad (\text{D9})$$

are offset by an angle $\delta_0/3$. Here, $m = \{1, 3, 5\}$ for $g > 0$ and $m = \{0, 2, 4\}$ for $g < 0$. In Table I, we signal this modified form of the Z_3 Potts model via Z_3^* .

To further visualize the effect of the offset angle, we rewrite the order parameter $\mathbf{d}^e = |\mathbf{d}^e|(\cos \gamma_e, \sin \gamma_e)$ in the (nml) representation of Eq. (14). To accomplish that, we define $n_e = \text{div}(\gamma_e, \pi/3)$ and $\tilde{\gamma}_e = \text{mod}(\gamma_e, \pi/3) = \gamma_e - n_e\pi/3 \in [0, \pi/3]$ with div , mod denoting integer division and modulo, respectively. Since the definition in Eq. (D7) implies $\delta_0 \in [-\pi/2, \pi/2]$, it follows that $n_e = m - [1 - \text{sign}(\delta_0)]/2$ and $\tilde{\gamma}_e = \delta_0/3 + \frac{\pi}{3}[1 - \text{sign}(\delta_0)]/2 \in [0, \pi/3]$. Then, for even n_e , the \mathbf{d}^e order parameter in the (nml) representation of Eq. (14) becomes

$$\alpha = \tilde{\gamma}_e, \quad \mathbf{n} = \mathbf{e}_{\tilde{n}_e+2}, \quad \mathbf{m} = \mathbf{e}_{\tilde{n}_e+1}, \quad \mathbf{l} = \mathbf{e}_{\tilde{n}_e}, \quad (\text{D10})$$

where $\tilde{n}_e = \frac{1}{2}n_e + 1 \in \{1, 2, 3\}$ and the summation in (D10) is understood as modulo three. Conversely, one obtains for odd n_e ,

$$\alpha = \frac{\pi}{3} - \tilde{\gamma}_e, \quad \mathbf{n} = \mathbf{e}_{\tilde{n}_e}, \quad \mathbf{m} = \mathbf{e}_{\tilde{n}_e+1}, \quad \mathbf{l} = \mathbf{e}_{\tilde{n}_e+2}, \quad (\text{D11})$$

with $\tilde{n}_e = \frac{1}{2}n_e + 1/2 \in \{1, 2, 3\}$. Interestingly, in this case of a Z_3^* Potts transition, the offset angle only affects α but leaves the nematic axes aligned with the coordinate axes \mathbf{e}_1 , \mathbf{e}_2 , and \mathbf{e}_3 . Thus, within the point groups T_h and T , the nematic doublet state is generically biaxial with $\alpha \neq \{0, \pi/3\}$. Only for $\gamma_e = n\frac{\pi}{3}$ ($n \in \mathbb{N}$), which is a symmetry-enforced condition in the point groups $\{O_h, O, T_d\}$, the state is uniaxial with $\alpha = \{0, \pi/3\}$.

APPENDIX E: LANDAU EXPANSION FOR THE HEXAGONAL GROUPS C_{6h} , C_{3h} , AND C_6

In this Appendix, we derive the nematic Landau expansion for the hexagonal point groups $\{C_{6h}, C_{3h}, C_6\}$. In contrast with the cases presented in Sec. IV B, the nematic in-plane and out-of-plane doublets \mathbf{d}^{ip} and \mathbf{d}^{op} transform according to complex IRs. For concreteness, we focus on the point group C_{6h} , for which the complex in-plane and out-of-plane nematic order parameters, $\Delta^{\text{ip}} = |\mathbf{d}^{\text{ip}}|e^{i\gamma_{\text{ip}}}$ and $\Delta^{\text{op}} = |\mathbf{d}^{\text{op}}|e^{i\gamma_{\text{op}}}$, transform according to the IRs E_{2g} and E_{1g} , respectively, whereas their complex conjugates transform as \bar{E}_{2g} and \bar{E}_{1g} . The same results hold for the other two groups.

To derive the Landau expansion for the in-plane nematic doublet, we first compute the decomposition of the symmetrized product for each expansion order,

$$[\otimes_{j=1}^2 (E_{2g} \oplus \bar{E}_{2g})]_s = A_g \oplus (E_{2g} \oplus \bar{E}_{2g}), \quad (\text{E1})$$

$$[\otimes_{j=1}^3 (E_{2g} \oplus \bar{E}_{2g})]_s = 2A_g \oplus (E_{2g} \oplus \bar{E}_{2g}), \quad (\text{E2})$$

$$[\otimes_{j=1}^4 (E_{2g} \oplus \bar{E}_{2g})]_s = A_g \oplus 2(E_{2g} \oplus \bar{E}_{2g}). \quad (\text{E3})$$

The four invariants are written in terms of the bilinears in Eq. (E1),

$$D^{A_g} = |\mathbf{d}^{\text{ip}}|^2, \quad D^{E_{2g}} = |\mathbf{d}^{\text{ip}}|^2 e^{-i2\gamma_{\text{ip}}}, \quad D^{\bar{E}_{2g}} = |\mathbf{d}^{\text{ip}}|^2 e^{i2\gamma_{\text{ip}}}. \quad (\text{E4})$$

resulting in $|\mathbf{d}^{\text{ip}}|^2$, $|\mathbf{d}^{\text{ip}}|^4$, $\Delta^{\text{ip}} D^{\bar{E}_{2g}}$, and $\bar{\Delta}^{\text{ip}} D^{E_{2g}}$. Thus, enforcing the invariants to be real-valued, we obtain the nematic Landau expansion

$$S_{\text{ip}} = \int_{\mathbf{x}} \{r_0 |\mathbf{d}^{\text{ip}}|^2 + g_{\text{ip}} |\mathbf{d}^{\text{ip}}|^3 \cos(3\gamma_{\text{ip}} - \delta_0) + u |\mathbf{d}^{\text{ip}}|^4\}, \quad (\text{E5})$$

with an angular-shifted cosine term obtained from the relationship (D6). The Landau expansion (E5) is that of a Z_3 clock model with an offset angle δ_0 , whose minimization gives

$$\gamma_{\text{ip}}^0 = \frac{1}{3}\delta_0 + \frac{\pi}{3} \left(\frac{1 + \mathfrak{s}_g}{2} \right) + \frac{2\pi}{3}n, \quad n = \{0, 1, 2\}, \quad (\text{E6})$$

where $\mathfrak{s}_g = \text{sign}g_{\text{ip}}$. In the nematic state, the Fermi surface is similar to that shown in Fig. 5(a), but arbitrarily rotated about the k_z axis according to the offset angle δ_0 , which is a Landau coefficient. To see this, we start from the parametrization of \mathbf{d}^{ip} in Eq. (87) and employ the identities

$$\begin{aligned} & \begin{pmatrix} \cos \frac{\gamma_{\text{ip}}^0}{2} \\ \sin \frac{\gamma_{\text{ip}}^0}{2} \end{pmatrix} \\ &= (-1)^n R_z \left(\frac{\delta_0}{6} \right) \left[\begin{pmatrix} \cos \tilde{\gamma}_{\text{ip}}^0 \\ -\sin \tilde{\gamma}_{\text{ip}}^0 \end{pmatrix} \frac{1 - \mathfrak{s}_g}{2} + \begin{pmatrix} \sin \tilde{\gamma}_{\text{ip}}^0 \\ \cos \tilde{\gamma}_{\text{ip}}^0 \end{pmatrix} \frac{1 + \mathfrak{s}_g}{2} \right], \end{aligned} \quad (\text{E7})$$

$$\begin{aligned} & \begin{pmatrix} -\sin \frac{\gamma_{\text{ip}}^0}{2} \\ \cos \frac{\gamma_{\text{ip}}^0}{2} \end{pmatrix} \\ &= (-1)^n R_z \left(\frac{\delta_0}{6} \right) \left[\begin{pmatrix} \sin \tilde{\gamma}_{\text{ip}}^0 \\ \cos \tilde{\gamma}_{\text{ip}}^0 \end{pmatrix} \frac{1 - \mathfrak{s}_g}{2} - \begin{pmatrix} \cos \tilde{\gamma}_{\text{ip}}^0 \\ -\sin \tilde{\gamma}_{\text{ip}}^0 \end{pmatrix} \frac{1 + \mathfrak{s}_g}{2} \right], \end{aligned} \quad (\text{E8})$$

with $\tilde{\gamma}_{\text{ip}}^0 = \frac{\pi}{3} \frac{1 + \mathfrak{s}_g}{2} + \frac{2\pi}{3}n$ and the rotation matrix

$$R_z(\delta) = \begin{pmatrix} \cos \delta & -\sin \delta \\ \sin \delta & \cos \delta \end{pmatrix}. \quad (\text{E9})$$

The relationships in Eqs. (E7) and (E8) explicitly show that the in-plane nematic axes are rotated by an angle $\delta_0/6$ away from the hexagonal high-symmetry directions listed in Eq. (97).

Repeating the same steps for the out-of-plane doublet order parameter \mathbf{d}^{op} , we obtain the symmetrized-product decompositions

$$[\otimes_{j=1}^2 (E_{1g} \oplus \bar{E}_{1g})]_s = A_g \oplus (E_{2g} \oplus \bar{E}_{2g}), \quad (\text{E10})$$

$$\left[\otimes_{j=1}^3 (E_{1g} \oplus \bar{E}_{1g}) \right]_s = 2B_g \oplus (E_{1g} \oplus \bar{E}_{1g}), \quad (\text{E11})$$

$$\left[\otimes_{j=1}^4 (E_{1g} \oplus \bar{E}_{1g}) \right]_s = A_g \oplus 2(E_{2g} \oplus \bar{E}_{2g}), \quad (\text{E12})$$

$$\left[\otimes_{j=1}^5 (E_{1g} \oplus \bar{E}_{1g}) \right]_s = 2B_g \oplus 2(E_{1g} \oplus \bar{E}_{1g}), \quad (\text{E13})$$

$$\left[\otimes_{j=1}^6 (E_{1g} \oplus \bar{E}_{1g}) \right]_s = 3A_g \oplus 2(E_{2g} \oplus \bar{E}_{2g}), \quad (\text{E14})$$

with the bilinears

$$D^A_g = |\mathbf{d}^{\text{op}}|^2, \quad D^{E_{2g}} = |\mathbf{d}^{\text{op}}|^2 e^{i2\gamma_{\text{op}}}, \quad D^{\bar{E}_{2g}} = |\mathbf{d}^{\text{op}}|^2 e^{-i2\gamma_{\text{op}}}. \quad (\text{E15})$$

Compared with the case of \mathbf{d}^{ip} , here the cubic terms $\Delta^{\text{op}} D^{E_{2g}}$ and $\bar{\Delta}^{\text{op}} D^{\bar{E}_{2g}}$ do not transform as A_g but as B_g . Thus, the five invariants in Eqs. (E10)–(E14) are $|\mathbf{d}^{\text{op}}|^2$, $|\mathbf{d}^{\text{op}}|^4$, $|\mathbf{d}^{\text{op}}|^6$, $(\Delta^{\text{op}} D^{E_{2g}})^2$, and $(\bar{\Delta}^{\text{op}} D^{\bar{E}_{2g}})^2$, yielding the Landau expansion

$$\mathcal{S}_{\text{op}} = \int_{\mathbf{x}} \left\{ r_0 |\mathbf{d}^{\text{op}}|^2 + u |\mathbf{d}^{\text{op}}|^4 + u_6 |\mathbf{d}^{\text{op}}|^6 + v_6 |\mathbf{d}^{\text{op}}|^6 \cos(6\gamma_{\text{op}} - \delta_0) \right\}, \quad (\text{E16})$$

with an offset angle δ_0 due to the relation (D6). Minimization leads to

$$\gamma_{\text{op}}^0 = \frac{1}{6} \delta_0 + \frac{\pi}{6} \frac{1 + \text{sign} v_6}{2} + \frac{2\pi}{6} n, \quad n \in \{0, 1, \dots, 5\}, \quad (\text{E17})$$

which, from Eq. (89), corresponds to a rotation of the nematic axes by $\delta_0/6$ about the k_z axis.

APPENDIX F: LANDAU EXPANSION FOR THE TRIGONAL GROUPS C_3 AND S_6

This Appendix presents the derivation of the Landau expansion for the trigonal groups $\{S_6, C_3\}$, which lack the in-plane symmetry directions $\mathcal{V}_1^{\text{hex}}, \mathcal{V}_2^{\text{hex}}$ in Eq. (97), thus complementing the analysis shown in Sec. IV C for the trigonal groups $\{D_3, D_{3d}, C_{3v}\}$. We consider the point group C_3 for concreteness; in this case, the combinations $\Delta^{\text{ip}} = |\mathbf{d}^{\text{ip}}| e^{i\gamma_{\text{ip}}}$ and $\Delta^{\text{op}} = |\mathbf{d}^{\text{op}}| e^{i\gamma_{\text{op}}}$ transform according to the complex IR E , whereas their complex conjugates $\bar{\Delta}^{\text{ip}}, \bar{\Delta}^{\text{op}}$ transform according to \bar{E} . Since we are interested in the Landau expansion of the total nematic order parameter $\mathbf{d}^E = (\mathbf{d}^{\text{ip}}, \mathbf{d}^{\text{op}})$, we need the symmetrized product decomposition of $(E \oplus \bar{E}) \oplus (E \oplus \bar{E})$:

$$\left[\otimes_{j=1}^2 ((E \oplus \bar{E}) \oplus (E \oplus \bar{E})) \right]_s = 4A \oplus 3(E \oplus \bar{E}), \quad (\text{F1})$$

$$\left[\otimes_{j=1}^3 ((E \oplus \bar{E}) \oplus (E \oplus \bar{E})) \right]_s = 8A \oplus 6(E \oplus \bar{E}), \quad (\text{F2})$$

$$\left[\otimes_{j=1}^4 ((E \oplus \bar{E}) \oplus (E \oplus \bar{E})) \right]_s = 9A \oplus 13(E \oplus \bar{E}). \quad (\text{F3})$$

The bilinear combinations obtained from Eq. (F1) are

$$\begin{aligned} D_{\text{ip}}^{A_1} &= |\mathbf{d}^{\text{ip}}|^2, & D_{\text{io}}^{A_1} &= |\mathbf{d}^{\text{ip}}| |\mathbf{d}^{\text{op}}| e^{i(\gamma_{\text{ip}} - \gamma_{\text{op}})}, \\ D_{\text{op}}^{A_1} &= |\mathbf{d}^{\text{op}}|^2, & D_{\text{ip}}^E &= |\mathbf{d}^{\text{ip}}|^2 e^{-i2\gamma_{\text{ip}}}, \\ D_{\text{op}}^E &= |\mathbf{d}^{\text{op}}|^2 e^{-i2\gamma_{\text{op}}}, & D_{\text{io}}^E &= |\mathbf{d}^{\text{ip}}| |\mathbf{d}^{\text{op}}| e^{-i(\gamma_{\text{ip}} + \gamma_{\text{op}})}, \end{aligned} \quad (\text{F4})$$

as well as the complex conjugates of the bilinears that are not real-valued. The eight cubic invariants transforming as A are

given by

$$\begin{aligned} \bar{\Delta}^{\text{ip}} D_{\text{ip}}^E &= |\mathbf{d}^{\text{ip}}|^3 e^{-i3\gamma_{\text{ip}}}, & \bar{\Delta}^{\text{ip}} D_{\text{io}}^E &= |\mathbf{d}^{\text{ip}}|^2 |\mathbf{d}^{\text{op}}| e^{-i(2\gamma_{\text{ip}} + \gamma_{\text{op}})}, \\ \bar{\Delta}^{\text{op}} D_{\text{op}}^E &= |\mathbf{d}^{\text{op}}|^3 e^{-i3\gamma_{\text{op}}}, & \bar{\Delta}^{\text{op}} D_{\text{io}}^E &= |\mathbf{d}^{\text{ip}}| |\mathbf{d}^{\text{op}}|^2 e^{-i(\gamma_{\text{ip}} + 2\gamma_{\text{op}})}, \end{aligned} \quad (\text{F5})$$

plus their complex conjugates. Similarly, the nine quartic invariants are

$$\begin{aligned} D_{\text{ip}}^A D_{\text{ip}}^A &= |\mathbf{d}^{\text{ip}}|^4, & D_{\text{ip}}^A D_{\text{io}}^A &= |\mathbf{d}^{\text{ip}}|^3 |\mathbf{d}^{\text{op}}| e^{i(\gamma_{\text{ip}} - \gamma_{\text{op}})}, \\ D_{\text{op}}^A D_{\text{op}}^A &= |\mathbf{d}^{\text{op}}|^4, & D_{\text{op}}^A D_{\text{io}}^A &= |\mathbf{d}^{\text{ip}}| |\mathbf{d}^{\text{op}}|^3 e^{i(\gamma_{\text{ip}} - \gamma_{\text{op}})}, \\ D_{\text{ip}}^A D_{\text{op}}^A &= |\mathbf{d}^{\text{ip}}|^2 |\mathbf{d}^{\text{op}}|^2, & D_{\text{io}}^A D_{\text{io}}^A &= |\mathbf{d}^{\text{ip}}|^2 |\mathbf{d}^{\text{op}}|^2 e^{i(2\gamma_{\text{ip}} - 2\gamma_{\text{op}})}, \end{aligned} \quad (\text{F6})$$

plus the complex conjugates of the terms on the right column. We can now write down the Landau expansion in terms of the real-valued combinations of these invariants. The resulting action becomes $\mathcal{S} = \mathcal{S}_2 + \mathcal{S}_3 + \mathcal{S}_4$, with

$$\begin{aligned} \mathcal{S}_2 &= \int_{\mathbf{x}} \left\{ r_{\text{ip}} (\mathbf{d}^{\text{ip}})^2 + r_{\text{op}} (\mathbf{d}^{\text{op}})^2 + r_{\text{io1}} (\mathbf{d}^{\text{ip}} \cdot \mathbf{d}^{\text{op}}) + r_{\text{io2}} (\mathbf{d}^{\text{ip}})^T (-i\sigma^y) \mathbf{d}^{\text{op}} \right\}, \end{aligned} \quad (\text{F7})$$

$$\begin{aligned} \mathcal{S}_3 &= \int_{\mathbf{x}} \left\{ |\mathbf{d}^{\text{ip}}|^3 [g_{\text{ip}}^c \mathbf{c}_{3\gamma_{\text{ip}}} + g_{\text{ip}}^s \mathbf{s}_{3\gamma_{\text{ip}}}] + |\mathbf{d}^{\text{op}}|^3 [g_{\text{op}}^c \mathbf{c}_{3\gamma_{\text{op}}} + g_{\text{op}}^s \mathbf{s}_{3\gamma_{\text{op}}}] + |\mathbf{d}^{\text{ip}}| |\mathbf{d}^{\text{op}}|^2 [g_2^c \mathbf{c}_{\gamma_{\text{ip}} + 2\gamma_{\text{op}}} + g_2^s \mathbf{s}_{\gamma_{\text{ip}} + 2\gamma_{\text{op}}}] + |\mathbf{d}^{\text{ip}}|^2 |\mathbf{d}^{\text{op}}| [g_1^c \mathbf{c}_{2\gamma_{\text{ip}} + \gamma_{\text{op}}} + g_1^s \mathbf{s}_{2\gamma_{\text{ip}} + \gamma_{\text{op}}}] \right\}, \end{aligned} \quad (\text{F8})$$

$$\begin{aligned} \mathcal{S}_4 &= \int_{\mathbf{x}} \left\{ u_{\text{ip}} |\mathbf{d}^{\text{ip}}|^4 + |\mathbf{d}^{\text{ip}}|^2 |\mathbf{d}^{\text{op}}|^2 [u_{\text{io}}^c \mathbf{c}_{2\gamma_{\text{ip}} - 2\gamma_{\text{op}}} + u_{\text{io}}^s \mathbf{s}_{2\gamma_{\text{ip}} - 2\gamma_{\text{op}}}] + u_{\text{io}}^0 |\mathbf{d}^{\text{ip}}|^2 |\mathbf{d}^{\text{op}}|^2 + [u_2^c \mathbf{c}_{\gamma_{\text{ip}} - \gamma_{\text{op}}} + u_2^s \mathbf{s}_{\gamma_{\text{ip}} - \gamma_{\text{op}}}] |\mathbf{d}^{\text{ip}}| |\mathbf{d}^{\text{op}}|^3 + u_{\text{op}} |\mathbf{d}^{\text{op}}|^4 + [u_1^c \mathbf{c}_{\gamma_{\text{ip}} - \gamma_{\text{op}}} + u_1^s \mathbf{s}_{\gamma_{\text{ip}} - \gamma_{\text{op}}}] |\mathbf{d}^{\text{ip}}|^3 |\mathbf{d}^{\text{op}}| \right\}, \end{aligned} \quad (\text{F9})$$

with 23 invariants. For brevity, we defined $\mathbf{c}_\gamma \equiv \cos \gamma$ and $\mathbf{s}_\gamma \equiv \sin \gamma$; the Pauli matrix $i\sigma^y$ in the quadratic action \mathcal{S}_2 acts on the two-dimensional subspace of \mathbf{d}^{ip} and \mathbf{d}^{op} .

To minimize \mathcal{S} , we proceed in the same way as the analysis carried out in Sec. IV C. Upon diagonalizing \mathcal{S}_2 , we obtain

$$\mathcal{S}_2 = \int_{\mathbf{x}} \left(\frac{\mathbf{d}^{\text{ip}}}{\mathbf{d}^{\text{op}}} \right)^T M \left(\frac{\mathbf{d}^{\text{ip}}}{\mathbf{d}^{\text{op}}} \right) = \int_{\mathbf{x}} \left\{ \lambda_+ |\mathbf{d}^+|^2 + \lambda_- |\mathbf{d}^-|^2 \right\}, \quad (\text{F10})$$

where

$$\lambda_{\pm} = \frac{1}{2} \left(r_{\text{ip}} + r_{\text{op}} \pm \sqrt{(r_{\text{ip}} - r_{\text{op}})^2 + r_{\text{io1}}^2 + r_{\text{io2}}^2} \right). \quad (\text{F11})$$

Here, we used the result $U^T M U = \text{diag}(\lambda_+, \lambda_+, \lambda_-, \lambda_-)$ and introduced the diagonal basis

$$\begin{pmatrix} \mathbf{d}^+ \\ \mathbf{d}^- \end{pmatrix} = U^T \begin{pmatrix} \mathbf{d}^{\text{ip}} \\ \mathbf{d}^{\text{op}} \end{pmatrix} = \begin{pmatrix} \beta_+ R_{\text{io}}^T \mathbf{d}^{\text{ip}} + \beta_- \mathbf{d}^{\text{op}} \\ -\beta_- R_{\text{io}}^T \mathbf{d}^{\text{ip}} + \beta_+ \mathbf{d}^{\text{op}} \end{pmatrix}, \quad (\text{F12})$$

with the rotation matrix

$$R_\gamma = \begin{pmatrix} \cos \gamma & -\sin \gamma \\ \sin \gamma & \cos \gamma \end{pmatrix}, \quad (\text{F13})$$

and the unitary matrix

$$U = \begin{pmatrix} \beta_+ \cos \delta_{io} & -\beta_+ \sin \delta_{io} & -\beta_- \cos \delta_{io} & \beta_- \sin \delta_{io} \\ \beta_+ \sin \delta_{io} & \beta_+ \cos \delta_{io} & -\beta_- \sin \delta_{io} & -\beta_- \cos \delta_{io} \\ \beta_- & 0 & \beta_+ & 0 \\ 0 & \beta_- & 0 & \beta_+ \end{pmatrix}, \quad (\text{F14})$$

where

$$\beta_{\pm} = \frac{1}{\sqrt{2}} \sqrt{1 \pm \frac{r_{ip} - r_{op}}{\sqrt{(r_{ip} - r_{op})^2 + r_{io1}^2 + r_{io2}^2}}}, \quad (\text{F15})$$

and

$$\cos \delta_{io} = \frac{r_{io1}}{\sqrt{r_{io1}^2 + r_{io2}^2}}, \quad \sin \delta_{io} = \frac{r_{io2}}{\sqrt{r_{io1}^2 + r_{io2}^2}}. \quad (\text{F16})$$

We emphasize that the corresponding expressions shown in Sec. IV C for the trigonal groups $\{D_3, D_{3d}, C_{3v}\}$ can be recovered from the expressions above upon setting $r_{io2} = 0$, which gives $\delta_{io} = 0, \pi$. The cubic and quartic actions can also be rewritten in the $\mathbf{d}^{\pm} = |\mathbf{d}^{\pm}|(\cos \gamma_{\pm}, \sin \gamma_{\pm})^T$ basis. For instance, \mathcal{S}_3 becomes

$$\begin{aligned} \mathcal{S}_3 = \int_{\mathbf{x}} \{ & |\mathbf{d}^+|^3 [g_+^c \mathbf{c}_{3\gamma_+} + g_+^s \mathbf{s}_{3\gamma_+}] \\ & + |\mathbf{d}^-|^3 [g_-^c \mathbf{c}_{3\gamma_-} + g_-^s \mathbf{s}_{3\gamma_-}] \\ & + |\mathbf{d}^+|^2 |\mathbf{d}^-| [\tilde{g}_1^c \mathbf{c}_{2\gamma_+ + \gamma_-} + \tilde{g}_1^s \mathbf{s}_{2\gamma_+ + \gamma_-}] \\ & + |\mathbf{d}^+| |\mathbf{d}^-|^2 [\tilde{g}_2^c \mathbf{c}_{\gamma_+ + 2\gamma_-} + \tilde{g}_2^s \mathbf{s}_{\gamma_+ + 2\gamma_-}] \}. \end{aligned} \quad (\text{F17})$$

Here, we defined the new Landau coefficients

$$\begin{aligned} \mathbf{g}_+ &= \beta_-^3 \mathbf{g}_{op} + \beta_-^2 \beta_+ R_{\delta_{io}}^T \mathbf{g}_2 + \beta_- \beta_+^2 R_{2\delta_{io}}^T \mathbf{g}_1 + \beta_+^3 R_{3\delta_{io}}^T \mathbf{g}_{ip}, \\ \mathbf{g}_- &= \beta_+^3 \mathbf{g}_{op} - \beta_- \beta_+^2 R_{\delta_{io}}^T \mathbf{g}_2 + \beta_-^2 \beta_+ R_{2\delta_{io}}^T \mathbf{g}_1 - \beta_-^3 R_{3\delta_{io}}^T \mathbf{g}_{ip}, \\ \tilde{\mathbf{g}}_1 &= 3\beta_-^2 \beta_+ \mathbf{g}_{op} + \beta_- (2\beta_+^2 - \beta_-^2) R_{\delta_{io}}^T \mathbf{g}_2 \\ &\quad + \beta_+ (\beta_+^2 - 2\beta_-^2) R_{2\delta_{io}}^T \mathbf{g}_1 - 3\beta_- \beta_+^2 R_{3\delta_{io}}^T \mathbf{g}_{ip}, \\ \tilde{\mathbf{g}}_2 &= 3\beta_- \beta_+^2 \mathbf{g}_{op} + \beta_+ (\beta_+^2 - 2\beta_-^2) R_{\delta_{io}}^T \mathbf{g}_2 \\ &\quad - \beta_- (2\beta_+^2 - \beta_-^2) R_{2\delta_{io}}^T \mathbf{g}_1 + 3\beta_-^2 \beta_+ R_{3\delta_{io}}^T \mathbf{g}_{ip}, \end{aligned} \quad (\text{F18})$$

where

$$\begin{aligned} \mathbf{g}_{ip} &= \begin{pmatrix} g_{ip}^c \\ g_{ip}^s \end{pmatrix}, \quad \mathbf{g}_{op} = \begin{pmatrix} g_{op}^c \\ g_{op}^s \end{pmatrix}, \quad \mathbf{g}_{1,2} = \begin{pmatrix} g_{1,2}^c \\ g_{1,2}^s \end{pmatrix}, \\ \mathbf{g}_{\pm} &= \begin{pmatrix} g_{\pm}^c \\ g_{\pm}^s \end{pmatrix}, \quad \tilde{\mathbf{g}}_{1,2} = \begin{pmatrix} \tilde{g}_{1,2}^c \\ \tilde{g}_{1,2}^s \end{pmatrix}. \end{aligned} \quad (\text{F19})$$

Similarly to the case of the trigonal groups investigated in Sec. IV C, we keep only the terms in the action that are linear and quadratic in the subleading-order parameter \mathbf{d}^+ . This results in $\mathcal{S} = \mathcal{S}_-[\mathbf{d}^-] + \mathcal{S}_{+-}[\mathbf{d}^+, \mathbf{d}^-]$ with

$$\mathcal{S}_- = \int_{\mathbf{x}} \{ \lambda_- |\mathbf{d}^-|^2 + g_- |\mathbf{d}^-|^3 \cos(3\gamma_- - \delta_-) + u_- |\mathbf{d}^-|^4 \}, \quad (\text{F20})$$

where

$$g_- = \text{sign}(g_-^c) \sqrt{(g_-^c)^2 + (g_-^s)^2}, \quad \delta_- = \arctan \frac{g_-^s}{g_-^c}, \quad (\text{F21})$$

and

$$\begin{aligned} \mathcal{S}_{+-} = \int_{\mathbf{x}} \{ & \lambda_+ |\mathbf{d}^+|^2 + |\mathbf{d}^+|^2 |\mathbf{d}^-| \tilde{g}_1 \cos(2\gamma_+ + \gamma_- - \tilde{\delta}_1) \\ & + |\mathbf{d}^+| |\mathbf{d}^-|^2 \tilde{g}_2 \cos(\gamma_+ + 2\gamma_- - \tilde{\delta}_2) \}, \end{aligned} \quad (\text{F22})$$

with relationships similar to Eq. (F21) holding for $\tilde{g}_{1,2}$ and $\tilde{\delta}_{1,2}$ in terms of the vectors $\tilde{\mathbf{g}}_{1,2}$ defined in Eq. (F18). Minimizing with respect to \mathbf{d}^+ gives

$$|\mathbf{d}^+| \approx \frac{-\tilde{g}_2 \cos(\gamma_+ + 2\gamma_- - \tilde{\delta}_2)}{2\lambda_+} |\mathbf{d}^-|^2 + O(|\mathbf{d}^-|^3), \quad (\text{F23})$$

which, when inserted back in Eq. (F22), results in an additional quartic term in \mathbf{d}^- :

$$\mathcal{S}_{+-} = \int_{\mathbf{x}} \left\{ -\frac{(\tilde{g}_2)^2 \cos^2(\gamma_+ + 2\gamma_- - \tilde{\delta}_2)}{4\lambda_+} |\mathbf{d}^-|^4 \right\}. \quad (\text{F24})$$

Combined with the condition that $|\mathbf{d}^+|$ in Eq. (F24) must be positive, this additional quartic term is minimized for the angle

$$\gamma_+ = -2\gamma_- + \tilde{\delta}_2 + \left(\frac{1 + \text{sign} \tilde{g}_2}{2} \right) \pi. \quad (\text{F25})$$

Consequently, the effect of integrating out the fluctuations in the subleading \mathbf{d}^+ channel is to renormalize the quartic Landau coefficient $u_- \rightarrow u_- - (\tilde{g}_2)^2 / (4\lambda_+)$ of the \mathbf{d}^- action (F20), analogously to what we found in Sec. IV C. The main difference of this action with respect to the action derived in Sec. IV C for the trigonal groups $\{D_3, D_{3d}, C_{3v}\}$ is the offset angle δ_- . Thus, the nematic order parameter \mathbf{d}^- behaves as a Z_3^* clock order parameter, characterized by the threefold-degenerate ground state:

$$\gamma_-^0 = \frac{\delta_-}{3} + \frac{\pi}{3} \frac{1 + \text{sign}(g_-)}{2} + \frac{2\pi}{3} n, \quad n = \{0, 1, 2\}. \quad (\text{F26})$$

For these values of γ_-^0 , the induced \mathbf{d}^+ nematic order parameter becomes

$$\mathbf{d}^+ = \text{sign}(g_-) \frac{|\tilde{g}_2|}{2\lambda_+} |\mathbf{d}^-| \mathcal{R}_{\tilde{\delta}_2 - \delta_-} \mathbf{d}^-. \quad (\text{F27})$$

Therefore, \mathbf{d}^+ is rotated against \mathbf{d}^- by the offset angle $\tilde{\delta}_2 - \delta_-$. Using Eq. (F12), it is straightforward to obtain the original nematic order-parameter doublets:

$$\mathbf{d}^{op} = \beta_- \mathbf{d}^+ + \beta_+ \mathbf{d}^-, \quad \mathbf{d}^{ip} = R_{-\delta_{io}} (\beta_+ \mathbf{d}^+ - \beta_- \mathbf{d}^-). \quad (\text{F28})$$

Because \mathbf{d}^+ is not collinear to \mathbf{d}^- , \mathbf{d}^{op} , and \mathbf{d}^{ip} are generally not going to be collinear either. One consequence of this property is that the nematic axes $\mathbf{n}, \mathbf{m}, \mathbf{l}$ will be offset from any high-symmetry axes. This is consistent with the fact that the groups $\{S_6, C_3\}$ have no residual symmetry axes in the nematic phase, see also Table I. In contrast, for the trigonal groups $\{D_3, D_{3d}, C_{3v}\}$, the Landau coefficients satisfy $r_{io2} = 0$, $g_{ip,op,1,2}^s = 0$, and $u_{io,1,2}^s = 0$. This causes the rotation matrix in Eq. (F27) to become the identity, $\mathcal{R}_{\tilde{\delta}_2 - \delta_-} = \mathbb{1}$, such that \mathbf{d}^+ and \mathbf{d}^- are collinear.

APPENDIX G: LANDAU EXPANSION FOR THE TETRAGONAL GROUPS C_{4h}, C_4 , AND S_4

In this Appendix, we consider the three tetragonal point groups $\{C_{4h}, C_4, S_4\}$ that do not possess in-plane twofold

rotational symmetry axes. This implies not only that the two in-plane nematic components $\{d_2, d_5\}$ transform as the same one-dimensional IR, but also that the out-of-plane nematic doublet \mathbf{d}^{op} transforms as a complex IR. For concreteness, we focus on the group C_{4h} , for which d_2 and d_5 transform as B_g while $\Delta^{\text{op}} = |\mathbf{d}^{\text{op}}|e^{i\gamma_{\text{op}}}$ and $\bar{\Delta}^{\text{op}} = |\mathbf{d}^{\text{op}}|e^{-i\gamma_{\text{op}}}$ transform as E_g and \bar{E}_g .

Since the in-plane components are degenerate, we consider the full in-plane doublet $\mathbf{d}^{\text{ip}} = (d_2, d_5)$, which transforms according to $(B_g \oplus B_g)$. The decomposition of the symmetrized product is straightforward:

$$[\otimes_{j=1}^2 (B_g \oplus B_g)]_s = 3A_g, \quad (\text{G1})$$

$$[\otimes_{j=1}^3 (B_g \oplus B_g)]_s = 4B_g, \quad (\text{G2})$$

$$[\otimes_{j=1}^4 (B_g \oplus B_g)]_s = 5A_g. \quad (\text{G3})$$

There are thus eight Landau invariants up to fourth-order. The resulting action $\mathcal{S} = \mathcal{S}_2 + \mathcal{S}_4$ is then

$$\mathcal{S}_2 = \int_{\mathbf{x}} \{r_1(d_2)^2 + r_2(d_5)^2 + r_3 d_2 d_5\}, \quad (\text{G4})$$

$$\mathcal{S}_4 = \int_{\mathbf{x}} \{u_1(d_2)^4 + u_2(d_5)^4 + u_3(d_2)^2(d_5)^2 + u_4 d_2(d_5)^3 + u_5(d_2)^3 d_5\}. \quad (\text{G5})$$

We follow the same procedure as with the trigonal case in Sec. IV C. The diagonalization of the quadratic action, Eq. (G4), is accomplished via the orthogonal matrix

$$U = \begin{pmatrix} \beta_+ & -\frac{r_3}{|r_3|}\beta_- \\ \frac{r_3}{|r_3|}\beta_- & \beta_+ \end{pmatrix}, \quad \beta_{\pm} = \frac{1}{\sqrt{2}} \sqrt{1 \pm \frac{\Delta r}{\sqrt{(\Delta r)^2 + r_3^2}}}, \quad (\text{G6})$$

with $\Delta r \equiv r_1 - r_2$. We obtain

$$\mathcal{S}_2 = \int_{\mathbf{x}} \{\lambda_+(d_+)^2 + \lambda_-(d_-)^2\}, \quad (\text{G7})$$

with eigenvalues

$$\lambda_{\pm} = \frac{1}{2} \left(r_1 + r_2 \pm \sqrt{(r_1 - r_2)^2 + r_3^2} \right), \quad (\text{G8})$$

and eigenvectors

$$(d_+, d_-)^T = U^T \mathbf{d}^{\text{ip}}. \quad (\text{G9})$$

Since $\lambda_- < \lambda_+$ by construction, the combination d_- orders first. We thus rewrite the action $\mathcal{S} = \mathcal{S}_- + \mathcal{S}_{+-}$ as

$$\mathcal{S}_- = \int_{\mathbf{x}} \{\lambda_-(d_-)^2 + u_-(d_-)^4\}, \quad (\text{G10})$$

$$\mathcal{S}_{+-} = \int_{\mathbf{x}} \{\lambda_+(d_+)^2 + \tilde{u}_1 d_+(d_-)^3 + \tilde{u}_2(d_+)^2(d_-)^2\}, \quad (\text{G11})$$

where we kept only terms that are linear or quadratic in the subleading channel d_+ and defined

$$\begin{pmatrix} u_- \\ \tilde{u}_1 \\ \tilde{u}_2 \end{pmatrix} = \beta_-^4 \begin{pmatrix} u_1 \\ -u_5 \\ u_3 \end{pmatrix} + \beta_+^4 \begin{pmatrix} u_2 \\ u_4 \\ u_3 \end{pmatrix} + \beta_-^2 \beta_+^2 \begin{pmatrix} u_3 \\ 3(u_5 - u_4) \\ 6u_1 + 6u_2 - 4u_3 \end{pmatrix} + \frac{r_3}{|r_3|} \beta_- \beta_+^3 \begin{pmatrix} -u_4 \\ 4u_2 - 2u_3 \\ 3u_4 - 3u_5 \end{pmatrix} - \frac{r_3}{|r_3|} \beta_-^3 \beta_+ \begin{pmatrix} u_5 \\ 4u_1 - 2u_3 \\ 3u_4 - 3u_5 \end{pmatrix}. \quad (\text{G12})$$

Minimizing Eq. (G11) gives $d_+ \approx -\frac{\tilde{u}_1}{2\lambda_+} d_-^3$, which upon reinsertion into \mathcal{S}_{+-} leads to a sixth-order term d_-^6 . Hence, fluctuations of the subleading channel only renormalize the sixth-order Landau coefficient of the Ising-nematic action of the leading channel, Eq. (G10). To express the ground state in the in-plane ($\mathbf{m}\mathbf{l}$) representation of Eq. (89), we can substitute $d_+ \approx -\frac{\tilde{u}_1}{2\lambda_+} d_-^3$ in Eq. (G9) and perform the inverse transformation to obtain both $|\mathbf{d}^{\text{ip}}|$ and the specific angle γ_{ip} , both of which will be determined by the Landau parameters of the original action (G4) and (G5).

Proceeding to the out-of-plane doublet \mathbf{d}^{op} , the decompositions of the symmetrized products are

$$[\otimes_{j=1}^2 (E_g \oplus \bar{E}_g)]_s = A_g \oplus 2B_g, \quad (\text{G13})$$

$$[\otimes_{j=1}^3 (E_g \oplus \bar{E}_g)]_s = 2(E_g \oplus \bar{E}_g), \quad (\text{G14})$$

$$[\otimes_{j=1}^4 (E_g \oplus \bar{E}_g)]_s = 3A_g \oplus 2B_g, \quad (\text{G15})$$

with the bilinears $D_{\text{op}}^A = |\mathbf{d}^{\text{op}}|^2$,

$$D_{\text{op}}^{B_g,1} = |\mathbf{d}^{\text{op}}|^2 \cos(2\gamma_{\text{op}}), \quad D_{\text{op}}^{B_g,2} = |\mathbf{d}^{\text{op}}|^2 \sin(2\gamma_{\text{op}}). \quad (\text{G16})$$

The four invariants can be expressed as $|\mathbf{d}^{\text{op}}|^2$, $|\mathbf{d}^{\text{op}}|^4$, $D_{\text{op}}^{B_g,1} D_{\text{op}}^{B_g,2}$, and $(D_{\text{op}}^{B_g,1})^2 - (D_{\text{op}}^{B_g,2})^2$ which, combined with the relationship (D6), give the Landau expansion:

$$\mathcal{S}_{\text{op}} = \int_{\mathbf{x}} \{r_0 |\mathbf{d}^{\text{op}}|^2 + u |\mathbf{d}^{\text{op}}|^4 + v_4 |\mathbf{d}^{\text{op}}|^4 \cos(4\gamma_{\text{op}} - \delta_0)\}. \quad (\text{G17})$$

As in the cases analyzed in the previous Appendixes, the offset angle δ_0 should be understood as a Landau coefficient. The Landau expansion (G17) has the shape of a modified four-state clock model, Z_4^* clock, with the fourfold degenerate angles offset from the high-symmetry tetragonal directions:

$$\gamma_{\text{op}}^0 = \frac{1}{4} \delta_0 + \frac{2\pi}{4} n + \frac{\pi}{4} \left(\frac{1 + \text{sign} v_4}{2} \right), \quad n \in \{0, 1, 2, 3\}. \quad (\text{G18})$$

Upon employing Eq. (89), we conclude that the offset angle δ_0 leads to a rotation of the nematic axes about the k_z axis by an angle $\delta_0/4$.

- [1] V. Hinkov, D. Haug, B. Fauqué, P. Bourges, Y. Sidis, A. Ivanov, C. Bernhard, C. T. Lin, and B. Keimer, Electronic liquid crystal state in the high-temperature superconductor $\text{YBa}_2\text{Cu}_3\text{O}_{6.45}$, *Science* **319**, 597 (2008).
- [2] M. J. Lawler, K. Fujita, J. Lee, A. R. Schmidt, Y. Kohsaka, C. K. Kim, H. Eisaki, S. Uchida, J. C. Davis, J. P. Sethna, and E.-A. Kim, Intra-unit-cell electronic nematicity of the high- T_c copper-oxide pseudogap states, *Nature (London)* **466**, 347 (2010).
- [3] J. Wu, A. T. Bollinger, X. He, and I. Božović, Spontaneous breaking of rotational symmetry in copper oxide superconductors, *Nature (London)* **547**, 432 (2017).
- [4] Y. Sato, S. Kasahara, H. Murayama, Y. Kasahara, E.-G. Moon, T. Nishizaki, T. Loew, J. Porras, B. Keimer, T. Shibauchi, and Y. Matsuda, Thermodynamic evidence for a nematic phase transition at the onset of the pseudogap in $\text{YBa}_2\text{Cu}_3\text{O}_y$, *Nat. Phys.* **13**, 1074 (2017).
- [5] S. Mukhopadhyay, R. Sharma, C. K. Kim, S. D. Edkins, M. H. Hamidian, H. Eisaki, S.-I. Uchida, E.-A. Kim, M. J. Lawler, A. P. Mackenzie, J. C. S. Davis, and K. Fujita, Evidence for a vestigial nematic state in the cuprate pseudogap phase, *Proc. Natl. Acad. Sci. USA* **116**, 13249 (2019).
- [6] T.-M. Chuang, M. P. Allan, J. Lee, Y. Xie, N. Ni, S. L. Bud'ko, G. S. Boebinger, P. C. Canfield, and J. C. Davis, Nematic electronic structure in the “parent” state of the iron-based superconductor $\text{Ca}(\text{Fe}_{1-x}\text{Co}_x)_2\text{As}_2$, *Science* **327**, 181 (2010).
- [7] J.-H. Chu, J. G. Analytis, K. D. Greve, P. L. McMahon, Z. Islam, Y. Yamamoto, and I. R. Fisher, In-plane resistivity anisotropy in an underdoped iron arsenide superconductor, *Science* **329**, 824 (2010).
- [8] M. Yi, D. Lu, J.-H. Chu, J. G. Analytis, A. P. Sorini, A. F. Kemper, B. Moritz, S.-K. Mo, R. G. Moore, M. Hashimoto, W.-S. Lee, Z. Hussain, T. P. Devereaux, I. R. Fisher, and Z.-X. Shen, Symmetry-breaking orbital anisotropy observed for detwinned $\text{Ba}(\text{Fe}_{1-x}\text{Co}_x)_2\text{As}_2$ above the spin density wave transition, *Proc. Natl. Acad. Sci. USA* **108**, 6878 (2011).
- [9] J.-H. Chu, H.-H. Kuo, J. G. Analytis, and I. R. Fisher, Divergent nematic susceptibility in an iron arsenide superconductor, *Science* **337**, 710 (2012).
- [10] H.-H. Kuo, J.-H. Chu, J. C. Palmstrom, S. A. Kivelson, and I. R. Fisher, Ubiquitous signatures of nematic quantum criticality in optimally doped Fe-based superconductors, *Science* **352**, 958 (2016).
- [11] A. E. Böhrer, J.-H. Chu, S. Lederer, and M. Yi, Nematicity and nematic fluctuations in iron-based superconductors, *Nat. Phys.* **18**, 1412 (2022).
- [12] M. P. Lilly, K. B. Cooper, J. P. Eisenstein, L. N. Pfeiffer, and K. W. West, Evidence for an anisotropic state of two-dimensional electrons in high Landau levels, *Phys. Rev. Lett.* **82**, 394 (1999).
- [13] B. E. Feldman, M. T. Randeria, A. Gyenis, F. Wu, H. Ji, R. J. Cava, A. H. MacDonald, and A. Yazdani, Observation of a nematic quantum Hall liquid on the surface of bismuth, *Science* **354**, 316 (2016).
- [14] R. A. Borzi, S. A. Grigera, J. Farrell, R. S. Perry, S. J. S. Lister, S. L. Lee, D. A. Tennant, Y. Maeno, and A. P. Mackenzie, Formation of a nematic fluid at high fields in $\text{Sr}_3\text{Ru}_2\text{O}_7$, *Science* **315**, 214 (2007).
- [15] Y. Sun, S. Kittaka, T. Sakakibara, K. Machida, J. Wang, J. Wen, X. Xing, Z. Shi, and T. Tamegai, Quasiparticle evidence for the nematic state above T_c in $\text{Sr}_x\text{Bi}_2\text{Se}_3$, *Phys. Rev. Lett.* **123**, 027002 (2019).
- [16] C.-W. Cho, J. Shen, J. Lyu, O. Atanov, Q. Chen, S. H. Lee, Y. San Hor, D. J. Gawryluk, E. Pomjakushina, M. Bartkowiak, M. Hecker, J. Schmalian, and R. Lortz, Z_3 vestigial nematic order due to superconducting fluctuations in the doped topological insulators $\text{Nb}_x\text{Bi}_2\text{Se}_3$ and $\text{Cu}_x\text{Bi}_2\text{Se}_3$, *Nat. Commun.* **11**, 3056 (2020).
- [17] Y. Jiang, X. Lai, K. Watanabe, T. Taniguchi, K. Haule, J. Mao, and E. Y. Andrei, Charge order and broken rotational symmetry in magic-angle twisted bilayer graphene, *Nature (London)* **573**, 91 (2019).
- [18] Y. Cao, D. Rodan-Legrain, J. M. Park, N. F. Q. Yuan, K. Watanabe, T. Taniguchi, R. M. Fernandes, L. Fu, and P. Jarillo-Herrero, Nematicity and competing orders in superconducting magic-angle graphene, *Science* **372**, 264 (2021).
- [19] C. Rubio-Verdú, S. Turkel, Y. Song, L. Klebl, R. Samajdar, M. S. Scheurer, J. W. Venderbos, K. Watanabe, T. Taniguchi, H. Ochoa, L. Xian, D. M. Kennes, R. M. Fernandes, Á. Rubio, and A. N. Pasupathy, Moiré nematic phase in twisted double bilayer graphene, *Nat. Phys.* **18**, 196 (2022).
- [20] N. J. Zhang, Y. Wang, K. Watanabe, T. Taniguchi, O. Vafek, and J. I. A. Li, Electronic anisotropy in magic-angle twisted trilayer graphene, *arXiv:2211.01352*.
- [21] F. Ronning, T. Helm, K. Shirer, M. Bachmann, L. Balicas, M. K. Chan, B. Ramshaw, R. D. McDonald, F. F. Balakirev, M. Jaime, E. Bauer, and P. Moll, Electronic in-plane symmetry breaking at field-tuned quantum criticality in CeRhIn_5 , *Nature (London)* **548**, 313 (2017).
- [22] E. W. Rosenberg, J.-H. Chu, J. P. Ruff, A. T. Hristov, and I. R. Fisher, Divergence of the quadrupole-strain susceptibility of the electronic nematic system YbRu_2Ge_2 , *Proc. Natl. Acad. Sci. USA* **116**, 7232 (2019).
- [23] S. Seo, X. Wang, S. M. Thomas, M. C. Rahn, D. Carmo, F. Ronning, E. D. Bauer, R. D. dos Reis, M. Janoschek, J. D. Thompson, R. M. Fernandes, and P. F. S. Rosa, Nematic state in CeAuSb_2 , *Phys. Rev. X* **10**, 011035 (2020).
- [24] P. Massat, J. Wen, J. M. Jiang, A. T. Hristov, Y. Liu, R. W. Smaha, R. S. Feigelson, Y. S. Lee, R. M. Fernandes, and I. R. Fisher, Field-tuned ferroquadrupolar quantum phase transition in the insulator TmVO_4 , *Proc. Natl. Acad. Sci. USA* **119**, e2119942119 (2022).
- [25] N. Drucker, T. Nguyen, M. Mandal, P. Siriviboon, Y. Quan, A. Boonkird, R. Okabe, F. Li, K. Buragge, F. Funuma, M. Matsuda, D. Abernathy, T. Williams, S. Chi, F. Ye, C. Nelson, B. Liao, P. Volkov, and M. Li, Incipient nematicity from electron flat bands in a kagome metal, *arXiv:2401.17141*.
- [26] G. Beaudin, L. M. Fournier, A. D. Bianchi, M. Nicklas, M. Kenzelmann, M. Laver, and W. Witczak-Krempa, Possible quantum nematic phase in a colossal magnetoresistance material, *Phys. Rev. B* **105**, 035104 (2022).
- [27] A. Little, C. Lee, C. John, S. Doyle, E. Maniv, N. L. Nair, W. Chen, D. Rees, J. W. Venderbos, R. M. Fernandes, J. G. Analytis, and J. Orenstein, Three-state nematicity in the triangular lattice antiferromagnet $\text{Fe}_{1/3}\text{NbS}_2$, *Nat. Mater.* **19**, 1062 (2020).
- [28] Z. Ni, D. S. Antonenko, W. J. Meese, Q. Tian, N. Huang, A. V. Haglund, M. Cothrine, D. G. Mandrus, R. M. Fernandes, J. W. F. Venderbos, and L. Wu, Signatures of Z_3

- Vestigial Potts-nematic order in van der Waals antiferromagnets, [arXiv:2308.07249](https://arxiv.org/abs/2308.07249).
- [29] Z. Sun, G. Ye, M. Huang, C. Zhou, N. Huang, Q. Li, Z. Ye, C. Nnokwe, H. Deng, D. Mandrus *et al.*, Dimensionality crossover to 2D vestigial nematicity from 3D zigzag antiferromagnetism in an XY -type honeycomb van der Waals magnet, [arXiv:2311.03493](https://arxiv.org/abs/2311.03493).
- [30] K. Hwangbo, J. Cenker, E. Rosenberg, Q. Jiang, H. Wen, D. Xiao, J.-H. Chu, and X. Xu, Strain tuning three-state Potts nematicity in a correlated antiferromagnet, [arXiv:2308.08734](https://arxiv.org/abs/2308.08734).
- [31] Q. Tan, C. A. Occhialini, H. Gao, J. Li, H. Kitadai, R. Comin, and X. Ling, Observation of three-state nematicity and domain evolution in atomically thin antiferromagnetic NiPS₃, *Nano Lett.* **24**, 7166 (2024).
- [32] H. Siddiquee, R. Munir, C. Dissanayake, P. Vaidya, C. Nickle, E. Del Barco, G. Lamura, C. Baines, S. Cahen, C. Hérold, P. Gentile, T. Shiroka, and Y. Nakajima, Nematic superconductivity in the topological semimetal CaSn₃, *Phys. Rev. B* **105**, 094508 (2022).
- [33] S. Jin, W. Zhang, X. Guo, X. Chen, X. Zhou, and X. Li, Evidence of Potts-nematic superfluidity in a hexagonal sp^2 optical lattice, *Phys. Rev. Lett.* **126**, 035301 (2021).
- [34] P. Chaikin and T. Lubensky, *Principles of Condensed Matter Physics*, 3rd ed. (Cambridge University Press, Cambridge, UK, 2000).
- [35] E. Kats, V. Lebedev, and A. Muratov, Weak crystallization theory, *Phys. Rep.* **228**, 1 (1993).
- [36] S. A. Kivelson, E. Fradkin, and V. J. Emery, Electronic liquid-crystal phases of a doped Mott insulator, *Nature (London)* **393**, 550 (1998).
- [37] E. Fradkin and S. A. Kivelson, Liquid-crystal phases of quantum Hall systems, *Phys. Rev. B* **59**, 8065 (1999).
- [38] J. Zaanen, Z. Nussinov, and S. Mukhin, Duality in 2+1D quantum elasticity: Superconductivity and quantum nematic order, *Ann. Phys. (NY)* **310**, 181 (2004).
- [39] L. Nie, G. Tarjus, and S. A. Kivelson, Quenched disorder and vestigial nematicity in the pseudogap regime of the cuprates, *Proc. Natl. Acad. Sci. USA* **111**, 7980 (2014).
- [40] L. Nie, A. V. Maharaj, E. Fradkin, and S. A. Kivelson, Vestigial nematicity from spin and/or charge order in the cuprates, *Phys. Rev. B* **96**, 085142 (2017).
- [41] M. Hecker and J. Schmalian, Vestigial nematic order and superconductivity in the doped topological insulator Cu_xBi₂Se₃, *npj Quantum Mater.* **3**, 26 (2018).
- [42] M. Hecker, R. Willa, J. Schmalian, and R. M. Fernandes, Cascade of vestigial orders in two-component superconductors: Nematic, ferromagnetic, s -wave charge- $4e$, and d -wave charge- $4e$ states, *Phys. Rev. B* **107**, 224503 (2023).
- [43] E. Fradkin, S. A. Kivelson, M. J. Lawler, J. P. Eisenstein, and A. P. Mackenzie, Nematic Fermi fluids in condensed matter physics, *Annu. Rev. Condens. Matter Phys.* **1**, 153 (2010).
- [44] R. M. Fernandes, A. V. Chubukov, and J. Schmalian, What drives nematic order in iron-based superconductors? *Nat. Phys.* **10**, 97 (2014).
- [45] E. Fradkin, S. A. Kivelson, and J. M. Tranquada, Colloquium: Theory of intertwined orders in high temperature superconductors, *Rev. Mod. Phys.* **87**, 457 (2015).
- [46] R. M. Fernandes, P. P. Orth, and J. Schmalian, Intertwined vestigial order in quantum materials: Nematicity and beyond, *Annu. Rev. Condens. Matter Phys.* **10**, 133 (2019).
- [47] I. I. Pomeranchuk, On the stability of a Fermi liquid, *Sov. Phys. JETP* **8**, 361 (1958).
- [48] V. Oganesyan, S. A. Kivelson, and E. Fradkin, Quantum theory of a nematic Fermi fluid, *Phys. Rev. B* **64**, 195109 (2001).
- [49] L. Dell'Anna and W. Metzner, Fermi surface fluctuations and single electron excitations near Pomeranchuk instability in two dimensions, *Phys. Rev. B* **73**, 045127 (2006).
- [50] M. Zacharias, P. Wölfle, and M. Garst, Multiscale quantum criticality: Pomeranchuk instability in isotropic metals, *Phys. Rev. B* **80**, 165116 (2009).
- [51] D. L. Maslov and A. V. Chubukov, Fermi liquid near Pomeranchuk quantum criticality, *Phys. Rev. B* **81**, 045110 (2010).
- [52] B. Valenzuela and M. A. Vozmediano, Pomeranchuk instability in doped graphene, *New J. Phys.* **10**, 113009 (2008).
- [53] M. L. Kiesel, C. Platt, and R. Thomale, Unconventional Fermi surface instabilities in the kagome Hubbard model, *Phys. Rev. Lett.* **110**, 126405 (2013).
- [54] A. V. Maharaj, E. W. Rosenberg, A. T. Hristov, E. Berg, R. M. Fernandes, I. R. Fisher, and S. A. Kivelson, Transverse fields to tune an Ising-nematic quantum phase transition, *Proc. Natl. Acad. Sci. USA* **114**, 13430 (2017).
- [55] C. Wu, K. Sun, E. Fradkin, and S.-C. Zhang, Fermi liquid instabilities in the spin channel, *Phys. Rev. B* **75**, 115103 (2007).
- [56] K. Liu, J. Nissinen, R.-J. Slager, K. Wu, and J. Zaanen, Generalized liquid crystals: Giant fluctuations and the vestigial chiral order of I , O , and T matter, *Phys. Rev. X* **6**, 041025 (2016).
- [57] Y. Xu, X.-C. Wu, C.-M. Jian, and C. Xu, Orbital order and possible non-Fermi liquid in moiré systems, *Phys. Rev. B* **101**, 205426 (2020).
- [58] I. Mandal and R. M. Fernandes, Valley-polarized nematic order in twisted moiré systems: In-plane orbital magnetism and crossover from non-Fermi liquid to Fermi liquid, *Phys. Rev. B* **107**, 125142 (2023).
- [59] V. Gali, M. Hecker, and R. M. Fernandes, A critical nematic phase with pseudogap-like behavior in twisted bilayers, [arXiv:2401.01844](https://arxiv.org/abs/2401.01844).
- [60] I. Boettcher and I. F. Herbut, Unconventional superconductivity in Luttinger semimetals: Theory of complex tensor order and the emergence of the uniaxial nematic state, *Phys. Rev. Lett.* **120**, 057002 (2018).
- [61] H.-Y. Kee, E. H. Kim, and C.-H. Chung, Signatures of an electronic nematic phase at the isotropic-nematic phase transition, *Phys. Rev. B* **68**, 245109 (2003).
- [62] J. Maciejko, B. Hsu, S. A. Kivelson, Y. Park, and S. L. Sondhi, Field theory of the quantum Hall nematic transition, *Phys. Rev. B* **88**, 125137 (2013).
- [63] Y. You, G. Y. Cho, and E. Fradkin, Theory of nematic fractional quantum Hall states, *Phys. Rev. X* **4**, 041050 (2014).
- [64] E. W. Carlson, K. A. Dahmen, E. Fradkin, and S. A. Kivelson, Hysteresis and noise from electronic nematicity in high-temperature superconductors, *Phys. Rev. Lett.* **96**, 097003 (2006).
- [65] C. Xu, M. Müller, and S. Sachdev, Ising and spin orders in the iron-based superconductors, *Phys. Rev. B* **78**, 020501(R) (2008).
- [66] C. Fang, H. Yao, W.-F. Tsai, J. Hu, and S. A. Kivelson, Theory of electron nematic order in LaFeAsO, *Phys. Rev. B* **77**, 224509 (2008).

- [67] S. Raghu, A. Paramekanti, E. A. Kim, R. A. Borzi, S. A. Grigera, A. P. Mackenzie, and S. A. Kivelson, Microscopic theory of the nematic phase in $\text{Sr}_3\text{Ru}_2\text{O}_7$, *Phys. Rev. B* **79**, 214402 (2009).
- [68] R. M. Fernandes, L. H. VanBebber, S. Bhattacharya, P. Chandra, V. Keppens, D. Mandrus, M. A. McGuire, B. C. Sales, A. S. Sefat, and J. Schmalian, Effects of nematic fluctuations on the elastic properties of iron arsenide superconductors, *Phys. Rev. Lett.* **105**, 157003 (2010).
- [69] M. A. Metlitski and S. Sachdev, Quantum phase transitions of metals in two spatial dimensions. I. Ising-nematic order, *Phys. Rev. B* **82**, 075127 (2010).
- [70] M. H. Fischer and E.-A. Kim, Mean-field analysis of intra-unit-cell order in the Emery model of the CuO_2 plane, *Phys. Rev. B* **84**, 144502 (2011).
- [71] R. M. Fernandes, A. V. Chubukov, J. Knolle, I. Eremin, and J. Schmalian, Preemptive nematic order, pseudogap, and orbital order in the iron pnictides, *Phys. Rev. B* **85**, 024534 (2012).
- [72] S. Onari and H. Kontani, Origin of diverse nematic orders in Fe-based superconductors: 45° rotated nematicity in AFe_2As_2 ($A = \text{Cs, Rb}$), *Phys. Rev. B* **100**, 020507 (2019).
- [73] Y. Wang, W. Hu, R. Yu, and Q. Si, Broken mirror symmetry, incommensurate spin correlations, and B_{2g} nematic order in iron pnictides, *Phys. Rev. B* **100**, 100502 (2019).
- [74] R. M. Fernandes and J. W. F. Venderbos, Nematicity with a twist: Rotational symmetry breaking in a moiré superlattice, *Sci. Adv.* **6**, eaba8834 (2020).
- [75] F. Lasse Buessen, S. Sorn, I. Martin, and A. Paramekanti, Nematic order driven by superconducting correlations, *Ann. Phys. (NY)* **435**, 168494 (2021).
- [76] J. Strockoz, D. S. Antonenko, D. LaBelle, and J. W. Venderbos, Excitonic instability towards a Potts-nematic quantum paramagnet, [arXiv:2211.11739](https://arxiv.org/abs/2211.11739).
- [77] H. Li and T. Li, Competing emergent Potts orders and possible nematic spin liquids in the kagome J_1 - J_3 Heisenberg model, *Phys. Rev. B* **106**, 035112 (2022).
- [78] S. Onari and H. Kontani, $\text{SU}(4)$ valley+spin fluctuation interference mechanism for nematic order in magic-angle twisted bilayer graphene: The impact of vertex corrections, *Phys. Rev. Lett.* **128**, 066401 (2022).
- [79] K. Kimura, M. Sigrist, and N. Kawakami, Probing three-state Potts nematic fluctuations by ultrasound attenuation, *Phys. Rev. B* **105**, 035130 (2022).
- [80] A.-M. Nedić, V. L. Quito, Y. Sizyuk, and P. P. Orth, Three-state Potts nematic order in stacked frustrated spin models with $\text{SO}(3)$ symmetry, *Phys. Rev. B* **107**, 184401 (2023).
- [81] A. R. Chakraborty and R. M. Fernandes, Strain-tuned quantum criticality in electronic Potts-nematic systems, *Phys. Rev. B* **107**, 195136 (2023).
- [82] D. Shechtman, I. Blech, D. Gratias, and J. W. Cahn, Metallic phase with long-range orientational order and no translational symmetry, *Phys. Rev. Lett.* **53**, 1951 (1984).
- [83] D. Levine and P. J. Steinhardt, Quasicrystals: A new class of ordered structures, *Phys. Rev. Lett.* **53**, 2477 (1984).
- [84] K. Kamiya, T. Takeuchi, N. Kabeya, N. Wada, T. Ishimasa, A. Ochiai, K. Deguchi, K. Imura, and N. Sato, Discovery of superconductivity in quasicrystal, *Nat. Commun.* **9**, 154 (2018).
- [85] A. Uri, S. C. de la Barrera, M. T. Randeria, D. Rodan-Legrain, T. Devakul, P. J. Crowley, N. Paul, K. Watanabe, T. Taniguchi, R. Lifshitz, L. Fu, R. C. Ashoori, and P. Jarillo-Herrero, Superconductivity and strong interactions in a tunable moiré quasiperiodic crystal, *Nature (London)* **620**, 762 (2023).
- [86] A. Goldman and M. Widom, Quasicrystal structure and properties, *Annu. Rev. Phys. Chem.* **42**, 685 (1991).
- [87] K. Deguchi, S. Matsukawa, N. K. Sato, T. Hattori, K. Ishida, H. Takakura, and T. Ishimasa, Quantum critical state in a magnetic quasicrystal, *Nat. Mater.* **11**, 1013 (2012).
- [88] J. E. S. Socolar, Simple octagonal and dodecagonal quasicrystals, *Phys. Rev. B* **39**, 10519 (1989).
- [89] D. A. Rabson, N. D. Mermin, D. S. Rokhsar, and D. C. Wright, The space groups of axial crystals and quasicrystals, *Rev. Mod. Phys.* **63**, 699 (1991).
- [90] J. Luck, A classification of critical phenomena on quasicrystals and other aperiodic structures, *Europhys. Lett.* **24**, 359 (1993).
- [91] R. Lifshitz, The symmetry of quasiperiodic crystals, *Phys. A (Amsterdam, Neth.)* **232**, 633 (1996).
- [92] S. J. Ahn, P. Moon, T.-H. Kim, H.-W. Kim, H.-C. Shin, E. H. Kim, H. W. Cha, S.-J. Kahng, P. Kim, M. Koshino, Y.-W. Son, C.-W. Yang, and J. R. Ahn, Dirac electrons in a dodecagonal graphene quasicrystal, *Science* **361**, 782 (2018).
- [93] R. Haenel, T. Tummuru, and M. Franz, Incoherent tunneling and topological superconductivity in twisted cuprate bilayers, *Phys. Rev. B* **106**, 104505 (2022).
- [94] Y.-B. Liu, J. Zhou, Y. Zhang, W.-Q. Chen, and F. Yang, Making chiral topological superconductors from nontopological superconductors through large angle twists, *Phys. Rev. B* **108**, 064508 (2023).
- [95] Y.-B. Liu, Y. Zhang, W.-Q. Chen, and F. Yang, High-angular-momentum topological superconductivities in twisted bilayer quasicrystal systems, *Phys. Rev. B* **107**, 014501 (2023).
- [96] S. Y. F. Zhao, X. Cui, P. A. Volkov, H. Yoo, S. Lee, J. A. Gardener, A. J. Akey, R. Engelke, Y. Ronen, R. Zhong, G. Gu, S. Plugge, T. Tummuru, M. Kim, M. Franz, J. H. Pixley, N. Poccia, and P. Kim, Time-reversal symmetry breaking superconductivity between twisted cuprate superconductors, *Science* **382**, 1422 (2023).
- [97] B. M. Fregoso, K. Sun, E. Fradkin, and B. L. Lev, Biaxial nematic phases in ultracold dipolar Fermi gases, *New J. Phys.* **11**, 103003 (2009).
- [98] R. A. Cowley, Acoustic phonon instabilities and structural phase transitions, *Phys. Rev. B* **13**, 4877 (1976).
- [99] R. Folk, H. Iro, and F. Schwabl, Critical statics of elastic phase transitions, *Z. Phys. B: Condens. Matter* **25**, 69 (1976).
- [100] T. Lookman, S. R. Shenoy, K. O. Rasmussen, A. Saxena, and A. R. Bishop, Ferroelastic dynamics and strain compatibility, *Phys. Rev. B* **67**, 024114 (2003).
- [101] S. Hayami, M. Yatsushiro, Y. Yanagi, and H. Kusunose, Classification of atomic-scale multipoles under crystallographic point groups and application to linear response tensors, *Phys. Rev. B* **98**, 165110 (2018).
- [102] H. Li, Classification of phase transitions and intertwined orders in crystallographic point groups, [arXiv:2108.01586](https://arxiv.org/abs/2108.01586).
- [103] R. Zia and D. Wallace, Critical behaviour of the continuous n-component Potts model, *J. Phys. A: Math. Gen.* **8**, 1495 (1975).
- [104] F. Y. Wu, The Potts model, *Rev. Mod. Phys.* **54**, 235 (1982).

- [105] D. S. Rokhsar, N. D. Mermin, and D. C. Wright, Rudimentary quasicrystallography: The icosahedral and decagonal reciprocal lattices, *Phys. Rev. B* **35**, 5487 (1987).
- [106] Y.-B. Liu, J. Zhou, and F. Yang, Nematic superconductivity and its critical vestigial phases in the quasi-crystal, [arXiv:2401.00750](https://arxiv.org/abs/2401.00750).
- [107] M. Hecker and R. M. Fernandes, Phonon-induced rotation of the electronic nematic director in superconducting Bi_2Se_3 , *Phys. Rev. B* **105**, 174504 (2022).
- [108] H. Watanabe and A. Vishwanath, Criterion for stability of Goldstone modes and Fermi liquid behavior in a metal with broken symmetry, *Proc. Natl. Acad. Sci. USA* **111**, 16314 (2014).
- [109] J. V. José, L. P. Kadanoff, S. Kirkpatrick, and D. R. Nelson, Renormalization, vortices, and symmetry-breaking perturbations in the two-dimensional planar model, *Phys. Rev. B* **16**, 1217 (1977).
- [110] M. Oshikawa, Ordered phase and scaling in Z_n models and the three-state antiferromagnetic Potts model in three dimensions, *Phys. Rev. B* **61**, 3430 (2000).
- [111] J. Manuel Carmona, A. Pelissetto, and E. Vicari, n -component Ginzburg-Landau Hamiltonian with cubic anisotropy: A six-loop study, *Phys. Rev. B* **61**, 15136 (2000).
- [112] P. Patil, H. Shao, and A. W. Sandvik, Unconventional $U(1)$ to Z_q crossover in quantum and classical q -state clock models, *Phys. Rev. B* **103**, 054418 (2021).
- [113] M. Suzuki, New universality of critical exponents, *Prog. Theor. Phys.* **51**, 1992 (1974).
- [114] S. Jin, A. Sen, W. Guo, and A. W. Sandvik, Phase transitions in the frustrated Ising model on the square lattice, *Phys. Rev. B* **87**, 144406 (2013).
- [115] D. Podolsky, E. Shimshoni, G. Morigi, and S. Fishman, Buckling transitions and clock order of two-dimensional Coulomb crystals, *Phys. Rev. X* **6**, 031025 (2016).
- [116] M. Arnold and R. Nigmatullin, Dynamics of vortex defect formation in two-dimensional Coulomb crystals, *Phys. Rev. B* **106**, 104106 (2022).
- [117] D. Park, C. Park, E. Ko, K. Yananose, R. Engelke, X. Zhang, K. Davydov, M. Green, S. H. Park, J. H. Lee, K. Watanabe, T. Taniguchi *et al.*, Tunable incommensurability and spontaneous symmetry breaking in the reconstructed moiré-of-moiré lattices, [arXiv:2402.15760](https://arxiv.org/abs/2402.15760).
- [118] Y. Gallais and I. Paul, Charge nematicity and electronic Raman scattering in iron-based superconductors, *C. R. Phys.* **17**, 113 (2016).
- [119] S. Lederer, Y. Schattner, E. Berg, and S. A. Kivelson, Superconductivity and non-Fermi liquid behavior near a nematic quantum critical point, *Proc. Natl. Acad. Sci. USA* **114**, 4905 (2017).
- [120] A. Klein and A. Chubukov, Superconductivity near a nematic quantum critical point: Interplay between hot and lukewarm regions, *Phys. Rev. B* **98**, 220501 (2018).
- [121] Y. Qi and C. Xu, Global phase diagram for magnetism and lattice distortion of iron-pnictide materials, *Phys. Rev. B* **80**, 094402 (2009).
- [122] U. Karahasanovic and J. Schmalian, Elastic coupling and spin-driven nematicity in iron-based superconductors, *Phys. Rev. B* **93**, 064520 (2016).
- [123] I. Paul and M. Garst, Lattice effects on nematic quantum criticality in metals, *Phys. Rev. Lett.* **118**, 227601 (2017).
- [124] V. S. de Carvalho and R. M. Fernandes, Resistivity near a nematic quantum critical point: Impact of acoustic phonons, *Phys. Rev. B* **100**, 115103 (2019).
- [125] D.-H. Ding, W. Yang, C. Hu, and R. Wang, Generalized elasticity theory of quasicrystals, *Phys. Rev. B* **48**, 7003 (1993).
- [126] H. Ochoa, Moiré-pattern fluctuations and electron-phason coupling in twisted bilayer graphene, *Phys. Rev. B* **100**, 155426 (2019).
- [127] Y. Loh, E. Carlson, and K. Dahmen, Noise predictions for STM in systems with local electron nematic order, *Phys. Rev. B* **81**, 224207 (2010).
- [128] W. J. Meese, T. Vojta, and R. M. Fernandes, Random strain induced correlations in materials with intertwined nematic and magnetic orders, *Phys. Rev. B* **106**, 115134 (2022).
- [129] M. Hamermesh, *Group Theory and Its Applications to Physical Problems* (Dover Publications, Mineola, NY, 1989).